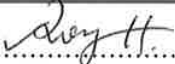


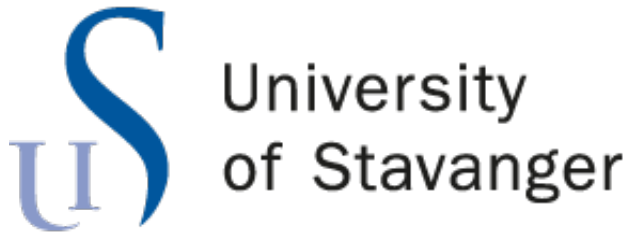


University of
Stavanger

Faculty of Science and Technology

MASTER'S THESIS

Study program/ Specialization: Master of Science in Mathematics and Physics, Physics Specialization	Spring semester, 2016 Open access
Writer: Wai Shing, Hung	 (Writer's signature)
Faculty supervisor: Helge Bøvik Larsen	
Thesis title: Size estimation of nano-particles from synchrotron X-ray data	
Credits (ECTS): 60	
Key words: Size estimation of nano-particles, X-ray diffraction, XRD, Scherrer equation, Diffraction peak broadening, Silver sulphate, Silver sizes growth, FWHM, integral breadth, TDS, Growth kinetics, Mathematica	Pages: 101 + enclosure: 2CD Stavanger, 15 th June/ 2016



Size estimation of nano-particles from synchrotron X-ray data

Hung Wai Shing

June 2016

MASTER'S THESIS

Department of Mathematics and Natural Sciences

University of Stavanger

Preface

This is a Master's thesis in department of mathematics and natural sciences at the University of Stavanger, as part of the study program of Master of Science in Mathematics and Physics during the 2015 Fall and 2016 Spring semesters.

As the need of reliable methods for determining nanoparticle size increases, so the aim of this study was to analysis the size estimation by synchrotron X-ray diffraction. Mathematica was used as the main tool for analysing diffractogram.

Stavanger, 15-6-2016

Hung Wai Shing

Acknowledgment

I would like to thank the following persons for their help during my thesis work. First and foremost, I sincerely thank my supervisor, Professor Helge Bøvik Larsen for suggesting an interesting project and providing with great support and guidance throughout the project. In addition, I would like to thank my family and friends for supporting and prayers. Lastly to God Almighty for his grace and love upon my life.

H.W.S

Abstract

Three samples of Ag_2SO_4 powder were heated up from 380 °C to 540 °C and then cooled down to 380 °C using an in-house made heat blower with a thermo-couple based temperature controller. During the heating process, synchrotron X-ray diffraction data including diffraction angles and intensities were obtained by diffractometer-setup found in the Swiss-Norwegian beamlines (SNBL- BM01A) at the ESRF. The diffractograms of each samples at different temperatures were studied by Mathematica.

Ag_2SO_4 powder procured at “Sigma-Aldrich” did not show any diffraction peak in the diffractograms, but the Ag_2SO_4 powder obtained from crushing a large single crystal by pestle and mortar showed silver peaks in all five lowest reflections, 111, 200, 220, 311 and 222.

The sizes of the silver were estimated by Scherrer equation. The ways of defining peak width and the choice of Scherrer constants were found to be vital for the accuracy of size estimations. Peak width was defined by two methods, namely FWHM and integral breadth. For FWHM method, the sizes of silver grew typically from around 50 ± 10 nm to 70 ± 10 nm when temperature increased from 380 °C to 432 °C. For integral breadth method, the sizes of silver grew typically from around 60 ± 10 nm to 80 ± 10 nm when temperature increased from 380 °C to 432 °C.

For both methods, silver crystallites were grown almost linearly with increasing temperature in all reflections within the temperature range of 380 °C to 432 °C. Then, silver crystallites stopped growing when temperature was over 432 °C that is close to the phase transition temperature of silver sulphate, 427 °C. It is very likely that the phase transition of silver sulphate prohibits the growth of metallic silver.

The main instrumental broadening was coming from the finite pixel size of the detector and the energy dispersion of the synchrotron radiation. The uncertainties in FWHM were $0.04^\circ \pm 0.01^\circ$ to $0.10^\circ \pm 0.01^\circ$. The magnitude of the instrumental broadening due to the energy dispersion of the synchrotron radiation was 10^{-5° and was insignificant.

Contents

Preface	i
Acknowledgment	ii
Abstract	iii
Table of Contents	iv
List of Tables	viii
List of Figures	xi
Abbreviations	xii
1 Introduction	1
1.1 Background	1
1.2 Method to study nanoparticles	2
1.3 Objectives	2
2 Experiment	3
3 Formation of metallic silver	6
3.1 Diffraction angle	7
3.1.1 Bragg's law	7
3.1.2 Extinction rule	7
3.1.3 Lattice constant of silver	7
3.2 Examining the presence of silver in the samples	10

3.2.1	Exponential model for decay of synchrotron beams	10
3.2.2	No silver formation in sample 1 and sample 3	11
3.2.3	Silver formation in sample 2	13
4	Size estimation of silver in sample 2	15
4.1	Scherrer equation	16
4.1.1	Limitation to Scherrer equation	17
4.1.2	Scherrer constant	18
4.1.3	Define peak breadth by FWHM	19
4.1.4	Define peak breadth by integral breadth	25
4.2	Silver growth	28
4.3	Uncertainty in size estimation	29
4.4	Comparison on FWHM and integral breadth	32
4.5	The important of Scherrer constant on size estimation	38
5	Factors leading to the broadening of diffraction peak	41
5.1	Instrumental broadening	41
5.1.1	Finite pixel size of the detector	41
5.1.2	Energy dispersion of the incoming synchrotron radiation	43
5.1.3	Method to remove instrumental broadening	44
5.2	Internal elastic strains	45
5.2.1	Macro-strain	46
5.2.2	Micro-strain	46
5.3	Thermal diffuse scattering	47
6	Growth kinetics	48
6.1	Isothermal kinetics	48
6.2	Non-isothermal kinetics	49
6.3	Shape of silver crystallites	52
7	Summary and suggestion to further investigation	53
7.1	Summary and conclusions	53

7.2 Suggestion to further investigation	55
A Diffraction angles of silver	56
B Scaling factors of exponential decay of synchrotron beam	61
C Maximum instrumental broadening due to energy dispersion	63
D Mathematica Code	66
Bibliography	84

List of Tables

2.1 Optics for BM01A	4
3.1 Interpolation of silver lattice constant by linear regression and exponential regression, where a is the lattice constant in Å and T is the temperature in °C	8
3.2 Mean absolute errors of linear regression linear regression and exponential regression with the experimental diffraction angle	8
3.3 Difference on interpolation of diffraction angle with data within 300 °C to 600 °C and interpolation with entire data set by exponential regression	10
4.1 Summary on silver growth estimated by FWHM and integral breadth method	28
4.2 Scherrer constants used in FWHM method for different shapes of silver crystallites and uncertainty of Scherrer constants, δK_w that is the maximum difference between the Scherrer constant of cubic shape with all other shapes	30
4.3 Scherrer constants used in integral breadth method for different shapes of silver crystallites and uncertainty of Scherrer constants, δK_β that is the maximum difference between the Scherrer constant of cubic shape with all other shapes	30
4.4 δB_{hkl} of FWHM method and integral breadth method at 380 °C	31
4.5 δB_{hkl} of FWHM method and integral breadth method at 432 °C	32
4.6 Summary on uncertainties in estimated silver sizes by FWHM and integral breadth method	32
5.1 Maximum Instrumental broadening due to energy dispersion of synchrotron radiation	44

A.1	Diffraction angles of silver estimated by linear regression	57
A.2	Diffraction angles of silver estimated by exponential regression	59
B.1	Scaling factor K for the samples at different elapsed time	61
C.1	Instrumental broadening due to energy dispersion of synchrotron radiation	64

List of Figures

2.1	Beamline layout at the Swiss-Norwegian beamline A	4
2.2	Experimental diffraction geometry	4
2.3	Diffraction pattern of powdered Ag_2SO_4 at 380 °C	5
3.1	Ag_2SO_4 peak nearby silver 220 reflection peak	9
3.2	Influence on peak intensities for silver 111 reflections without proper scaling	11
3.3	Decreasing in peak intensities for silver 111 reflection without proper scaling after reaching the phase transition temperature of silver sulphate	12
3.4	Intensities of silver 111 reflection of the 3 different samples along with temperature	12
3.5	Diffraction pattern to examining the presence of silver in the samples at temperature 530 °C in 111 reflection	13
3.6	Diffraction pattern of sample 2 at 530 °C that showing the five lowest reflection peaks of silver	14
4.1	The function $\frac{\sin^2 Nx}{\sin^2 x}$ for $N = 500$	16
4.2	The function $\frac{\sin^2 Nx}{\sin^2 x}$ for $N = 5$	16
4.3	Diffraction pattern showing FWHM of 200 reflection of silver peak at 398 °C	19
4.4	Diffraction patterns showing the silver 200 reflection peak at 398 °C with and without background intensities	20
4.5	Recorded diffraction angles and intensities within the range of 200 reflection at 398 °C	21
4.6	Gaussian fitting of silver 200 reflection at 398 °C	22
4.7	Calculated FWHM for all five reflections	22

4.8	The size estimations of silver for the five lowest reflections by defining peak breadth by FWHM	23
4.9	The size estimations of silver for the five lowest reflections by defining peak breadth by FWHM with x-axis as elapsed time in minutes and y-axis in nano-meter	24
4.10	Diffraction showing peak intensity and the total area under diffraction peak profile of 200 reflection of silver peak at 398 °C	25
4.11	Calculated integral breadth for all five lowest reflections of silver	26
4.12	The size estimations of silver for the five lowest reflections by defining peak breadth by integral breadth and x-axis as elapsed time in minutes	27
4.13	95% confidence interval of Gaussian fitting of silver 200 reflection at 398 °C	31
4.14	The uncertainties in size estimations of silver for the five lowest reflections by defining peak breadth by FWHM	33
4.15	The uncertainties in size estimations of silver for the five lowest reflections by defining peak breadth by integral breadth	34
4.16	Difference on size estimations of silver by defining peak breadth by FWHM and integral breadth	36
4.17	Comparing the estimated sizes growth rates of silver by FWHM and integral breadth method by shifting up the plot of sizes estimated by FWHM method	37
4.18	Difference on size estimations for 311 reflection by assuming spherical crystallite where Scherrer constant equal to 0.94; and assuming cubic crystallite where Scherrer constant equal to 0.9082	38
4.19	Difference on size estimations for 111 reflection by assuming spherical crystallite where Scherrer constant equal to 0.94; and assuming cubic crystallite where Scherrer constant equal to 0.8551	39
4.20	Difference on size estimations for 200 reflection by assuming spherical crystallite where Scherrer constant equal to 0.94; and assuming cubic crystallite where Scherrer constant equal to 0.8859	39
4.21	Difference on size estimations for 220 reflection by assuming spherical crystallite where Scherrer constant equal to 0.94; and assuming cubic crystallite where Scherrer constant equal to 0.8340	40

4.22	Difference on size estimations for 222 reflection by assuming spherical crystallite where Scherrer constant equal to 0.94; and assuming cubic crystallite where Scherrer constant equal to 0.8551	40
5.1	Theoretical and experiment values of diffraction angle of 200 reflection	42
5.2	Diffraction pattern of silver 200 reflection at 388 °C, 390 °C, 392 °C and 394 °C	42
5.3	Size estimations of silver in sample 2 111 reflection with and without eliminating the energy dispersion broadening	45
5.4	TDS contribution to silver 200 reflection peak at 432 °C, where the TDS intensity is not to scale	47
6.1	The plotting of $\ln[-\ln(1-x(t))]$ against $\ln t$ within the temperature range of 380 °C to 432 °C, for the five lowest reflections by defining peak breadth by FWHM	50
6.2	The plotting of $\ln[-\ln(1-x(t))]$ against $\ln t$ within the temperature range of 380 °C to 432 °C, for the five lowest reflections by defining peak breadth by integral breadth	51
6.3	Shape of silver crystallites by FWHM method, which was estimated by using thickness in [111], [200], [220] as the principal axes of ellipsoid	52
6.4	Shape of silver crystallites by integral breadth method, which was estimated by using thickness in [111], [200], [220] as the principal axes of ellipsoid	52

Abbreviations

ESRF European Synchrotron Radiation Facility

FCC Face Centered Cubic

FWHM Full Width at Half Maximum

MAE Mean Absolute Error

TDS Thermal Diffuse Scattering

TEM Transmission Electron Microscope

XRD X-Ray Diffraction

Chapter 1

Introduction

1.1 Background

Nanoparticles refer to particles with dimensions measured in nanometer (nm) . In 2008, the International Organization for Standardization (ISO) defined a nanoparticle to be a discrete nano-object that all three Cartesian dimensions have to be less than 100 nm [1]. Nanoparticles can be found in natural or can be made by human. During the last few decades, nanoparticles have become more important due to the practical applications in a variety of areas, including medicine, engineering, catalysis, and environmental remediation [1].

Therefore, the need of reliable methods for determining nanoparticle size has increased and this study was dedicated to improve the size estimation by X-ray diffraction.

Nanoparticles to be studied

Silver nanoparticles have special optical, electronic and chemical properties, so they are used in many fields such as antibacterial application [2], catalysis [3, 4]. The study of silver nanoparticles has become more important, so silver nanoparticles were chosen to be studied.

In this research project, silver nanoparticles precipitating in silver sulphate matrix were studied. According to Larsen et al. [5], during the heating process of silver sulphate, metallic silver precipitated inside the silver sulphate matrix. The metallic silver will modify the physical properties associated with silver sulphate like ionic conduction property, so it is useful to understand the growth of silver precipitates in silver sulphate.

1.2 Method to study nanoparticles

Transmission electron microscopy (TEM) and X-ray diffraction (XRD) [6] are the most common methods to estimate the size of nanoparticles.

TEM is a direct observation method. The size of particles can be read directly. TEM is mostly used for studying the fine structure of crystallites. However, the samples have to be made into very thin layers so that they are observable in TEM. The preparations of the samples are difficult for some materials. In addition, some very small particles can be transparent for electrons [6]. Also, TEM provides information about the local structure, but the nanoparticles can have a distribution of sizes. So, the size estimations by TEM can have great error if there are a great variety of sizes in the nanoparticles [6, 7].

XRD method is the study of diffraction pattern from the crystallites. The size of the crystallites can be estimated from the information in the diffraction profiles, like peak breadth and peak intensity, by Scherrer equation. XRD can overcome the difficulties and limitations faced when using TEM. Firstly, XRD can be used with large powder, so preparations of very small samples are not necessary. Secondly, the recorded X-ray diffraction patterns come from a larger sample volume and thus XRD gives a volume averaged result. Therefore, XRD is more favorable than TEM in this study. However, it is worth to mention that there are some limitations in the use of Scherrer equation, which would be mentioned in Chapter 4.

1.3 Objectives

There are four main goals in this study:

- To examine the presence of silver in the silver sulphate in different samples.
- To study the growth of metallic silver in silver sulphate during the heating process.
- To compare the size estimations by FWHM and integral breadth method.
- To study the growth kinetics of silver

Chapter 2

Experiment

The experimental data were coming from research project done by Larsen et al. [5]. Below was given, for the sake of completeness, a resume of the experimental work. The majority of experimental data were analyzed by Mathematica, while some were by Excel.

Experimental details

Three samples of silver sulphate were tested in this study. Sample 1 was some silver sulphate powder procured at “Sigma-Aldrich” and sample 3 was the same as sample 1 but having smaller grain sizes. Sample 2 was silver sulphate powder obtained from crushing a large single crystal by pestle and mortar. The single crystal was prepared according to a procedure given in research project done by Larsen et al. [5].

Each sample was filled in thin-walled glass capillaries with an outer diameter of 0.3 mm and mounted on a rotary axis with rotation speed ω at the diffractometer-setup found in the Swiss-Norwegian beamlines (SNBL- BM01A) at the ESRF. After that, the sample was heated up to 540 °C from 380 °C, and then cooled down back to 380 °C at a rate of 2 °C per minute, excepting sample 2 was cooled down to 510 °C only due to some technical errors in software communication setup. The temperature measurements were conducted using an in-house made heat blower with a thermo-couple based temperature controller. This was placed closed to the sample. The error of the thermo-couple was ± 0.5 °C.

During the heating process, collimated synchrotron beams of wavelength 0.6941 Å were produced by Swiss-Norwegian beamline A setup as shown in Figure 2.1 [8] with optics shown in Ta-

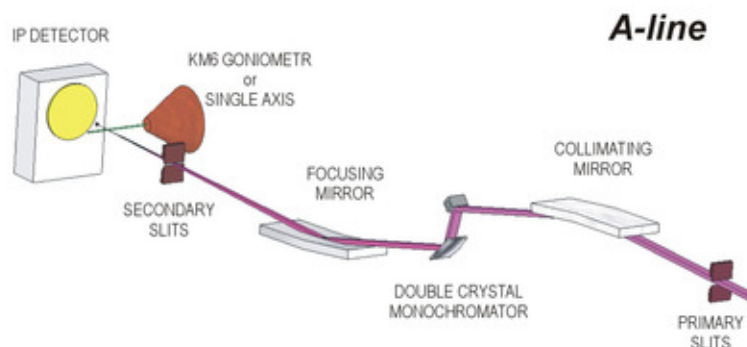


Figure 2.1: Beamline layout at the Swiss-Norwegian beamline A

Table 2.1: Optics for BM01A

Optical elements	Mirror 1	Double-crystal mono.	Mirror 2
Distance from source	25.9 m	28.5 m	30.8 m
Focusing type	Rh coated Vert. collim.	Si (111) Sagittally focusing	Rh coated Vert. focusing
Beam size at sample	Nominally $0.5 \times 0.5 \text{ mm}^2$ FWHM focused		
Spectral range	6 - 22 (30) keV		
Horizontal acceptance	2 mrad		

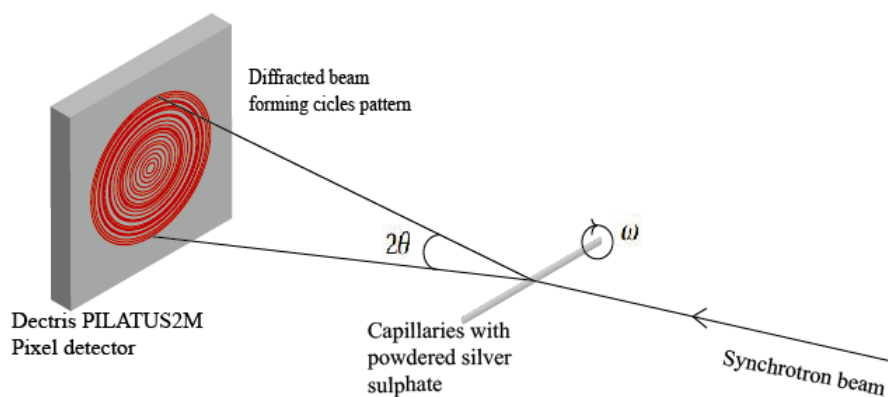


Figure 2.2: Experimental diffraction geometry

ble 2.1 [8]. Diffraction pattern was produced as shown in Figure 2.2. The diffracted angles and diffracted intensities were recorded by the Dectris PILATUS2M Pixel detector with $0.172 \text{ mm} \times 0.172 \text{ mm}$ pixel size. As shown in Figure 2.2, the diffracted angles 2θ were the angles spread by each circle from the reference point of the powdered sample to the detector, while the recorded diffracted intensities were the azimuthal integration using the software package "Fit2D".

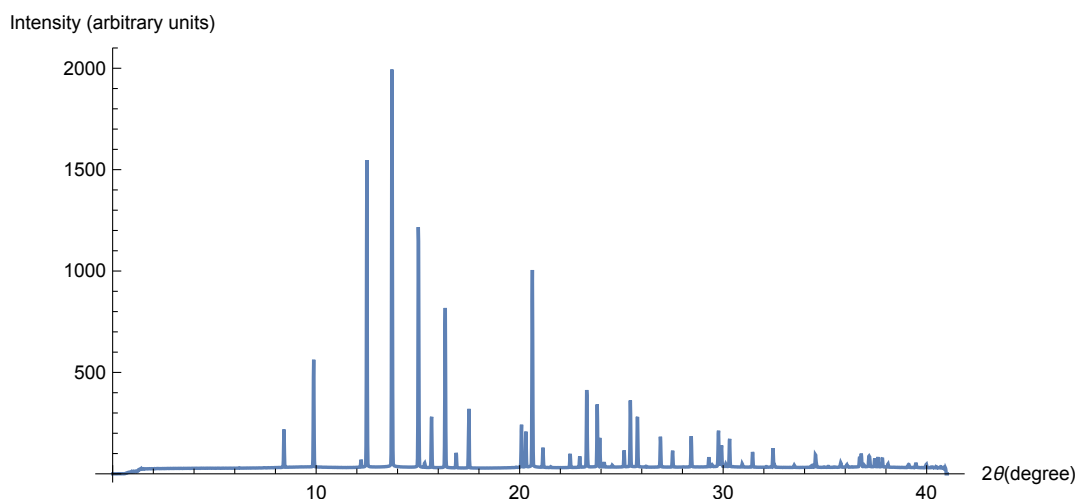


Figure 2.3: Diffractogram of powdered Ag_2SO_4 at $380 \text{ }^\circ\text{C}$

Then, diffractograms were plotted by Mathematica with the recorded diffraction angles and the diffracted intensities at different temperature respectively. Figure 2.3 shows an example of diffractogram of sample 1 at $380 \text{ }^\circ\text{C}$. The diffraction peak profiles for all crystallites contained in the samples and all valid reflections of silver and silver sulphate can be found from the diffractogram.

In this study, the five lowest orders of silver peaks were tried to be found in each sample so as to examine the presence of silver throughout the heating process of silver sulphate. To do so, the diffraction angles were calculated with Bragg's law. Then, the diffractograms of that particular angles range were studied to identify the presence of silver peaks. If the diffractograms show silver peaks at the diffraction angle calculated, the presence of silver in the sample is proved. By studying the silver peak profiles, the size of the silver crystallites can be calculated with Scherrer equation.

Chapter 3

Formation of metallic silver

The work of Masciocchi and Parrish [9] stated that when powder of silver sulphate was heated up to 425 °C, silver sulphate would transit from the low-temperature orthorhombic phase to hexagonal phase and would produce metallic silver. According to the research project done by Masciocchi and Parrish [9], the diffractograms showed that all silver sulphate was transited to hexagonal phase at 425 °C. Meanwhile, by looking at silver 111 reflection peak, it showed that the powder only contained a small volume of silver precipitate at 38.1 °C, and remained small until temperature was increased up to 350 °C. The silver precipitate grew rapidly at higher temperature, but Masciocchi and Parrish [9] did not mention about the change of volume of silver precipitate when temperature was heated up to temperature beyond 430 °C.

In this study, three samples of silver sulphate were tested. In each sample, the silver sulphate was heated up from 380 °C to 540 °C and then cooled down back to 380 °C at a rate of 2 °C per minute, excepting sample 2 which was cooled down to 510 °C only because of the technical error occurred in the experiment. The objectives of this part of the experiment were:

- To test which samples would produce metallic silver when they were heated up.
- To look at the growth of metallic silver when the samples were heated up to temperature over the phase transition temperature of silver sulphate, which was 427 °C in this study.

3.1 Diffraction angle

3.1.1 Bragg's law

The diffraction angle of the silver can be found by Bragg's law [10]:

$$2d_{hkl} \sin \theta = \lambda \quad (3.1)$$

where hkl is the Miller index, d_{hkl} is the inter-planar spacing at hkl reflection, θ is the Bragg angle and λ is the wavelength of X-ray used, which is 0.6941 Å in this study. Since the metallic silver is FCC structure, the inter-planar spacing is [11]:

$$d_{hkl} = \frac{a_{silver}}{\sqrt{h^2 + k^2 + l^2}} \quad (3.2)$$

where a_{silver} is the lattice parameter of silver.

3.1.2 Extinction rule

Some of the reflections of silver can not be observed in diffractograms, due to the extinction rule of FCC structure. The corresponding extinction rule is: [12]:

- FCC structure extinction rule: all h, k, l are mixed odd or even.

Therefore, the five lowest orders of non-extinct reflections are 111, 200, 220, 311 and 222. By putting hkl equal to 111, 200, 220, 311 and 222 in Equation 3.2 respectively, d_{hkl} of the five lowest orders of reflections were found and with these values, the diffraction angles were found by Equation 3.1.¹

3.1.3 Lattice constant of silver

Since lattice constant changes with temperature [13, 14], to find an accurate diffraction angle of the silver, the lattice constants of silver at different temperatures have to be found.

¹See Appendix A for the calculated diffraction angles by linear regression and exponential regression

In this study, data of silver's lattice constants at different temperatures from the [Spreadborough and Christian's](#) experiment [15] were collected. The data were used to interpolate the lattice constants of silver at different temperatures. The result is shown as Table 3.1

Table 3.1: Interpolation of silver lattice constant by linear regression and exponential regression, where a is the lattice constant in Å and T is the temperature in °C

Linear regression	Exponential Regression
$a = 0.00009*T + 4.083$	$a = 4.0831*\exp(0.00002*T)$

The difference between the lattice constants generated by linear regression and exponential regression² [16] were of magnitude smaller than 0.001 (2θ , degree), which would not affect the identification of silver peaks. The silver peaks could be identified by both methods. However, overlapping of Ag_2SO_4 peaks with Ag peaks could occur. The solution to this problem would be discussed in the coming section.

To compare the accuracy of linear and exponential regression, mean absolute error (MAE) [17] was used.

$$MAE = \frac{1}{n} \sum_{i=1}^n |f_i - y_i| \quad (3.3)$$

where n is the number of data, f_i is the predicted value by regression and y_i is the true value. As shown in Table 3.2, exponential regression on average, had a slightly lower mean absolute error than linear regression, so exponential regression is slightly better.

Table 3.2: Mean absolute errors of linear regression linear regression and exponential regression with the experimental diffraction angle

Reflection	MAE of linear regression, 2θ (degree)	MAE of exponential regression, 2θ (degree)
111	0.0102	0.0098
220	0.0113	0.0109
222	0.0163	0.0158
311	0.0140	0.0133
222	0.0209	0.0202
Average	0.0145	0.0140

²See Appendix A for the calculated diffraction angles by linear regression and exponential regression

One thing worth to mention is that for 220 reflection, the silver peaks should be identified with caution, as there was a side peak originating from Ag_2SO_4 next to the silver peak that would affect the identification of silver peak as shown in Figure 3.1. So, addition code in Mathematica had to be added to avoid recording wrong diffraction angle and intensity.³

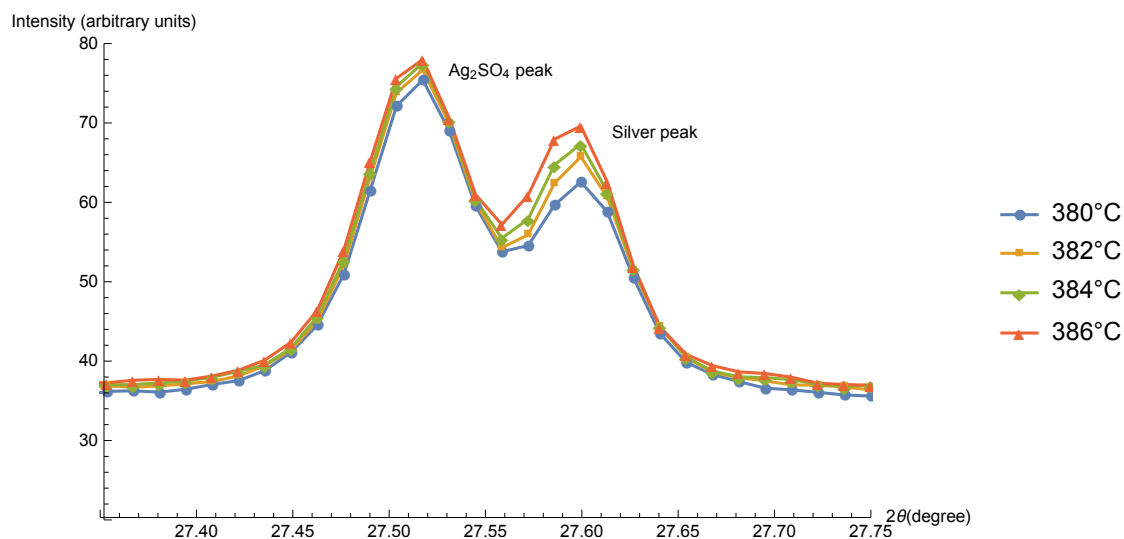


Figure 3.1: Ag_2SO_4 peak nearby silver 220 reflection peak

Interpolation of lattice constants

The data of lattice constants in the experiment were done by Spreadborough and Christian [15]. It contained values that were not within our experimental temperature range. So, the interpolation of lattice constants was performed again, with those values which were close to our experimental temperatures. These values were then compared with lattice constants that were interpolated by entire data set.

Table 3.3 shows that the mean absolute error on average became lower, if we interpolated with only lattice constants that were closed to our experimental temperature range, which was within 300 °C to 600 °C. It implies that if no further experiment data can be provided, and interpolation of lattice constant is needed for future studies, then interpolation with those values, which are close to your experimental temperature range is recommended.

³See Appendix D for the code to avoid recording the side peak.

Table 3.3: Difference on interpolation of diffraction angle with data within 300 °C to 600 °C and interpolation with entire data set by exponential regression

Reflection	MAE of exponential regression with data within 300 °C to 600 °C, 2θ (°)	MAE of exponential regression with entire data set, 2θ (°)
111	0.00548	0.0098
220	0.00579	0.0109
222	0.01103	0.0158
311	0.00664	0.0133
222	0.00996	0.0202
Average	0.00778	0.0140

3.2 Examining the presence of silver in the samples

To test if the samples contained silver, the diffractograms of the three samples were examined by Mathematica.⁴

From the last section, the diffraction angles of silver 111 reflection were calculated. According to Appendix A, diffraction angles of silver 111 reflection were within the range of 16.65 (2θ) to 16.85 (2θ). So, the maximum peak intensities within the range of 16.65 (2θ) to 16.85 (2θ) were recorded to test if 111 reflection silver peaks were there.

3.2.1 Exponential model for decay of synchrotron beams

Since the synchrotron beams will decay exponentially and it implies that the intensity of the diffracted beams will decrease with time. This depends on the mode of operation of the synchrotron, which is the amount of electrons that are injected into the storage ring. The exponential decay equation is [18]:

$$\frac{dN}{dt} = -t_{1/2}N \quad (3.4)$$

where N is the quantity or the intensity in this study, $t_{1/2}$ is the half life which is 10 hours for the synchrotron beams being used and t is the elapsed time. The solution to Equation 3.4 is [18]:

$$N = N_0 e^{-t_{1/2}t} \quad (3.5)$$

⁴See Appendix D for the Mathematica code.

where N_0 is the initial quantity. By simple manipulation of Equation 3.5, the scaling factor K is shown in Equation 3.6.

$$K = \frac{N_0}{N} = \frac{1}{e^{-t/12t}} \quad (3.6)$$

The effect of the exponential decay can then be cancelled by multiply the recorded diffraction intensities by the scaling factor K ⁵.

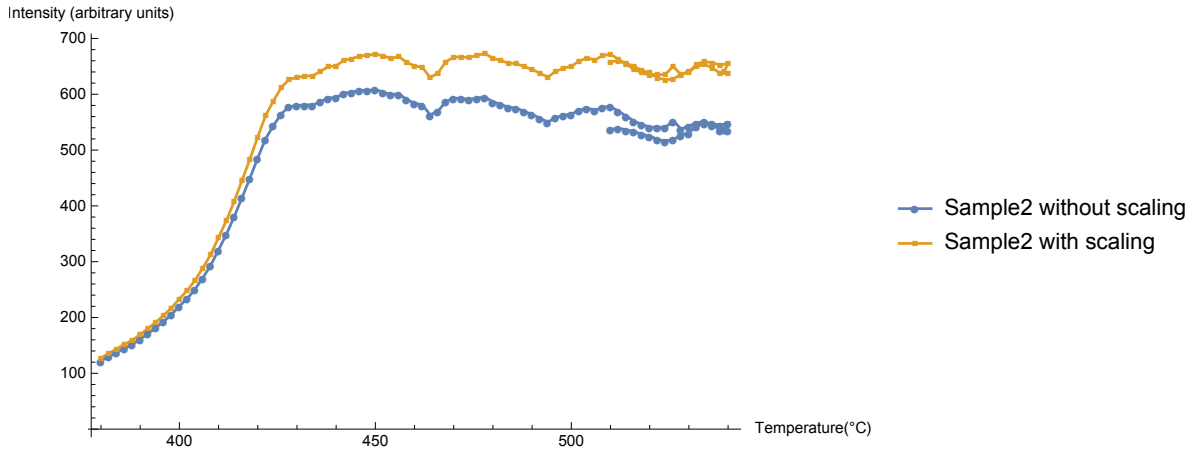


Figure 3.2: Influence on peak intensities for silver 111 reflections without proper scaling

Figure 3.2 shows that the peaks intensities became higher after scaling and that means the actual diffracted intensities should be higher than the recorded intensities. Also, Figure 3.3 illustrates that when sample was heated up to 430 °C, the peak intensities for the scaled data set remained at certain level, while the peak intensities for the non-scaled data set trended to decrease across the temperatures. This implies that the actual silver peak intensity will only increase when the heating process is below 430 °C, and remain more or less the same after 430 °C.

3.2.2 No silver formation in sample 1 and sample 3

With the scaling factor calculated from the previous section, the intensities of silver 111 reflections of the 3 different samples at different temperatures were calculated. Figure 3.4 shows that the maximum peak intensities within the range of 16.65 (2θ) to 16.85 (2θ) for sample 1 and sample 3 remained low across the temperature range of 380 °C to 530 °C. Also, by taking a closer

⁵See Appendix B for the calculated scaling factors

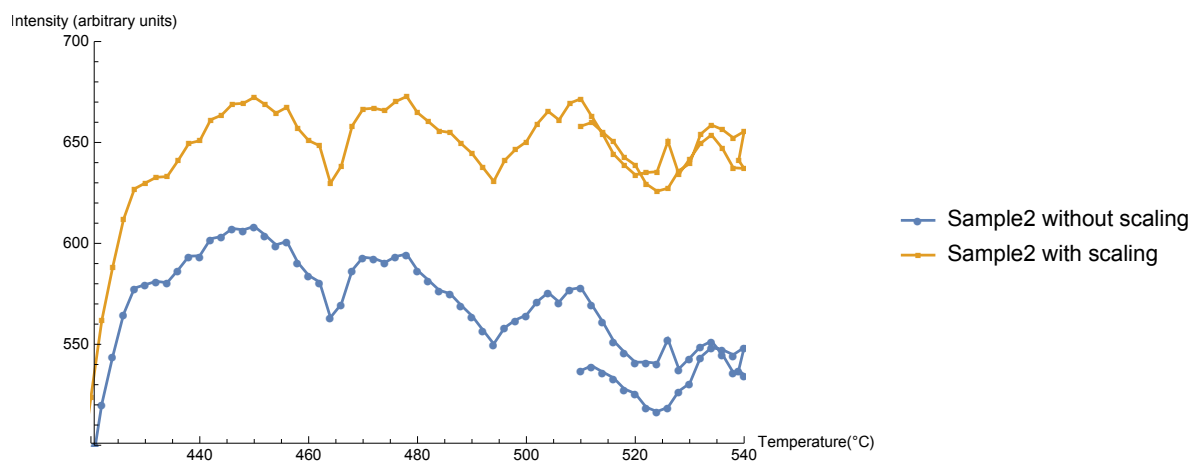


Figure 3.3: Decreasing in peak intensities for silver 111 reflection without proper scaling after reaching the phase transition temperature of silver sulphate

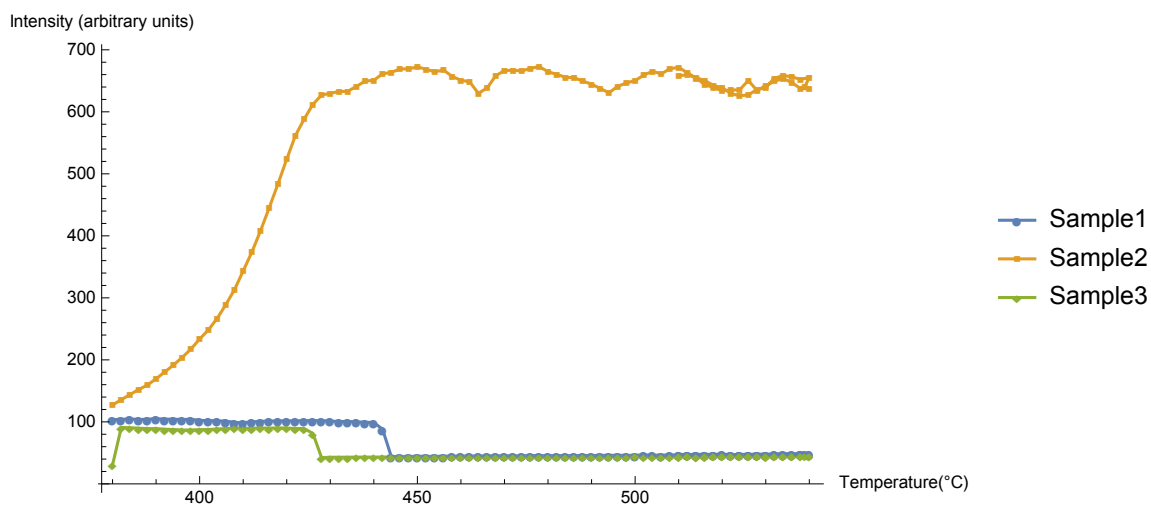


Figure 3.4: Intensities of silver 111 reflection of the 3 different samples along with temperature

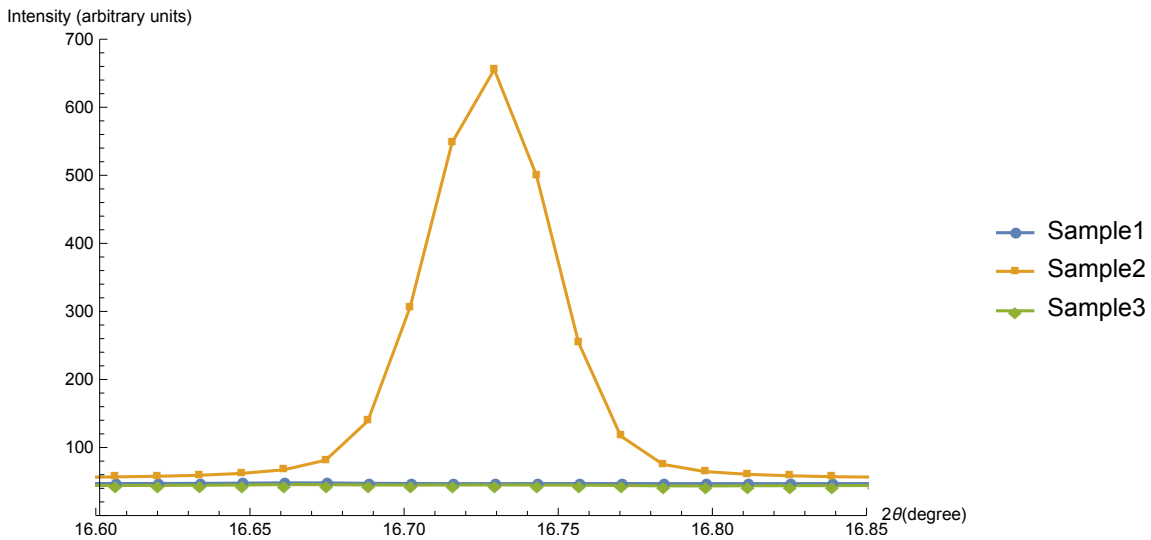


Figure 3.5: Diffractogram to examining the presence of silver in the samples at temperature 530 °C in 111 reflection

look of the diffractogram at 530 °C in Figure 3.5, it is observed there was no silver peak for sample 1 and sample 3. These prove that there is no silver formation for sample 1 and sample 3 throughout the process.

3.2.3 Silver formation in sample 2

Figure 3.4 and Figure 3.5 indicate that silver peaks were found and that means silver was formed in sample 2. Figure 3.6 shows an example of diffractogram of sample 2 at 430 °C that indicating the presence of silver peaks for the five lowest reflections. The reason of why only sample 2 had silver peaks might be explained by the difference in producing the silver sulphate powder. Since, sample 2 was made from one single silver sulphate crystal, metallic silver was precipitated inside the silver sulphate matrix, possibly by disproportionation. Metallic silver crystallites were embedded in sample 2 before the heating process and started to grow in size when they were heated up, while the sample 1 and sample 3 were coming from the commercial powder that did not contain any metallic silver. More details about the origin of the metallic silver would be discussed in Chapter 7.

From Figure 3.4, silver was formed at 380 °C, which was before the heating process was started. That means silver can be formed at temperature lower than the phase transition temperature of silver sulphate. This disagrees with Masciocchi and Parrish [9]'s saying that silver

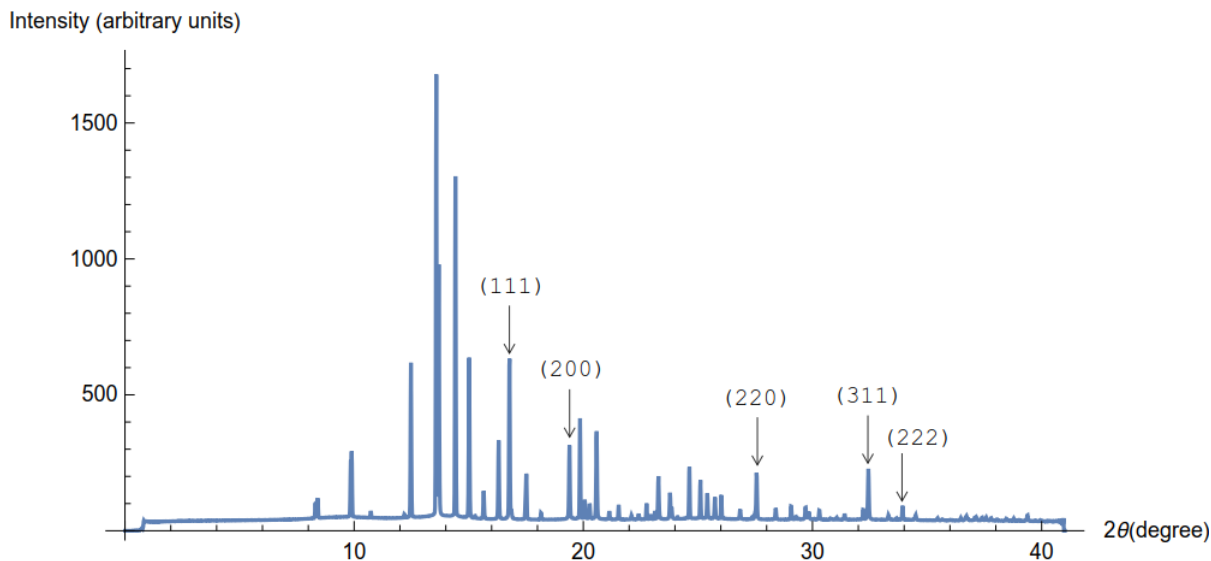


Figure 3.6: Diffractogram of sample 2 at 530 °C that showing the five lowest reflection peaks of silver

sulphate would transit from the low-temperature orthorhombic phase to hexagonal phase and produce metallic silver, because silver can be formed before the phase transition begins. Also, Figure 3.4 reveals that the peak intensity reached plateau after the phase transition. It is very likely that the phase transition of silver sulphate prohibits the growth of metallic silver rather than leads to the growth of silver. Further investigation is needed to understand the mechanism for the growth of metallic silver and some considerations would be given later in the thesis.

From Figure 3.4, it is shown that the peak intensity increased with the temperature and reached a plateau when temperature was increased to 430 °C which was close to the phase transition temperature of the silver sulphate, 427 °C. However, the peak intensity does not represent the size of the silver. To study the growth of the silver size, Scherrer equation is needed and the size growth would be discussed in chapter 4.

Chapter 4

Size estimation of silver in sample 2

The size estimation of small crystallite powder from diffraction pattern is rooted from equation that describes the intensity of a diffracted peak from a small single parallelepipedon crystal [19]:

$$I = I_e F^2 \frac{\sin^2(\pi/\lambda)(\mathbf{s} - \mathbf{s}_0) \cdot N_1 \mathbf{a}_1}{\sin^2(\pi/\lambda)(\mathbf{s} - \mathbf{s}_0) \cdot \mathbf{a}_1} \frac{\sin^2(\pi/\lambda)(\mathbf{s} - \mathbf{s}_0) \cdot N_2 \mathbf{a}_2}{\sin^2(\pi/\lambda)(\mathbf{s} - \mathbf{s}_0) \cdot \mathbf{a}_2} \frac{\sin^2(\pi/\lambda)(\mathbf{s} - \mathbf{s}_0) \cdot N_3 \mathbf{a}_3}{\sin^2(\pi/\lambda)(\mathbf{s} - \mathbf{s}_0) \cdot \mathbf{a}_3} \quad (4.1)$$

and [19],

$$I_e = I_0 \frac{e^4}{m^2 c^4 R^2} p$$

where I indicates the diffracted beam intensity, I_0 is the intensity of the polarized primary beam, p is the polarization factor, for conventional X-ray source, p is equal to $\frac{1+\cos^2 2\theta}{2}$ and for ideal synchrotron X-ray source, p is equal to 1 in the plane [20]. F represents the structure factor, e and m represent the charge and mass of electron, c is the velocity of light, \mathbf{s}_0 and \mathbf{s} are unit vectors that give the direction of the primary beam and the direction to the point of observation, R is the distance from the crystal to the point of observation for the scattered beam and $N_{1,2,3}$, are the numbers of unit cells along the lattice directions $\mathbf{a}_{1,2,3}$.

In general, if the crystallite size is large which is $N_{1,2,3}$ are large numbers, then each of the three quotients are non-zero only if the three Laue equations are closely satisfied and the diffraction peaks are sharp [19]. As shown in Figure 4.1, no size information can be told from the peak profile.

On the other hand, if the crystallite size is small where $N_{1,2,3}$ are small enough, the three

quotients are broadened as shown in Figure 4.2, and the breadth of the diffracted peak is inversely proportional to the size of the crystallite. So, the peak breadth can then be used to find the crystallite size with size range up to about 1000 Å [19].



Figure 4.1: The function $\frac{\sin^2 Nx}{\sin^2 x}$ for $N = 500$

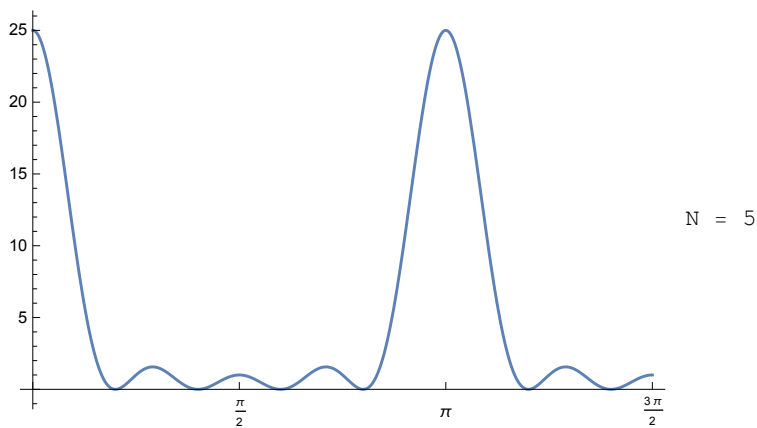


Figure 4.2: The function $\frac{\sin^2 Nx}{\sin^2 x}$ for $N = 5$

The size estimation depends on the definition of the peak breadth and the estimation of the crystallite shape factor[21] or the Scherrer constant. These two factors would be discussed in the following sections.

4.1 Scherrer equation

Scherrer came up with the idea of size estimation of crystallites from the diffraction profile, and the Scherrer equation is [22, 23]:

$$D_{hkl} = \frac{K\lambda}{B_{hkl} \cos\theta} \quad (4.2)$$

where D_{hkl} is the crystallite size in the direction perpendicular to the lattice plane, hkl represents the Miller index, K is the Scherrer constant, λ is the wavelength of the synchrotron radiation, B_{hkl} represents the peak breadth of the diffracted peak and θ is the Bragg angle.

By studying the diffraction profile, the size of crystallite can then be told with known wavelength of radiation, and the corresponding diffraction angle.

4.1.1 Limitation to Scherrer equation

Warren [19] showed the detail derivation of Scherrer equation from Equations 4.1 and there are actually some assumptions during the derivation that limit the use of Scherrer equation. The assumptions include:

1. $N_1 = N_2 = N_3 = N$
2. $\mathbf{a}_1, \mathbf{a}_2, \mathbf{a}_3$ are equal and orthogonal
3. Peak broadening is due to the small crystallite size only
4. Crystals are free from stains and faulting
5. $\frac{\sin^2 Nx}{\sin^2 x}$ is approximated by Gaussian function $N^2 e^{-(Nx)^2/\pi}$

Crystallites shape and size distribution

Assumption 1 implies that the powder crystallites are assumed to be cubic and all of the same size. Therefore, if the powder crystallites are not cubic in shape or have a size distribution, then Scherrer equation cannot be applied directly. Langford and Wilson [22] have summarized the modification needed for the choice of Scherrer constant if the crystallites were of other shape. The important of the choice of Scherrer constant would be discussed later in this Chapter. Wilson [24, 25] have considered the effect to the use of Scherrer equation when there was a size distribution and Langford and Wilson [22] have summarized the modification needed for the choice of Scherrer constant.

Cubic symmetry

Assumption 2 means that the crystallites are assumed to be cubic symmetry. So, strictly speaking, Scherrer equation is only valid in cubic symmetry structure crystallites. The Scherrer equation holds for Ag, since its structure is indeed cubic (FCC). Warren [19] stated that for other structure, it is not a bad approximation if for each hkl -reflection, the value of D_{hkl} is assumed to be an average crystal dimension perpendicular to the reflecting planes.

Broadening due to other factors

Assumptions 3 and 4 implies that diffraction peak profiles are only due to the small crystallite size. In reality, there are always others factors that will also contribute to the broadening, for instance, instrumental broadening, stains and faulting. These broadenings effect have to be eliminated before applying the Scherrer equation. Many researches [19, 26–29] have made effort on studying broadening due to other factors. These factors would be discussed in Chapter 5.

Gaussian approximation

Assumption 5 implies that the diffraction peak profile is assumed to be a Gaussian function. The Gaussian fitting would be discussed in detail later in this Chapter. Langford and Wilson [22] have summarized the modification needed for diffraction peak profile having other functional form.

4.1.2 Scherrer constant

Before starting with the size estimation, the Scherrer constant and the peak breadth have to be defined. According to Langford and Wilson [22] Scherrer constant depends on three things:

- Definition of the breadth
- Crystallite shape
- Crystallite-size distribution

Different definitions of the breadth will give different values of Scherrer constant, the corresponding Scherrer constant value can be found from researches done by Langford and Wilson

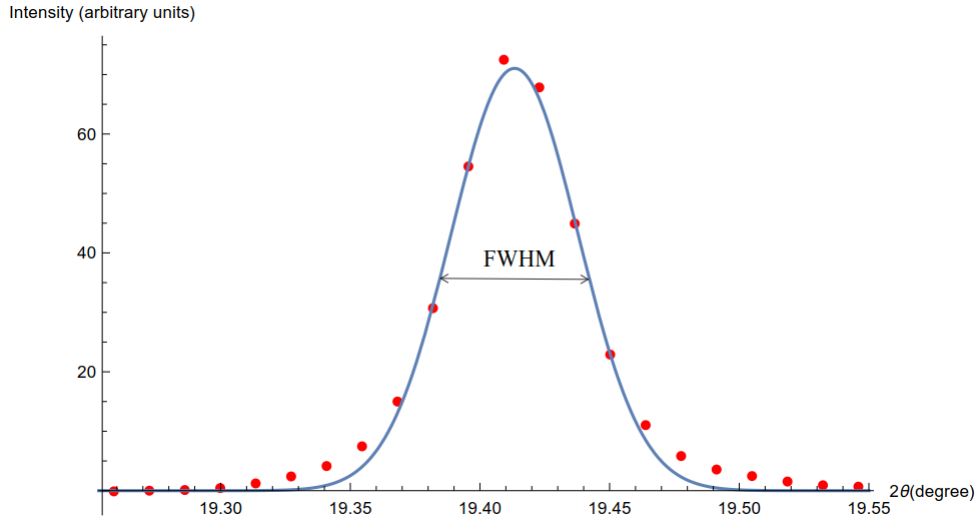


Figure 4.3: Diffractogram showing FWHM of 200 reflection of silver peak at 398 °C

[22], Patterson [30, 31]. TEM can be used to find shape of crystallite and the corresponding Scherrer constant can be found from research done by Langford and Wilson [22].

In this study, there was no TEM indication on the crystallite shape and crystallite size distribution. So, crystallites were assumed to be cubic and the Scherrer constants for the 5 lowest reflections were found by Langford and Wilson's research [22]. Also, the effect of the crystallite-size distribution was omitted.

4.1.3 Define peak breadth by FWHM

The first way of defining the peak breadth was stated by Scherrer [23], that is the full width of the diffracted maximum at the height, which is half of the background and the maximum peak intensity (FWHM). Figure 4.3 shows an example of FWHM of 200 reflection of silver peak at 398 °C.

Background intensity

There was some background intensities, for example TDS, that would contribute to the silver peak intensity. So, as a first step to find the FWHM, the background intensities were cancelled by calculating the average value of recorded background intensities as shown in Figure 4.4.

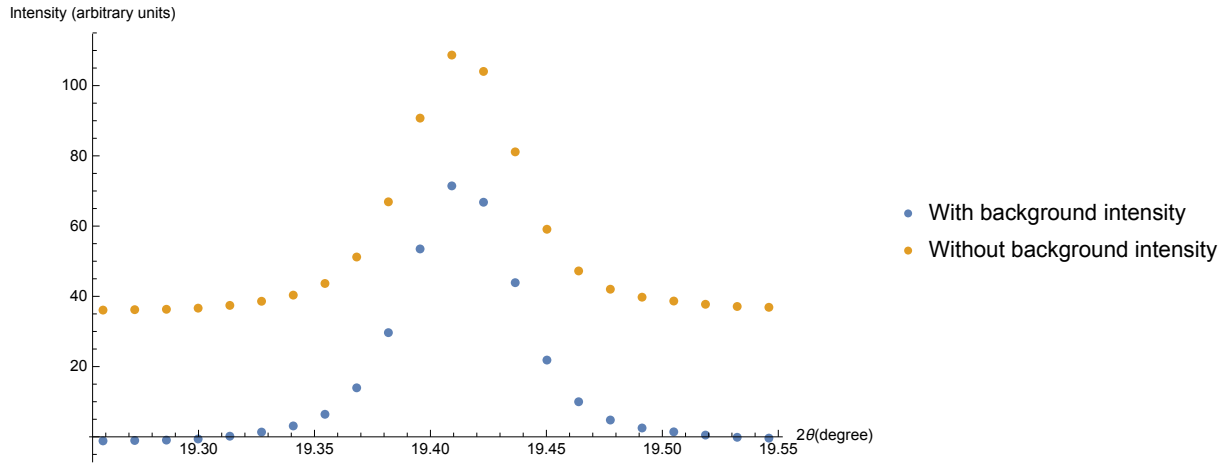


Figure 4.4: Diffractograms showing the silver 200 reflection peak at 398 °C with and without background intensities

Gaussian fitting

Due to the finite pixel size of the detector, the FWHM could not be found from the diffractogram directly. As an example, the 200 reflection peak at 398 °C is shown in Figure 4.5. The peak profile was composed of only few data points, and the FWHM could not be recorded directly.

The Gaussian fitting based on the data points that were recorded, and the Gaussian Equation is [32]:

$$f(x) = Ae^{-\frac{(x-\mu)^2}{\sigma^2}} \quad (4.3)$$

where A is the height of the peak, μ is the position of the center of the peak and σ is the standard derivation.

It is worthwhile to mention that in Mathematica, the parameters A , μ , σ have to be set as some reasonable pre-set values so that the Gaussian fitting can function properly¹. The guesses can be made by observing the range of the diffraction angle and diffraction intensities for that particular reflection.

Another thing that is needed to pay attention to is the Gaussian fittings for 111 reflection and 220 reflections because there were side peaks nearby the silver peaks. So, those values have to be excluded from the fitting by choosing fitting range carefully¹.

¹See Appendix D for the Mathematica code.

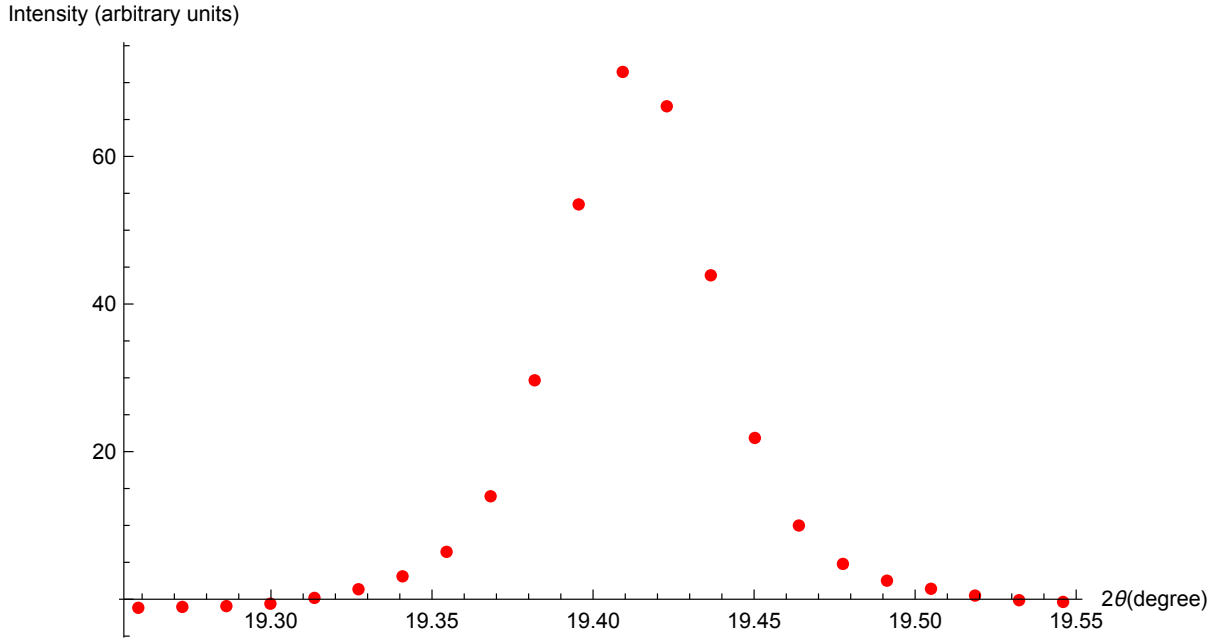


Figure 4.5: Recorded diffraction angles and intensities within the range of 200 reflection at 398 °C

One of the examples of Gaussian fitting is shown in Figure 4.6. The peak profile is now completed and the FWHM can then be recorded from the Gaussian fitting curve by the following equation [33]:

$$\text{FWHM} = 2\sqrt{2\ln 2}\sigma \quad (4.4)$$

Figure 4.7 shows the calculated FWHM for all five lowest reflections of silver.

Size estimation

With the calculated FWHM and the corresponding Scherrer constants from Langford and Wilson's research [22], the sizes of silver were estimated by Scherrer Equation 4.2. The results of the size estimations of silver for the 111, 200, 220, 311 and 222 reflections are shown in Figure 4.8.

Since the sample was heated up to 540 °C and then cooled back to 510 °C, the plots were somehow overlapping in the tail. To make the plots clearer, the x-axis was changed to elapsed time in minutes and y-axis to nano-meter, as shown in Figure 4.9.

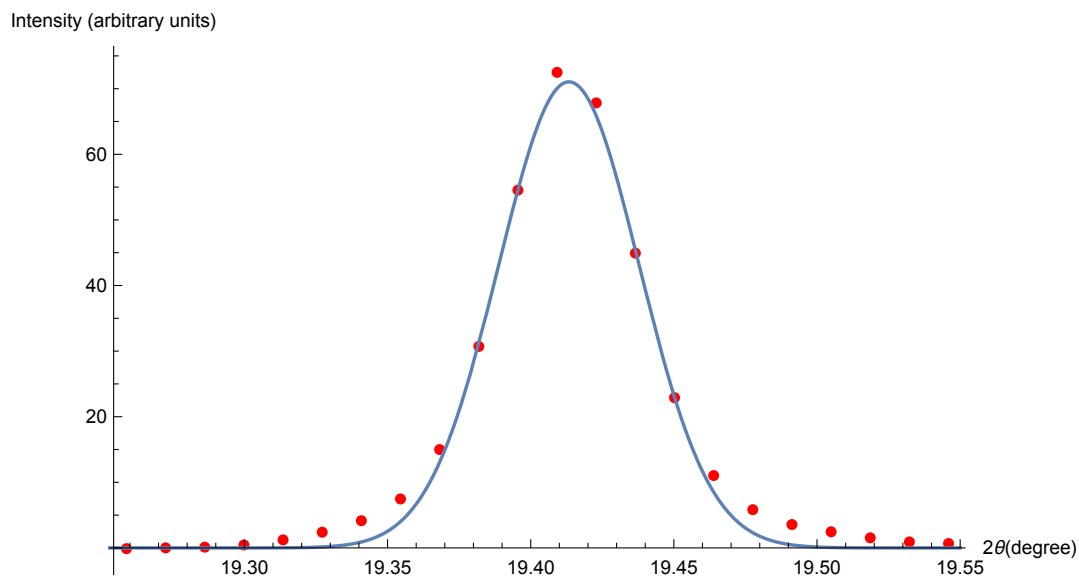


Figure 4.6: Gaussian fitting of silver 200 reflection at 398 °C

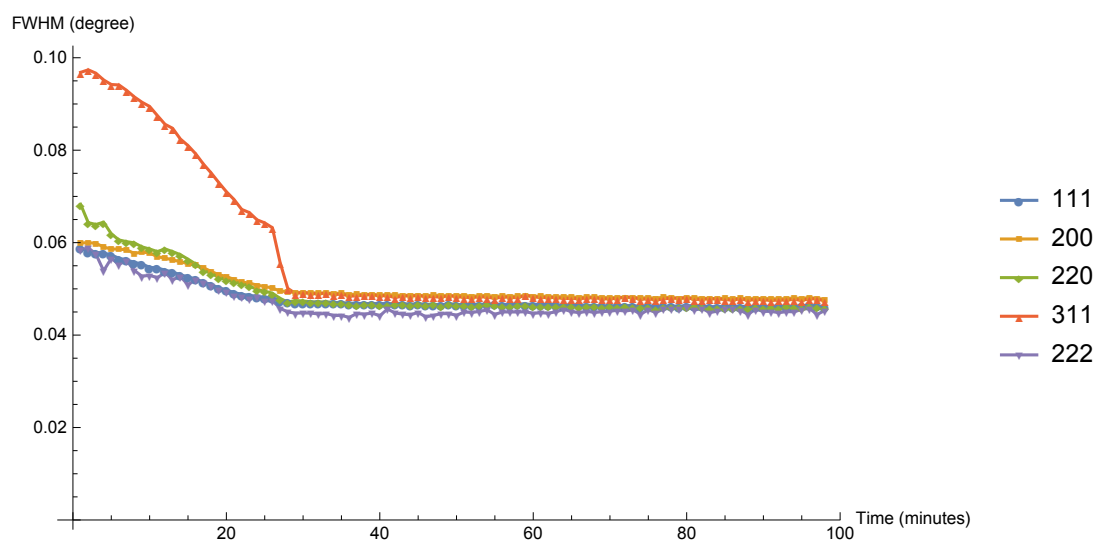


Figure 4.7: Calculated FWHM for all five reflections

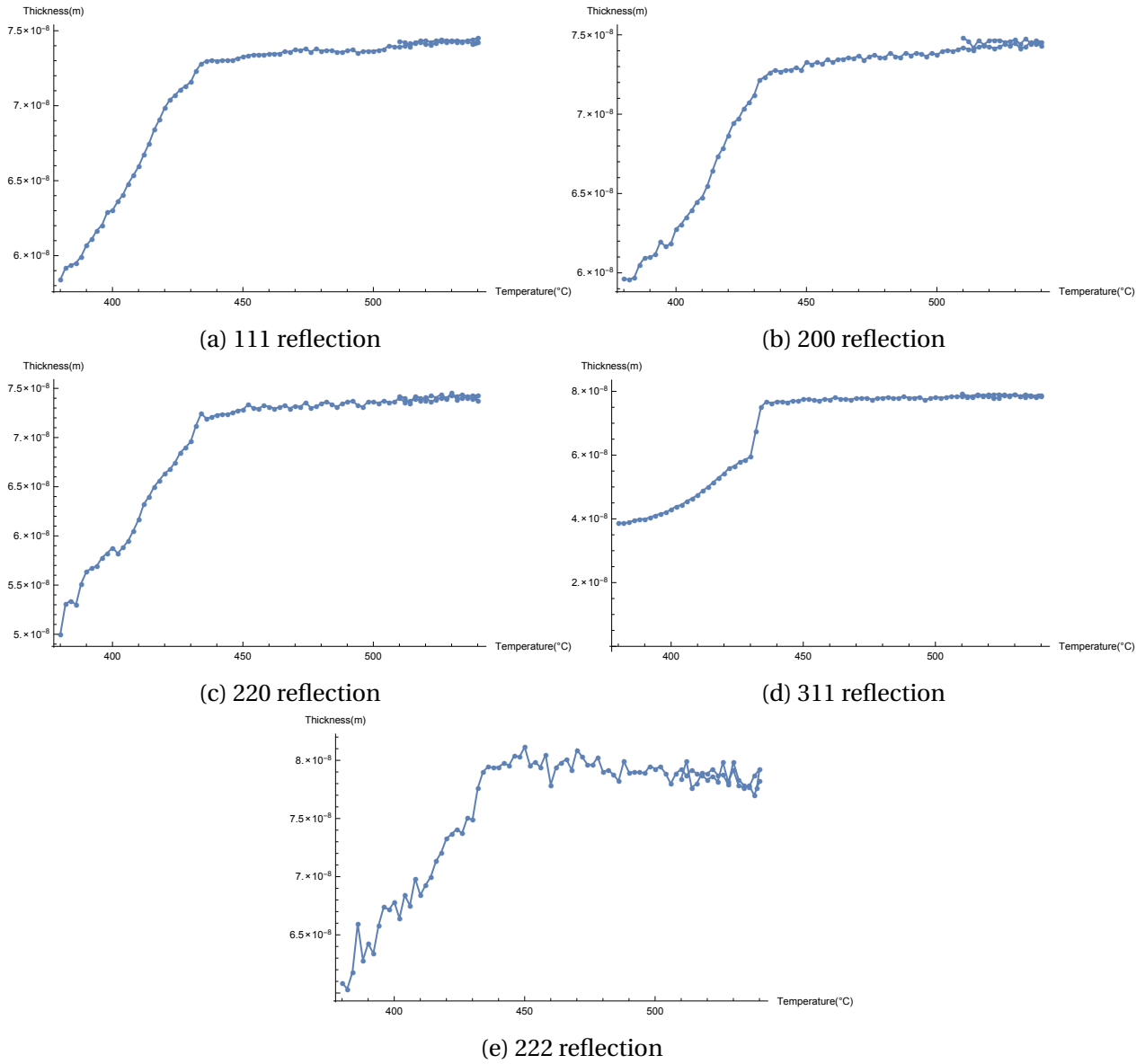


Figure 4.8: The size estimations of silver for the five lowest reflections by defining peak breadth by FWHM

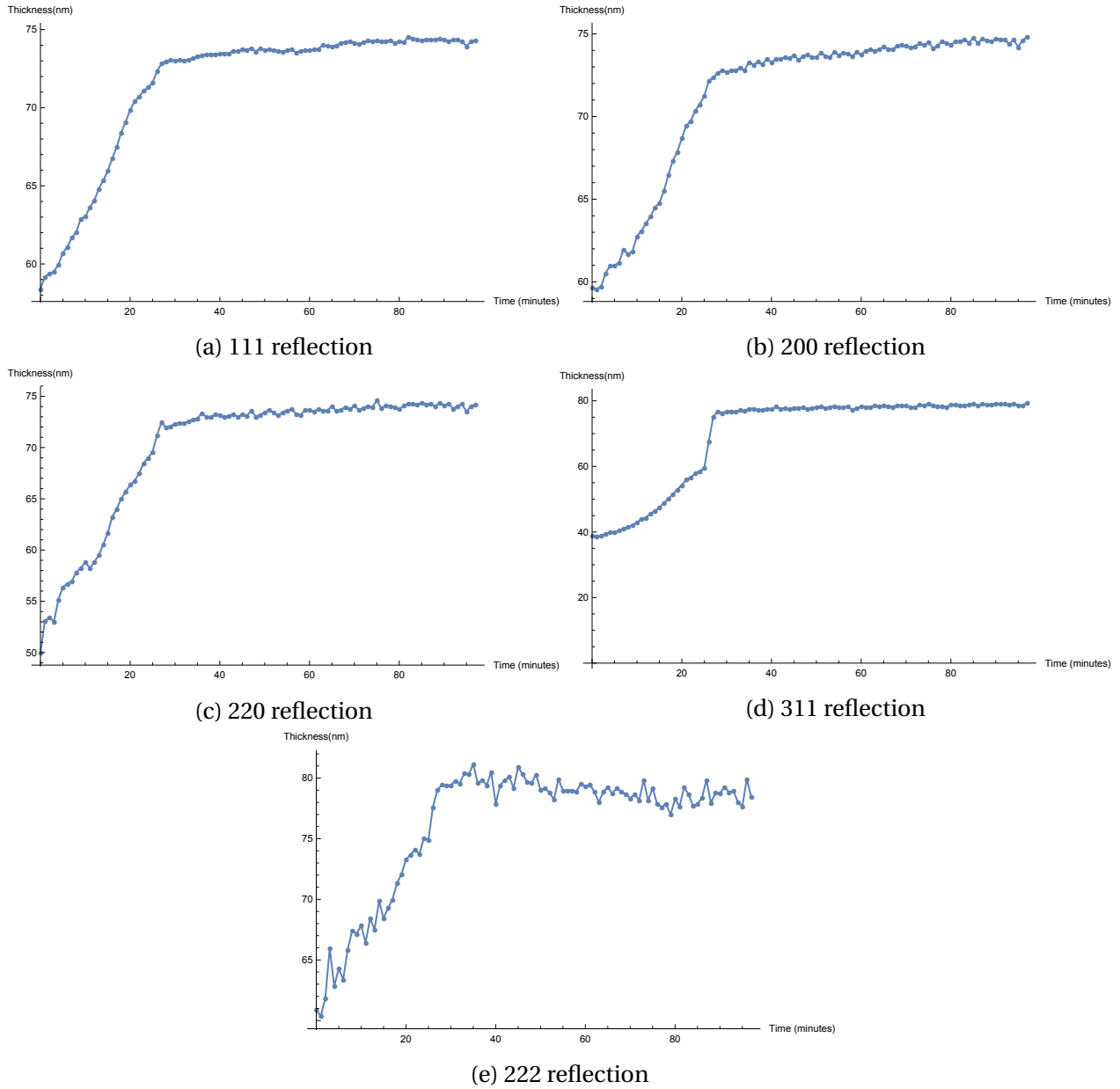


Figure 4.9: The size estimations of silver for the five lowest reflections by defining peak breadth by FWHM with x-axis as elapsed time in minutes and y-axis in nano-meter

4.1.4 Define peak breadth by integral breadth

The second way of defining the peak breadth was first introduced by Laue [34] (see also Stokes and Wilson [35] and Jones [36]), the peak breadth or the integral breadth is defined as the total area under the diffraction peak profile and divided by the peak intensity.

Background and Gaussian fitting

The background intensity was cancelled with the same method as previous section shown in Figure 4.4. Also, the same Gaussian fitting was performed as the previous section shown in Figure 4.6.

Size estimation

The total area under the silver peak profile generated by Gaussian fitting, as shown in Figure 4.10, was calculated by Mathematica. Then, the areas were divided by the peak intensity so as to find the integral breadth. Figure 4.11 shows the calculated integral breadth for all five reflections. Together with the corresponding Scherrer constants from Langford and Wilson's research [22], the result of size estimations was shown in Figure 4.12.

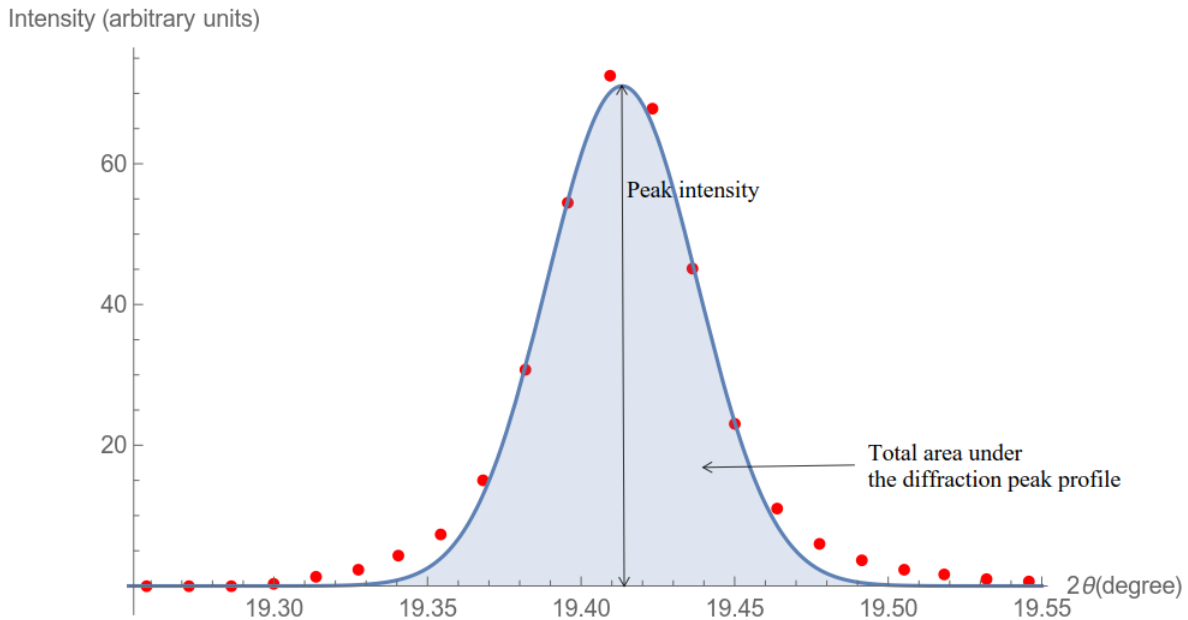


Figure 4.10: Diffractogram showing peak intensity and the total area under diffraction peak profile of 200 reflection of silver peak at 398 °C

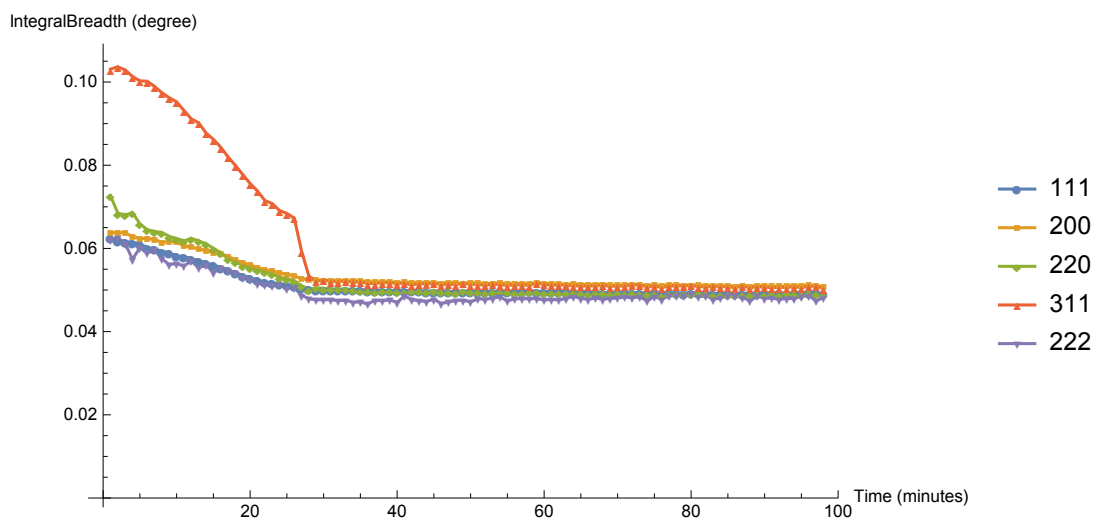


Figure 4.11: Calculated integral breadth for all five lowest reflections of silver

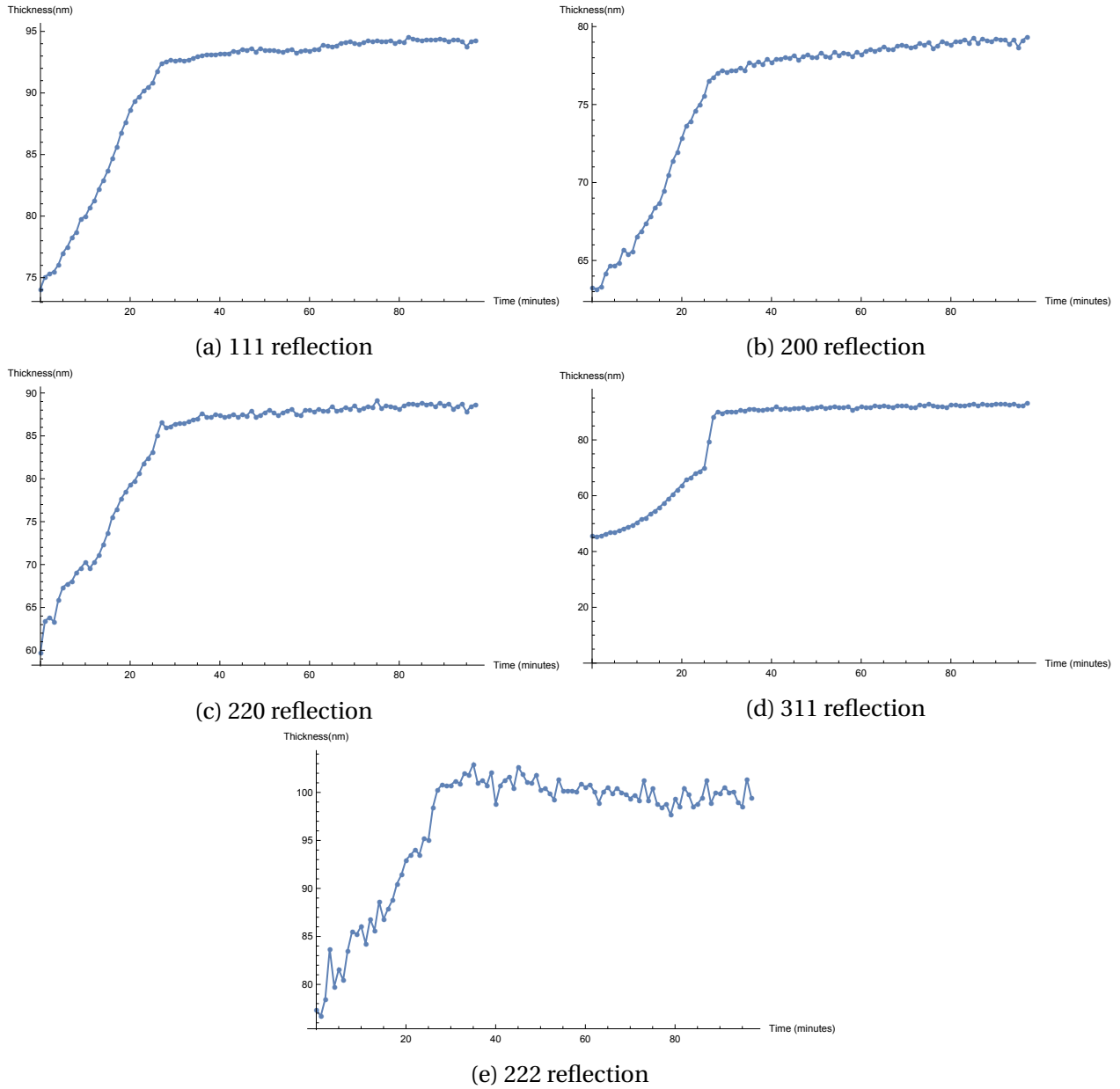


Figure 4.12: The size estimations of silver for the five lowest reflections by defining peak breadth by integral breadth and x-axis as elapsed time in minutes

4.2 Silver growth

From Figure 4.9 and 4.12 in the last section, the silver growth shows three features:

- Silver crystallites were growing almost linearly with temperature in all reflections.
- The size of silver crystallites was smallest in the beginning at 380 °C and became the largest at around 432 °C in all reflections.
- The silver crystallites stopped growing after reaching 432 °C in all reflections

and Table 4.1 summarizes the size estimations of silver by FWHM method and integral breadth method.

Table 4.1: Summary on silver growth estimated by FWHM and integral breadth method

	Temperature	Reflections				
		111	200	220	311	222
Size estimated by FWHM (nm)	380 °C	58.40	59.64	50.00	38.84	60.87
	432 °C	72.82	72.34	72.45	75.06	79.00
Size estimated by Integral Breadth (nm)	380 °C	74.08	63.25	59.74	45.64	77.36
	432 °C	92.37	76.71	86.57	88.19	100.22

Validity of Scherrer equation

According to Holzwarth and Gibson [37], the Scherrer equation can only be applied for size estimation up to about 100 nm to 200 nm, while the sizes of silver estimated by both methods were within the range of 50 nm to 100 nm. This implies that the size estimations with Scherrer equation are valid.

Growth of metallic silver

Figures 4.9 and 4.12 show that silver sizes were growing during the heating process of silver sulphate. One of the suggestions to the growth of silver is the disproportionation theorem and more details would be discussed in Chapter 7.

Stopping of metallic silver growth

With reference to Figures 4.9 and 4.12, the silver stopped growing at 432 °C which was close to the phase transition temperature which is 427 °C. This supports the observation from Chapter 3, which is the phase transition of silver sulphate prohibits the growth of metallic silver rather than leads to the growth of silver, because the silver crystallites grew before the phase transition and stopped at temperature near to the phase transition. To test the hypothesis, see Chapter 7 for further investigation suggested.

Another suggestion to the growth stop is coming from the saturation of metallic silver. According to Klimovich et al. [38], when the standard free energy change of the chemical reaction is non-negative, the reaction will stop. The metallic silver grow because it can reduce the standard free energy of the silver sulphate matrix. However, upon some levels, further growing of metallic silver can no longer reduce the free energy of the system. Therefore, the growth stops. Another effect could be due to some sort of site saturation. Further investigation is needed to test this hypothesis.

4.3 Uncertainty in size estimation

The uncertainty in size estimation can be expressed by Equation 4.5 [39].

$$\delta D_{hkl} = \sqrt{\left(\frac{\partial D}{\partial K} \delta K\right)^2 + \left(\frac{\partial D}{\partial \lambda} \delta \lambda\right)^2 + \left(\frac{\partial D}{\partial B_{hkl}} \delta B_{hkl}\right)^2 + \left(\frac{\partial D}{\partial \theta} \delta \theta\right)^2} \quad (4.5)$$

By performing the partial derivatives, Equation 4.5 becomes:

$$\delta D_{hkl} = \sqrt{\left(\frac{\lambda}{B_{hkl} \cos \theta} \delta K\right)^2 + \left(\frac{K}{B_{hkl} \cos \theta} \delta \lambda\right)^2 + \left(-\frac{K \lambda}{B_{hkl}^2 \cos \theta} \delta B_{hkl}\right)^2 + \left(\frac{K \lambda \sin \theta}{B_{hkl} \cos^2 \theta} \delta \theta\right)^2} \quad (4.6)$$

Uncertainty in Scherrer constant δK

The shapes of the silver crystallites were unknown, and the size estimations of silver crystallites were based on the Scherrer constant values for cubic shape crystallites. So, the uncertainty would be the maximum difference between the Scherrer constant of cubic shape with all other shapes listed in Table 4.2 and Table 4.3 [22]. δK_w represents the uncertainty in Scherrer constant

for FWHM method and δK_β represents the uncertainty in Scherrer constant for integral breadth method.

Table 4.2: Scherrer constants used in FWHM method for different shapes of silver crystallites and uncertainty of Scherrer constants, δK_w that is the maximum difference between the Scherrer constant of cubic shape with all other shapes

Reflection	Scherrer constants for different shape of crystallites, K_w				δK_w
	Cubic	Spherical	Tetrahedral	Octahedral	
111	0.8551	0.9400	0.8894	0.9354	0.0849
200	0.8859	0.9400	1.0220	0.8151	0.2069
220	0.8340	0.9400	0.7262	0.8613	0.2138
311	0.9082	0.9400	0.9289	0.8863	0.0426
222	0.8551	0.9400	0.8894	0.9354	0.0849

Table 4.3: Scherrer constants used in integral breadth method for different shapes of silver crystallites and uncertainty of Scherrer constants, δK_β that is the maximum difference between the Scherrer constant of cubic shape with all other shapes

Reflection	Scherrer constants for different shape of crystallites, K_β				δK_β
	Cubic	Spherical	Tetrahedral	Octahedral	
111	1.1547	1.0747	0.8894	1.1438	0.2544
200	1.0000	1.0747	1.3867	1.1006	0.3120
220	1.0607	1.0747	0.9806	1.0377	0.0941
311	1.1359	1.0747	1.3156	1.1211	0.2409
222	1.1547	1.0747	1.2009	1.1438	0.1262

Uncertainty in wavelength $\delta\lambda$

The uncertainty in wavelength was mainly coming from energy dispersion of the incoming synchrotron radiation. $\delta\lambda$ is 0.694×10^{-15} and detail calculation is shown in Chapter 5.

Uncertainty in peak breadth δB_{hkl}

The uncertainty in peak breadth was coming from the Gaussian fitting. The 95% confidence interval of Gaussian fitting was found by Mathematica function and was used to find the uncertainty in peak breadth. Figure 4.13 shows an example of 95% confidence interval of Gaussian fitting of 200 reflection at 398 °C. The uncertainty in peak breadth was calculated by the

difference between the peak breadth of Gaussian fitting model and the peak breadth of 95% confidence interval. The value of δB_{hkl} is taken as:

$$\delta B_{hkl} = \frac{|B_G - B_u| + |B_G - B_l|}{2}$$

where B_G is the peak breadth of Gaussian fitting model, B_u is peak breadth of the upper limit of 95% confidence interval and B_l is peak breadth of the lower limit of 95% confidence interval.

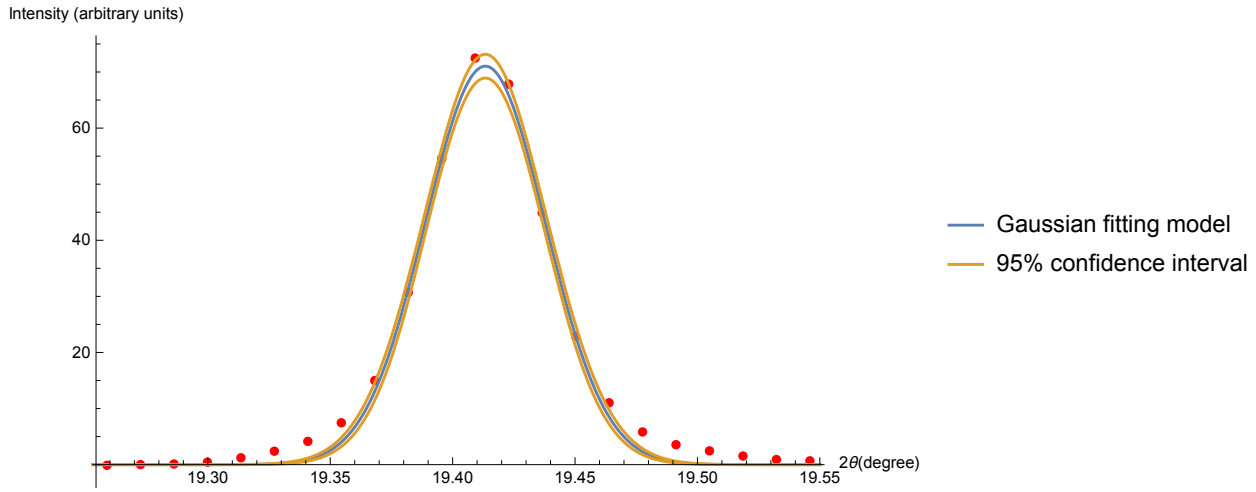


Figure 4.13: 95% confidence interval of Gaussian fitting of silver 200 reflection at 398 °C

Table 4.4 and 4.5 show an example of δB_{hkl} of FWHM method and integral breadth method at 380 °C and 432 °C respectively.

Table 4.4: δB_{hkl} of FWHM method and integral breadth method at 380 °C

Reflection	B_{FWHM}	δB_{FWHM}	$B_{Integralbreadth}$	$\delta B_{Integralbreadth}$
111	0.0589	0.0022	0.0627	0.0018
200	0.0599	0.0023	0.0638	0.0021
220	0.0683	0.0047	0.0727	0.0031
311	0.0968	0.0022	0.1031	0.0020
222	0.0584	0.0035	0.0621	0.0033

Uncertainty in diffraction angle $\delta\theta$

The dominating part of uncertainty in diffraction angle was coming from finite pixel size of the detector and $\delta\theta$ is 0.35. The detail calculated can be found in Chapter 5.

Table 4.5: δB_{hkl} of FWHM method and integral breadth method at 432 °C

Reflection	B_{FWHM}	δB_{FWHM}	$B_{Integralbreadth}$	$\delta B_{Integralbreadth}$
111	0.0475	0.0012	0.0506	0.0011
200	0.0495	0.0012	0.0527	0.0011
220	0.0480	0.0018	0.0510	0.0013
311	0.0557	0.0022	0.0593	0.0020
222	0.0458	0.0009	0.0488	0.0009

The uncertainty of size estimation

The uncertainties of size estimations δD_{hkl} were calculated by putting all the calculated values above into Equation 4.6. Table 4.6 summarizes the results at 380 °C and 432 °C. Figure 4.14 and 4.15 show the uncertainties in size estimations for the five lowest reflections of silver throughout the entire experimental range.

Table 4.6: Summary on uncertainties in estimated silver sizes by FWHM and integral breadth method

	Temperature	Reflections				
		111	200	220	311	222
Size estimated by FWHM (nm)	380 °C	58±6	60±14	50±13	39±2	61±7
	432 °C	73±7	72±17	72±18	75±4	79±8
Size estimated by Integral Breadth (nm)	380 °C	74±16	63±20	60±6	46±10	77±9
	432 °C	92±20	77±24	87±8	88±17	100±10

4.4 Comparison on FWHM and integral breadth

Silver growth pattern

According to Figure 4.16, the growth patterns of silver crystallites were the same in all reflections. For each reflection, the estimated sizes of silver by both methods grew linearly in between temperature range of 380 °C to 432 °C and stopped at temperature around 432 °C. This implies that both methods are for sure studying the same crystallites as their estimated sizes have the same pattern.

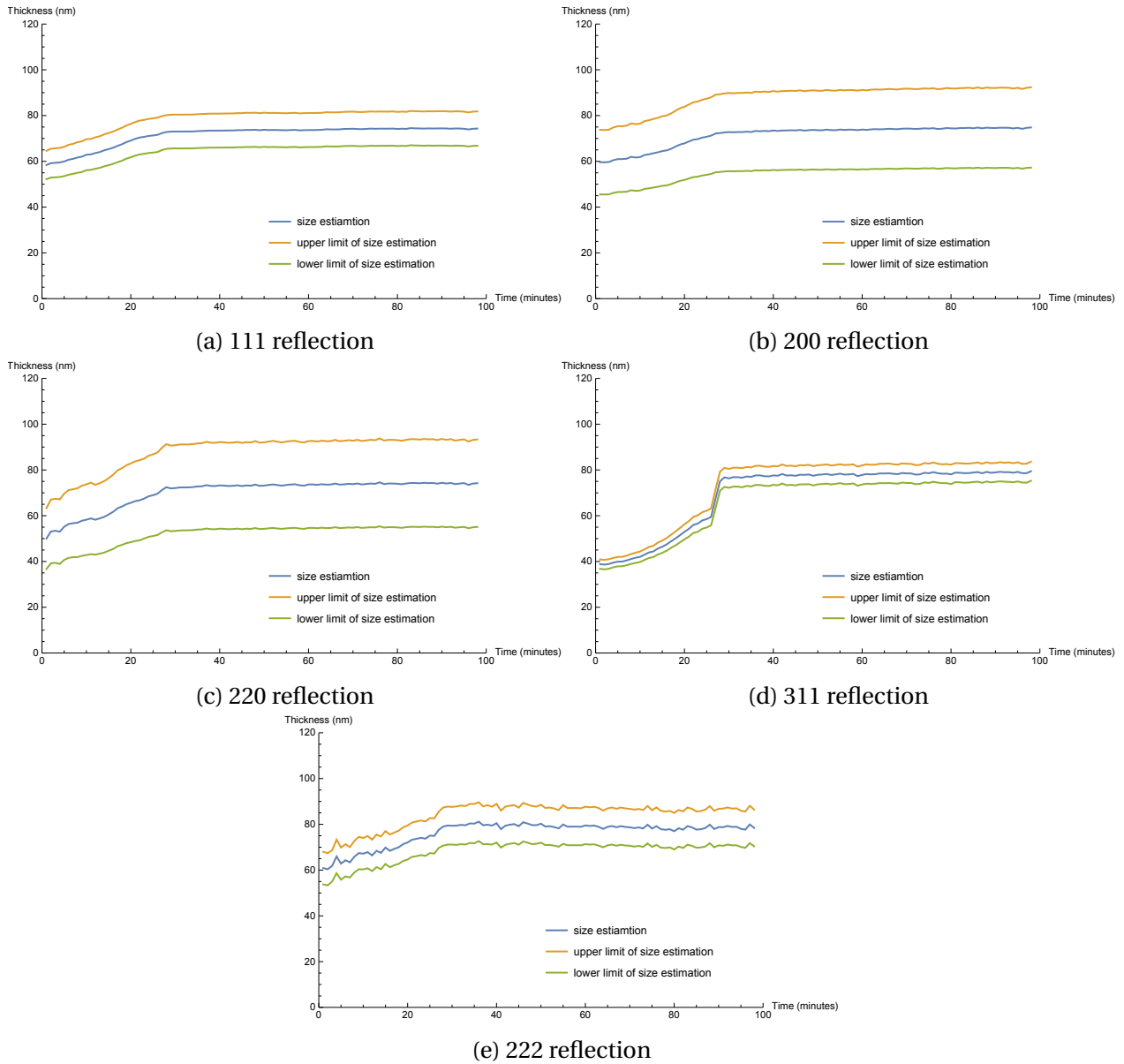


Figure 4.14: The uncertainties in size estimations of silver for the five lowest reflections by defining peak breadth by FWHM

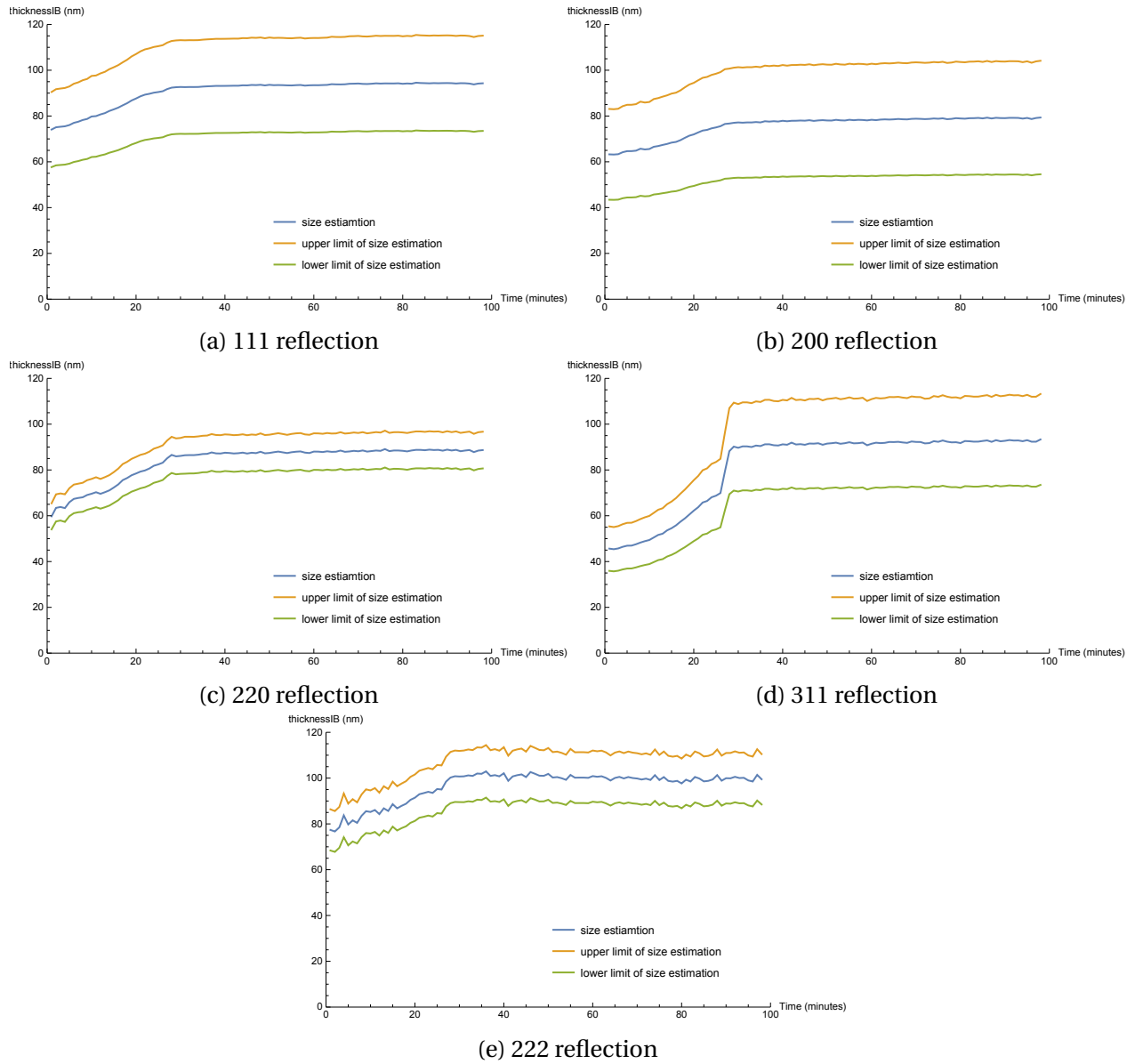


Figure 4.15: The uncertainties in size estimations of silver for the five lowest reflections by defining peak breadth by integral breadth

Estimated size difference

Figure 4.16 shows that the estimated sizes between FWHM method and integral breadth method have some difference throughout the temperature range of the experiment in all five reflections. This is possibly because of the difference in defining peak breadth and the values of Scherrer constant that were used. However, this does not mean that one of the methods is more accurate than the other. To compare the accuracy of size estimations from these two methods in this study, further investigation is needed to examine the true size of silver.

Silver growth rate

The average difference between size estimations by FWHM and integral breadth were calculated. This average value was added to the sizes estimated by FWHM, so that the two plots reached almost the same level, for better comparison between the estimated growth rates.

As shown in Figure 4.17, the integral breadth method showed a faster growth rate in between temperature range of 380 °C to 432 °C for all five reflections. This is possibly due to the difference in defining the integral breadth. While, the growth rate reach almost zero for temperature higher than 432 °C for all five reflections.

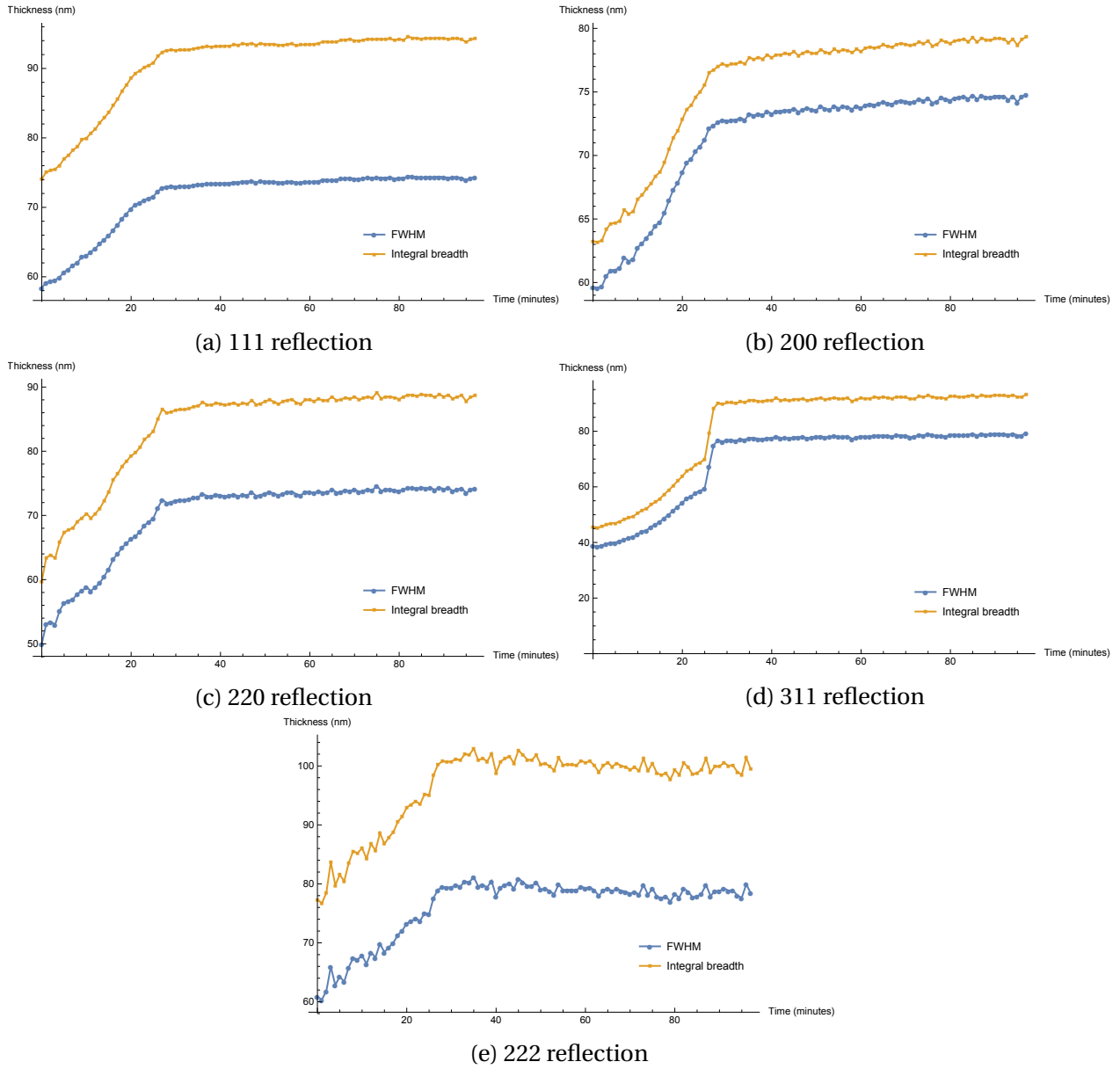


Figure 4.16: Difference on size estimations of silver by defining peak breadth by FWHM and integral breadth

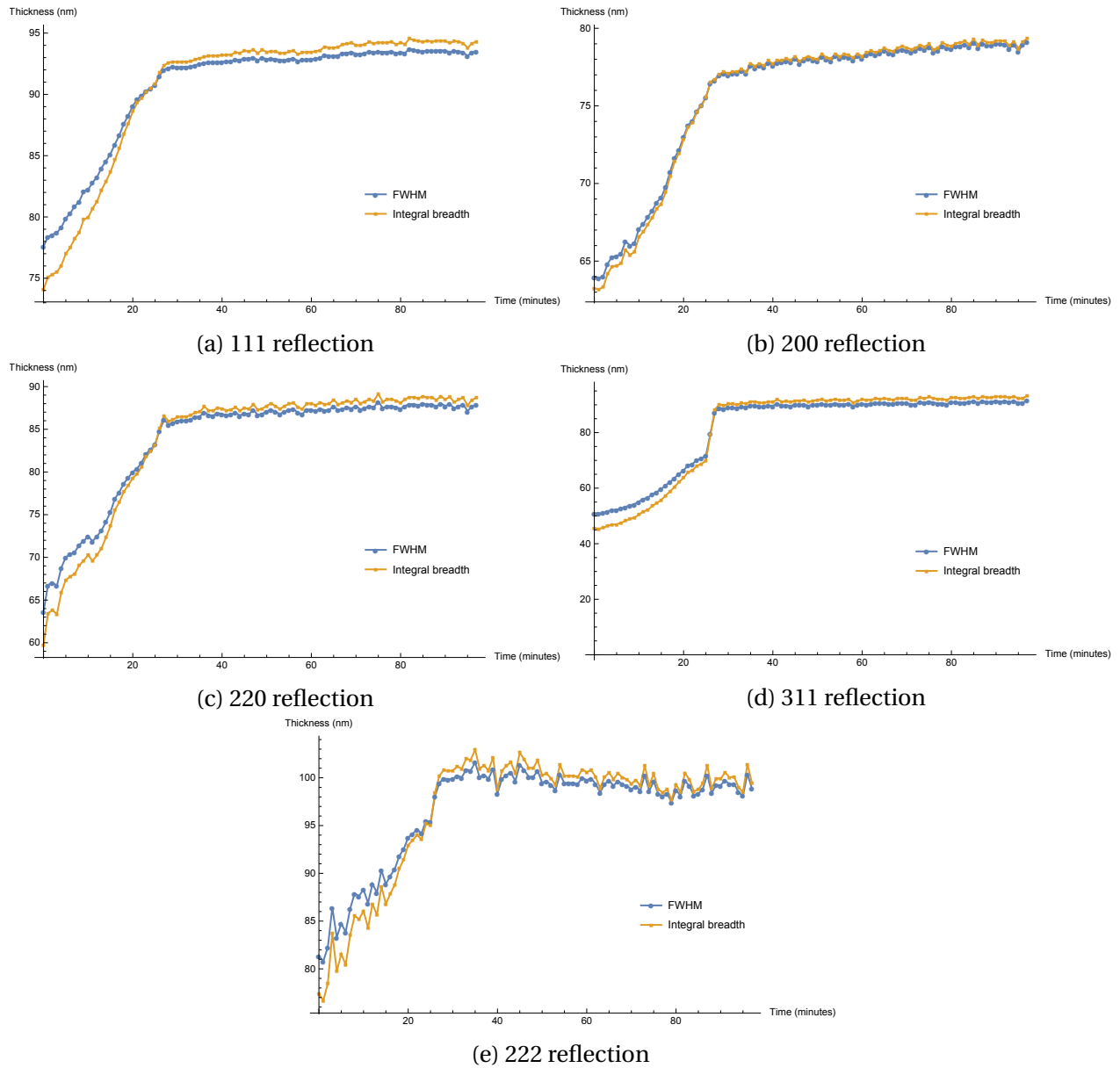


Figure 4.17: Comparing the estimated sizes growth rates of silver by FWHM and integral breadth method by shifting up the plot of sizes estimated by FWHM method

4.5 The important of Scherrer constant on size estimation

From Figure 4.18, it is known that there was not much difference in size estimations for silver 311 reflection by assuming spherical crystallite where Scherrer constant equal to 0.94; and assuming cubic crystallite where numerical value of Scherrer constant was found from the [Langford and Wilson's \[22\]](#) research.

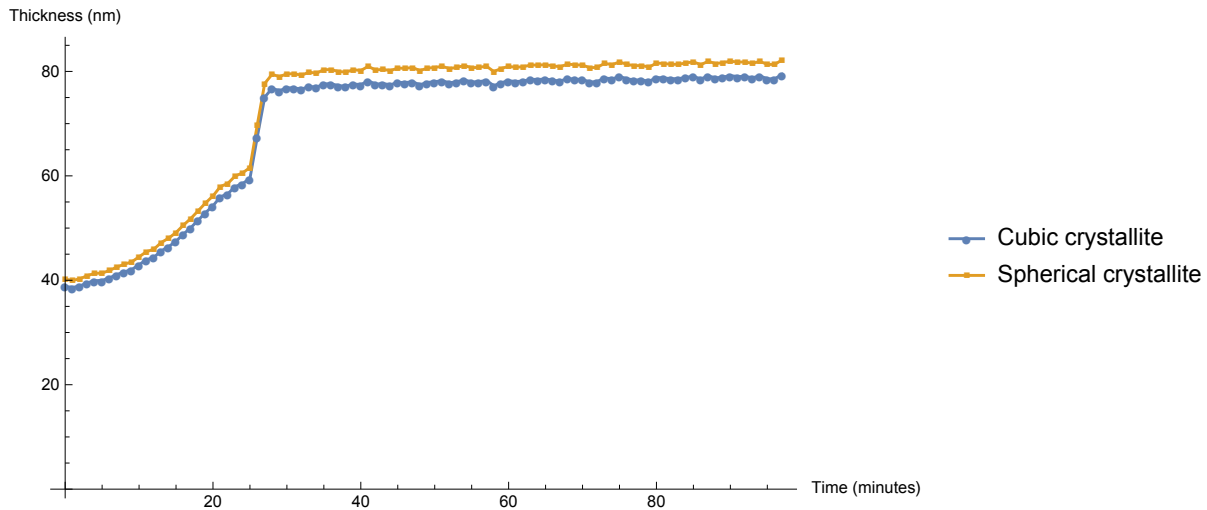


Figure 4.18: Difference on size estimations for 311 reflection by assuming spherical crystallite where Scherrer constant equal to 0.94; and assuming cubic crystallite where Scherrer constant equal to 0.9082

However, Figure 4.19, 4.20, 4.21, 4.22 illustrate an obvious difference in size estimations for 111, 200, 200, 222 reflections by assuming spherical crystallite and assuming cubic crystallite. This implies that the size estimations can be quite different from real size if crystallite shape is unknown. Therefore, TEM-indication is necessary for an accurate size estimation.

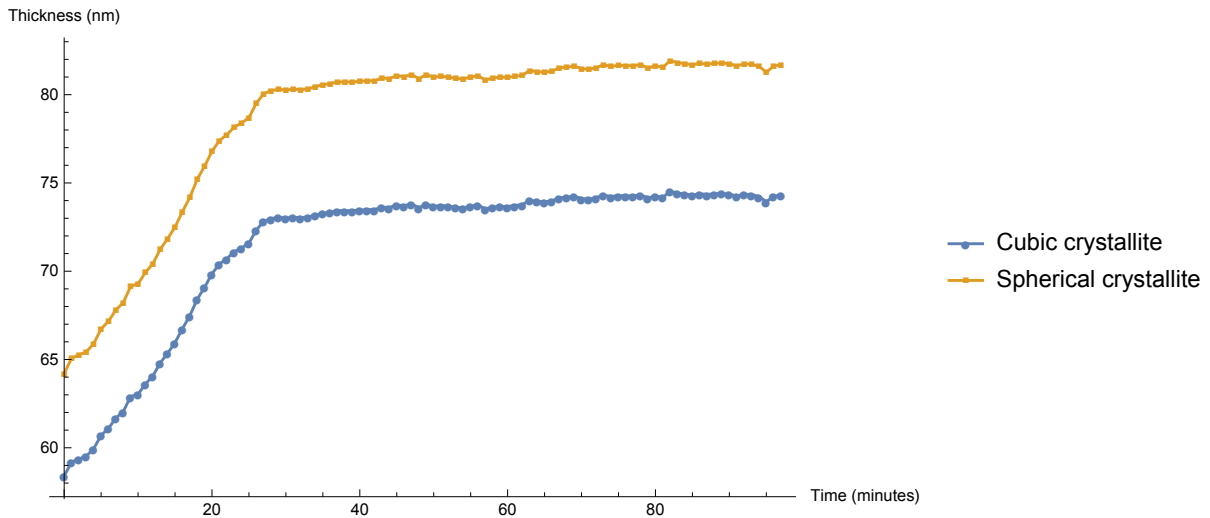


Figure 4.19: Difference on size estimations for 111 reflection by assuming spherical crystallite where Scherrer constant equal to 0.94; and assuming cubic crystallite where Scherrer constant equal to 0.8551

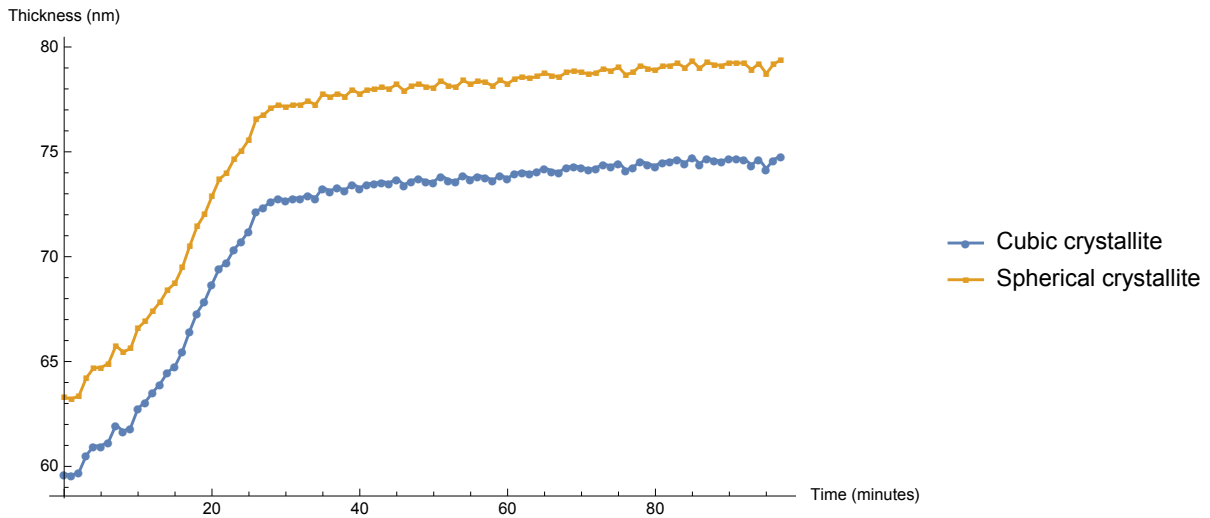


Figure 4.20: Difference on size estimations for 200 reflection by assuming spherical crystallite where Scherrer constant equal to 0.94; and assuming cubic crystallite where Scherrer constant equal to 0.8859

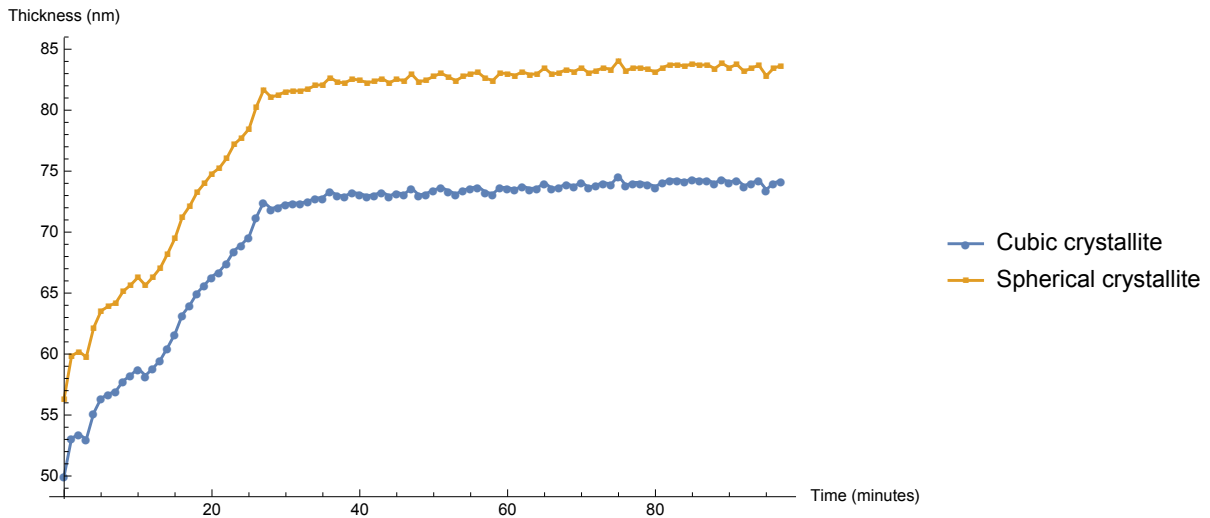


Figure 4.21: Difference on size estimations for 220 reflection by assuming spherical crystallite where Scherrer constant equal to 0.94; and assuming cubic crystallite where Scherrer constant equal to 0.8340

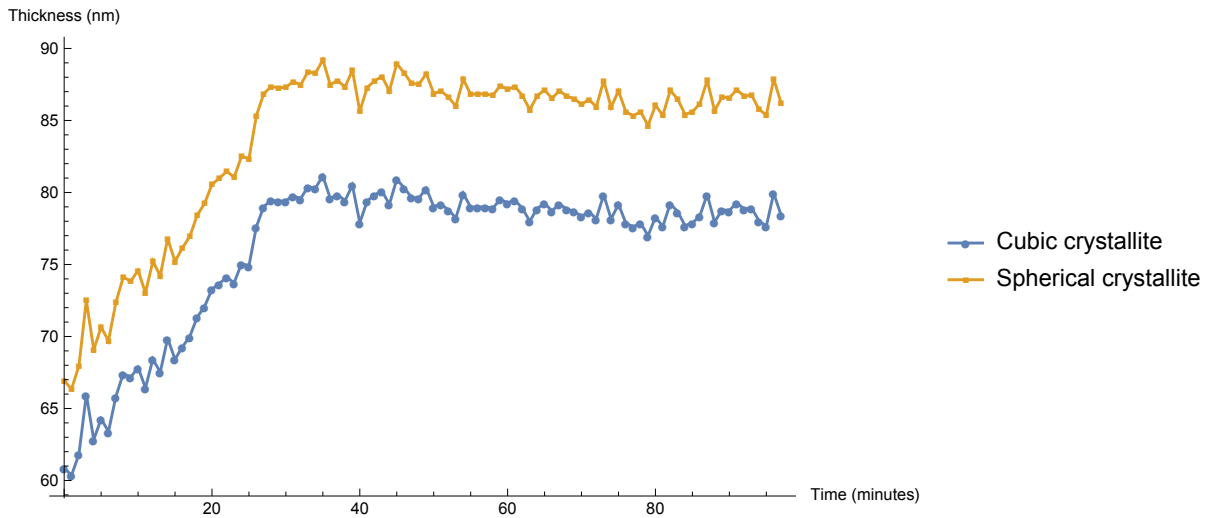


Figure 4.22: Difference on size estimations for 222 reflection by assuming spherical crystallite where Scherrer constant equal to 0.94; and assuming cubic crystallite where Scherrer constant equal to 0.8551

Chapter 5

Factors leading to the broadening of diffraction peak

As mentioned in the previous chapters, the particle size affects the diffraction peak profile, but this is not the only factor. Many researches [27, 29, 37, 40–42] have stated that there are other factors that will affect the diffraction peak profile. To get a more accurate size estimation of the crystallite, these kinds of broadening have to be studied and eliminated.

5.1 Instrumental broadening

There are many types of instrumental broadening, such as slit widths, imperfect focusing, beam size, penetration into the sample[26], etc. Depending on the experimental setup, different instrumental broadenings should be considered.

In this study, Dectris PILATUS2M Pixel detector and double crystal monochromator setup were used. The main instrumental broadening was coming from the finite pixel size of the detector and the energy dispersion of the synchrotron radiation.

5.1.1 Finite pixel size of the detector

According to Bragg's law (Equation 3.1), the diffraction angle is inversely proportional to interplanar distance d and d is proportional to temperature. So, diffraction angles should decrease

with increasing temperatures. However, the experimental diffraction angles were found to be

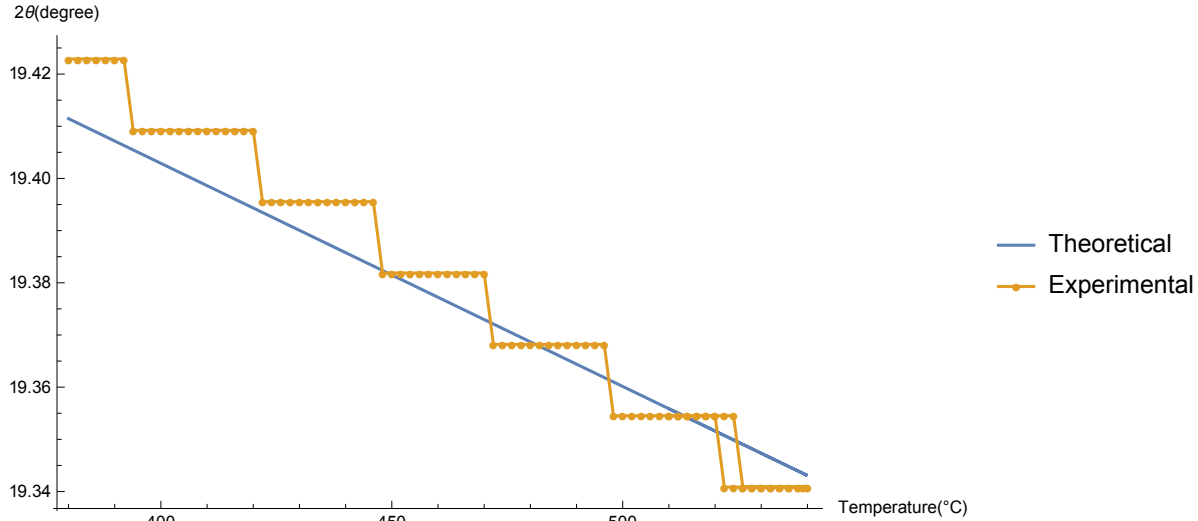


Figure 5.1: Theoretical and experiment values of diffraction angle of 200 reflection

decreased in a zig-zag way and Figure 5.1 shows an example from silver 200 reflection that the diffraction angles did not decrease linearly as predicted theoretically.

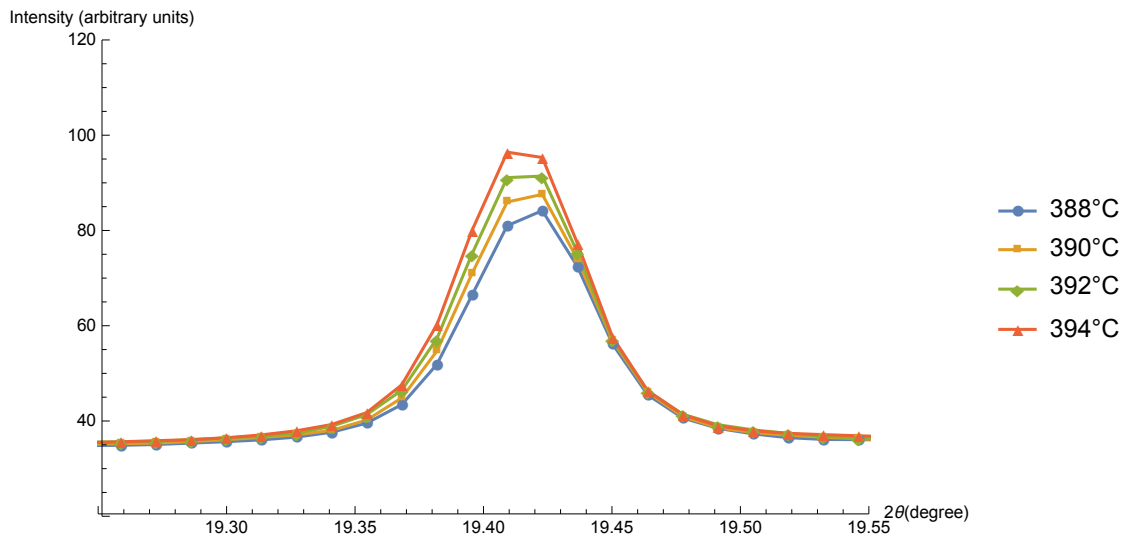


Figure 5.2: Diffractogram of silver 200 reflection at 388 °C, 390 °C, 392 °C and 394 °C

The reason to these results is due to the finite pixel size of the detector. Figure 5.2 shows that for 200 reflection, when temperature increased, the diffraction angle decreased. However, due to the finite pixel size of the detector, the peak position remain the same from 388 °C to 392 °C and then jumped to other position at 394 °C and made the zig-zag curve shown in Figure 5.1.

Magnitude of error on size estimations of silver

The uncertainties in recorded diffraction angles due to finite pixel size of the detector were found by Equation 5.1.

$$\delta\theta = \tan^{-1}\left(\frac{l}{d}\right) \quad (5.1)$$

where,

$$l = \sqrt{\left(\frac{w}{2}\right)^2 + \left(\frac{w}{2}\right)^2}$$

where $\delta\theta$ is the uncertainty in recorded diffraction angle due to finite pixel size of the detector, l is the maximum possible error of the diffracted position measured, d is the sample to detector distance and w is the width of the pixel.

The pixel size of the detector was 0.172 mm \times 0.172 mm, so w was 0.172 mm and sample to detector distance of the experimental setup d was 20 cm. Therefore, uncertainty in recorded diffraction angle or the uncertainty in measured FWHM was of the magnitude 10^{-2} .

With reference to Chapter 4, the broadenings due to the samples were within the range of 4 to 10×10^{-2} (degree), and the magnitude of the instrumental broadening due to finite pixel size of the detector was 10^{-2} (degree). This implies that instrumental broadening due to finite pixel size of the detector is probably the dominating instrumental broadening factor and the uncertainties in FWHM were 0.04 ± 0.01 (degree) to 0.10 ± 0.01 (degree).

5.1.2 Energy dispersion of the incoming synchrotron radiation

The double crystal monochromator setup was used to select the required energy of synchrotron radiation. The maximum possible error during the energy selection is:

$$\frac{\Delta E}{E} = \frac{\Delta\lambda}{\lambda} = 10^{-4} \quad (5.2)$$

where E is the energy of the synchrotron radiation and λ is the wavelength of the synchrotron radiation. By differentiate Equation 3.1 with d_{hkl} fixed,

$$2d_{hkl} \cos\theta = \frac{d\lambda}{d\theta} \quad (5.3)$$

and by simple manipulation, Equation 5.3 become,

$$d\theta = \frac{d\lambda}{2d_{hkl} \cos\theta} \quad (5.4)$$

by substituting Equation 3.2 and 5.2 into Equation 5.4,

$$d\theta = \frac{\lambda \times 10^{-4}}{2 \frac{a}{\sqrt{h^2+k^2+l^2}} \cos\theta} \quad (5.5)$$

With reference to diffraction angles of silver at Appendix A, the maximum possible errors for the 5 lowest reflections due to energy dispersion of sample 2 at 380 °C were shown in Table 5.1¹.

Table 5.1: Maximum Instrumental broadening due to energy dispersion of synchrotron radiation

	Reflections, 2θ (degree)				
Temperature	111	200	220	311	222
380 °C	2.89×10^{-5}	3.33×10^{-5}	4.63×10^{-5}	5.37×10^{-5}	5.59×10^{-5}

Table 5.1 and Appendix C show that the maximum possible errors due to energy dispersion were of magnitude 10^{-5} (degree), while the magnitude of the instrumental broadening due to the sample was 10^{-2} (degree). This implies that instrumental broadening due to finite pixel size of the detector is negligible.

To double check if the errors affect the results, Equation 5.6 was used to calculate the difference in size estimations with and without eliminating the energy dispersion errors. Figure 5.3 illustrates that, the size estimations of silver in sample 2 111 reflection were almost the same for estimations with or without eliminating the energy dispersion broadening. This proves that the broadening is negligible.

5.1.3 Method to remove instrumental broadening

It is worth to mention the general method to remove the instrumental broadening. Warren [19] stated that, by running a standard peak using a large powder size sample, all particle size broadening is eliminated. Then, the recorded diffraction peak profile will be mainly contributed by

¹See Appendix C for errors at other temperatures

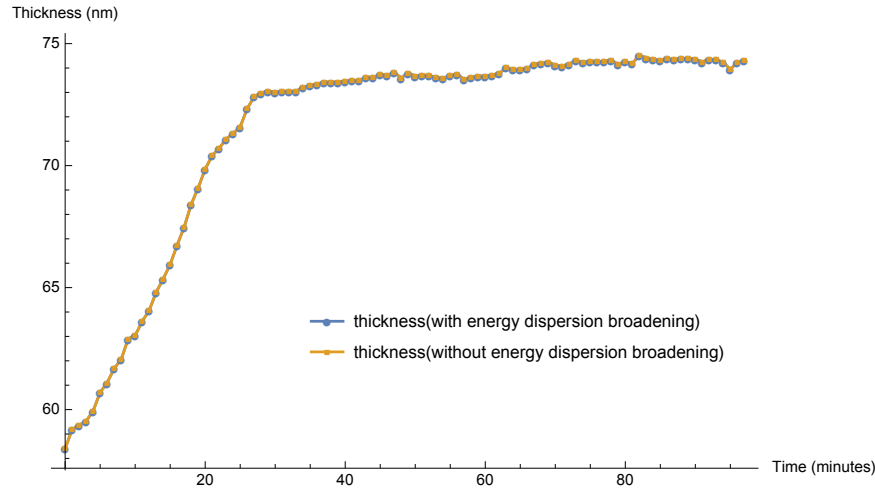


Figure 5.3: Size estimations of silver in sample 2 111 reflection with and without eliminating the energy dispersion broadening

instrumental broadening. So, the instrumental broadening can be removed by using Equation 5.6 or 5.7 [19, 28] depending on the shape of the peak profile.

$$\text{Gaussian shape : } B^2(h) = B^2(g) + B^2(f) \quad (5.6)$$

$$\text{Cauchy shape : } B(h) = B(g) + B(f) \quad (5.7)$$

where $B(g)$ is the half maximum breadth due to instrumental broadening, $B(f)$ is the half maximum breadth due to particle size and $B(h)$ is the half maximum breadth due to both instrumental broadening and particle size.

5.2 Internal elastic strains

According to Hammond [26], the elastic strains can be separated into macro-strain and micro-strain, and both of them will affect the diffracted peaks. The macro-strain will shift the diffraction peaks and affect the identification of specific peaks, while the micro-strain will affect the broadening of the peak and thus alter the size estimation of samples.

5.2.1 Macro-strain

Macro-strain means that the whole material is under directional residual tension or compression, so that the inter-planar spacing d_{hkl} will be increase or decrease in certain direction. Therefore, the diffraction peak profile will be shifted [26].

Hammond [26] suggested that the macro-strain can be measured by rotating the specimen for various settings, and thus the direction and magnitude of the macro-strain can then be extrapolated.

5.2.2 Micro-strain

Micro-strain means that the directions or the magnitude of the internal strains are different from crystallites to crystallites [26]. These may be coming from, for instance faulting, dislocation [42], non-uniform lattice distortions [21], etc. The contribution to the broadening by micro-strain can be calculated by differentiate Bragg's Law (Equation 3.1) with λ fixed [26]:

$$0 = 2d \cos\theta \delta\theta + 2 \sin\theta \delta d \quad (5.8)$$

since micro-strain ϵ is equal to $\delta d/d$, so Equation 5.8 becomes [26]:

$$\epsilon = -\cot\theta \delta\theta \quad (5.9)$$

Therefore the broadening due to micro-strain is:

$$B(2\theta) = -\frac{2\epsilon}{\cot\theta} = -2\epsilon \tan\theta \quad (5.10)$$

As mentioned by Hammond [26], broadening due to particle size varies as $1/\cos\theta$ while the broadening due to micro-strain varies as $1/\cot\theta$.

5.3 Thermal diffuse scattering

Atoms in the crystal vibrate, and these vibrations affect the diffracted intensities. The vibrations occurred for two reasons. The first one is purely quantum mechanical in origin from the uncertainty principle; the second one is due to elastic waves, or phonons, that are thermally excited in crystal. Equation 5.11 shows the scattered intensity with the consideration of these vibrations [43].

$$I = \sum_m \sum_n f(\mathbf{Q}) e^{-M} e^{i\mathbf{Q}\cdot\mathbf{R}_m} f^*(\mathbf{Q}) e^{-M} e^{i\mathbf{Q}\cdot\mathbf{R}_n} + \sum_m \sum_n f(\mathbf{Q}) e^{-M} e^{i\mathbf{Q}\cdot\mathbf{R}_m} f^*(\mathbf{Q}) e^{-M} e^{i\mathbf{Q}\cdot\mathbf{R}_n} \{e^{Q^2(u_{Qm}u_{Qn})} - 1\} \quad (5.11)$$

where f is atomic form factor, \mathbf{Q} is the wave-vector transfer, e^{-M} is the Debye-Waller factor, R_n is the time-averaged mean position for n 'th atom, u_{Qn} is the component of displacement parallel to \mathbf{Q} for the n 'th atom.

The first term in Equation 5.11 is the elastic Bragg scattering. The second term is thermal diffuse scattering (TDS) [43]. Figure 5.4 shows the idea of TDS contribution to the diffracted peak profile, but due to lack of experimental data, the TDS in Figure 5.4 is not to scale. The actual value of TDS can be found by experiment.

In general, TDS have to be eliminated to give a more accurate size estimation. Chapter 4 shows how background intensity was eliminated in this study.

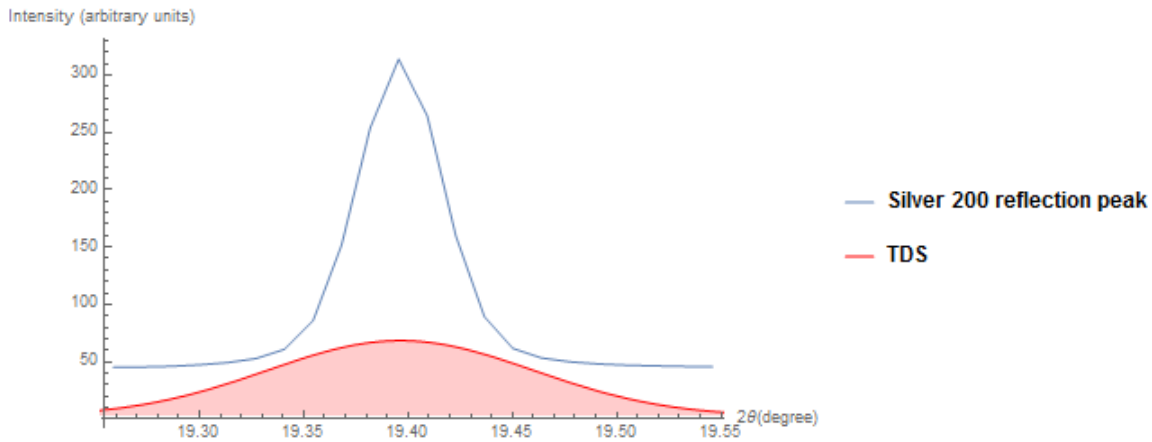


Figure 5.4: TDS contribution to silver 200 reflection peak at 432 °C, where the TDS intensity is not to scale

Chapter 6

Growth kinetics

6.1 Isothermal kinetics

The Johnson-Mehl-Avrami (JMA) equation can be used to describe many types of isothermal solid state transformations [44]. The JMA equation has the form [44]:

$$x(t) = 1 - e^{-(Kt)^n} \quad (6.1)$$

where $x(t)$ is the volume fraction transformed after time t , t is the elapsed time, K is the reaction rate constant and n is the kinetic exponent. By taking natural logarithm twice on both sides of Equation 6.1, JMA equation becomes:

$$\ln[-\ln(1 - x(t))] = n \ln K - n \ln t \quad (6.2)$$

In this study, $x(t)$ was assumed to be reached 100% when the estimated size of silver reached the plateau at 432 °C and $x(t)$ from 380 °C to 432 °C was defined by Equation 6.3.

$$x(t) = \frac{D_t^3}{D_{100\%}^3} \quad (6.3)$$

where D_t is the size estimated at elapsed time t and $D_{100\%}$ is the size estimated at 432 °C.

By plotting $\ln[-\ln(1 - x(t))]$ against $\ln t$, the kinetics exponent n can be found by reading the slope of the plot and the reaction rate constant K can be calculated from the intercept $n \ln(K)$.

However, the initial value of elapsed time t at 380 °C was unknown. The initial value of t was assumed to be 0 at 380 °C in the following part, so as to have a general picture of the growth kinetics.

Figure 6.1 and 6.2 show that, the plotting of $\ln[-\ln(1-x(t))]$ against $\ln t$ did not give a straight line for all five reflections by both FWHM method and integral breadth method. So, the growth kinetics could not be calculated directly from this model. However, it could be possible to assign two straight lines for each plots, one line for $\ln t < 6.5$ and the other line for $\ln t > 6.5$. Two sets of rate constants and kinetics exponents could possibly use to study the growth of silver.

One of the main reasons that plots did not show one straight line is that, the experiment was not done in non-isothermal condition, but readily increasing temperature at a rate of 2 °C per minutes. If this model will be used in future study, an isothermal experimental condition will be recommended.

6.2 Non-isothermal kinetics

According to Vazquez et al. [44], the non-isothermal kinetics model is much more complicated than the isothermal model, and contains some values that were not measured in this study. So, using the model in this study was not possible.

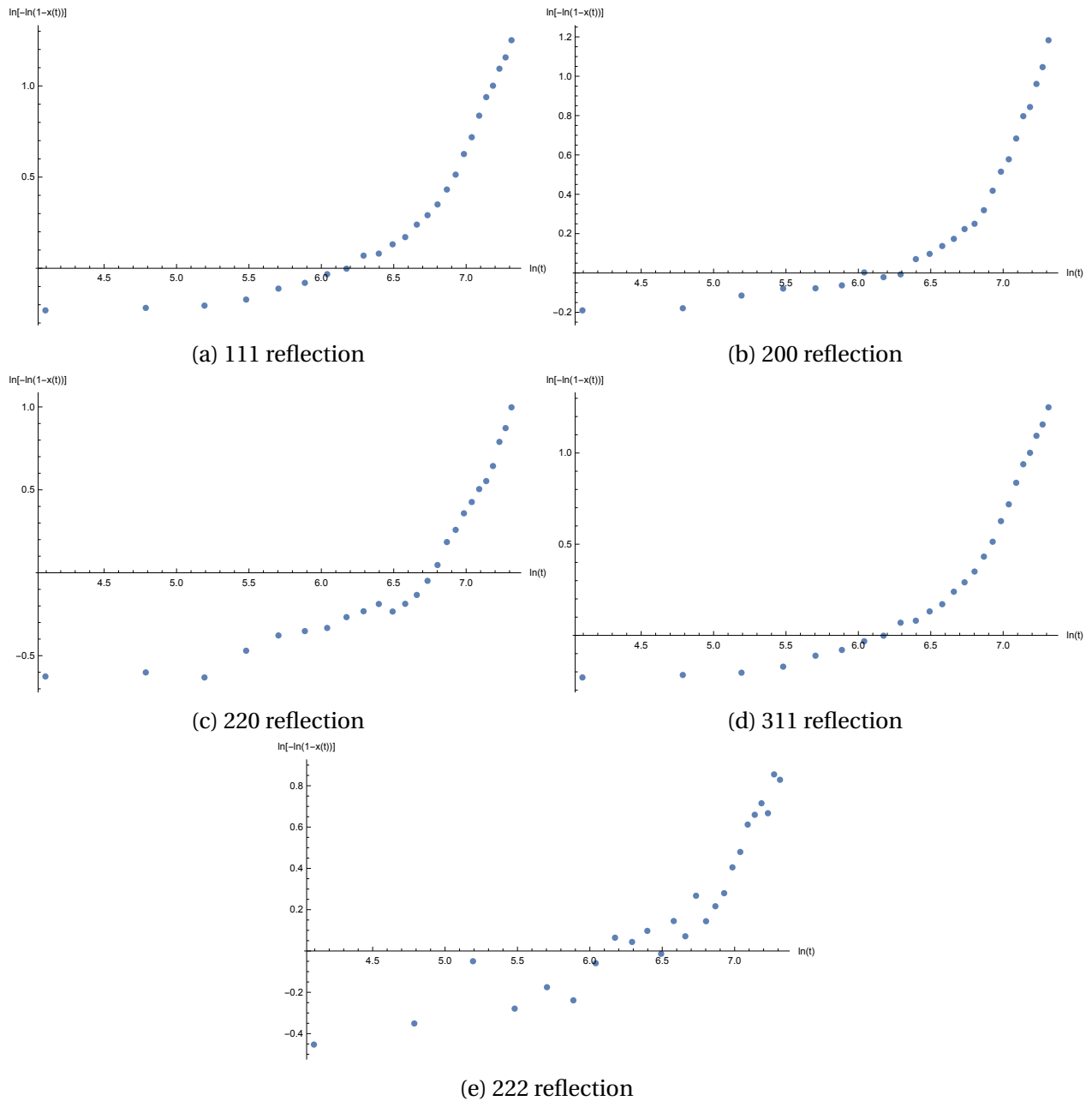


Figure 6.1: The plotting of $\ln[-\ln(1-x(t))]$ against $\ln t$ within the temperature range of 380 °C to 432 °C, for the five lowest reflections by defining peak breadth by FWHM

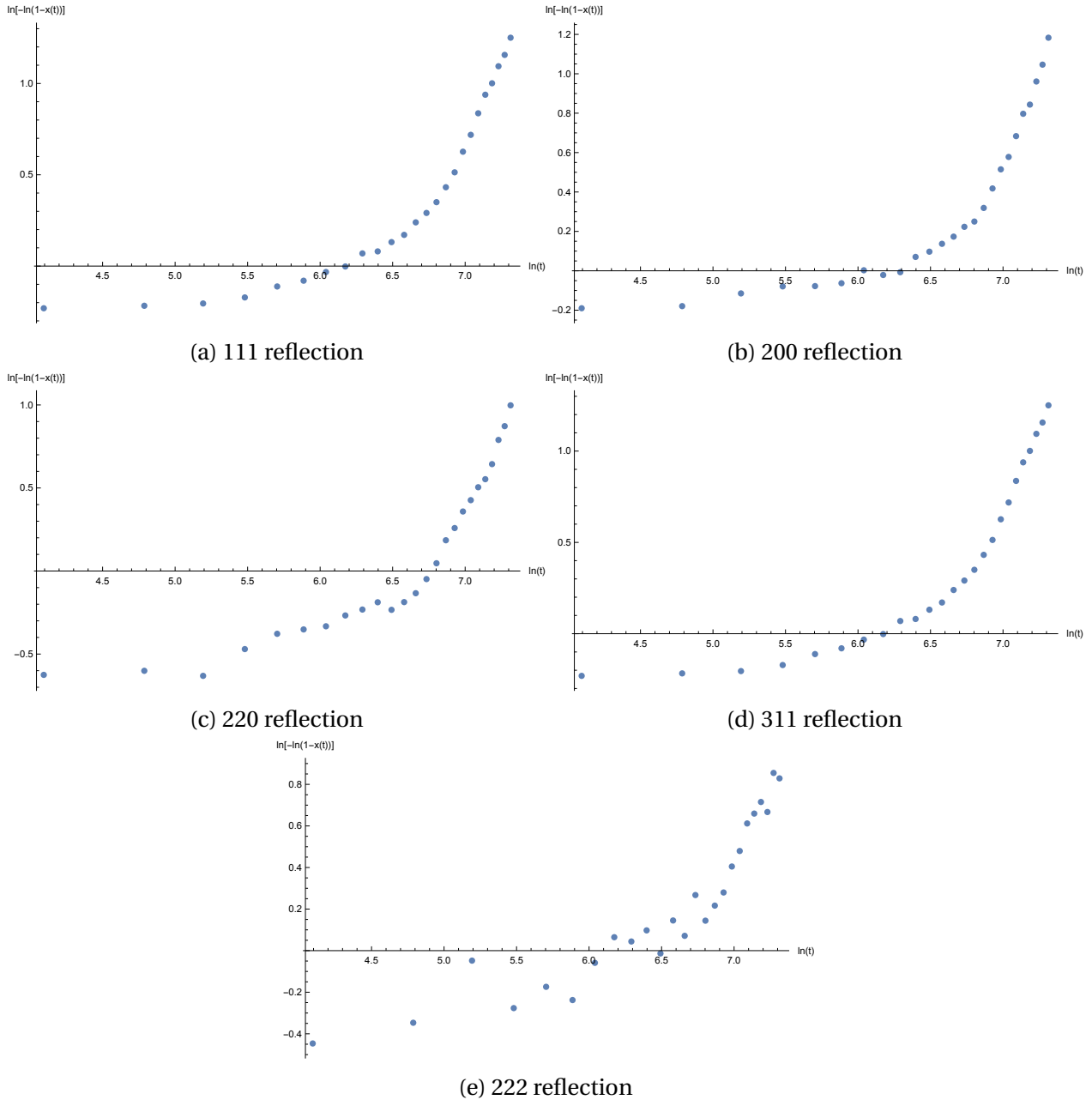


Figure 6.2: The plotting of $\ln[-\ln(1-x(t))]$ against $\ln t$ within the temperature range of 380 °C to 432 °C, for the five lowest reflections by defining peak breadth by integral breadth

6.3 Shape of silver crystallites

Although the growth kinetics cannot be found through the model, the shape of silver crystallites can be estimated by using the sizes calculated from Table 4.1. As the silver is FCC structure, (hkl) is equal to $[hkl]$. The estimated sizes of silver for each reflection can act as a probe for thickness in different directions. Therefore, the silver crystallites can be visualized. Since some of the directions cannot be measured due to extinction principle, the shapes of the silver crystallites were estimated by using thickness in $[111]$, $[200]$, $[220]$ as the principal axes of ellipsoid. The estimated shape of silver crystallites by FWHM method was almost like a sphere shown in Figure 6.3, while the estimated shape of silver crystallites by integral breadth method was more like an ellipsoid shown in Figure 6.4.

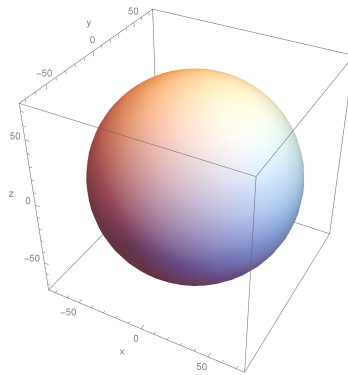


Figure 6.3: Shape of silver crystallites by FWHM method, which was estimated by using thickness in $[111]$, $[200]$, $[220]$ as the principal axes of ellipsoid

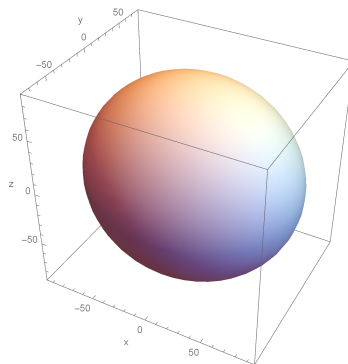


Figure 6.4: Shape of silver crystallites by integral breadth method, which was estimated by using thickness in $[111]$, $[200]$, $[220]$ as the principal axes of ellipsoid

Chapter 7

Summary and suggestion to further investigation

7.1 Summary and conclusions

Presence of silver in silver sulphate sample

In Chapter 3, Bragg's law and extinction rule were used to calculate the silver peak position as a function of temperature. Also, the effect of increasing temperature to silver lattice constants was also considered so as to have a more accurate estimation on the diffraction angle. Furthermore, exponential decay of synchrotron beams was also evaluated, so that the silver peak intensities could represent the true values.

The results in Chapter 3 show that, diffractograms in sample 1 and 3 did not show any silver peaks in the five lowest orders of reflections throughout the temperature range of this study. While sample 2 shows silver peaks in all five lowest orders of reflections. The difference between sample 2 and sample 1, 3 may be due to the difference resulted from the manufacturing process. The detailed mechanism concerning this point is not known yet and needs further investigation. Therefore, if silver size growth in silver sulphate during heating process is to be studied, sample 2 is recommended.

Silver growth

Scherrer equation was applied in Chapter 4 to estimate the size of silver. The results show that silver crystallites were grown almost linearly with increasing temperature in all reflections within the temperature range of 380 °C to 432 °C. The sizes of silver grew typically from around 50 ± 10 nm to 70 ± 10 nm. Then, silver crystallites stopped growing when temperature was over 432 °C. Therefore, it is very likely that the phase transition of silver sulphate prohibits the growth of metallic silver rather than leads to the growth of silver, because the silver crystallites grew at temperature below the phase transition temperature and stopped at temperature near to the phase transition. The origin of the silver growth is suspected to be the disproportionation mechanism of silver sulphate.

Comparison on FWHM and integral breadth

With reference to Chapter 4, both FWHM and integral breadth methods were tested in order to estimate the sizes of silver. The estimated sizes of silver by both methods grew at almost the same rate and pattern throughout the temperature range of the experiment. However, the estimated sizes have a constant difference throughout the temperature range of the experiment, and this might be due to the difference in defining peak breadth and the values of Scherrer constant. For FWHM method, the sizes of silver grew typically from around 50 ± 10 nm to 70 ± 10 nm. For integral breadth method, the sizes of silver grew typically from around 60 ± 10 nm to 80 ± 10 nm.

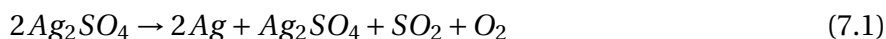
Others factor leading to the broadening of diffraction peak

In this study, two of the main instrumental broadenings were coming from the finite pixel size of the detector and the energy dispersion of the synchrotron radiation. The uncertainties in FWHM due to finite pixel size of the detector were $0.04^\circ \pm 0.01^\circ$ to $0.10 \pm 0.01^\circ$. The magnitude of the instrumental broadening due to the energy dispersion of the synchrotron radiation was 10^{-5}° and is insignificant. While other factors that lead to the broadening of diffraction peak like micro-strain were difficult to estimate quantitatively in this study, because of the lack of experimental data.

7.2 Suggestion to further investigation

Origin of the silver metal

From Chapter 4, silver crystallites were found to be growing during the heating process of metallic silver. One of the suggestion to the growth of metallic silver during the heating process of silver sulphate is the disproportionation mechanism [45]:



Disproportionation is a redox reaction that Ag_2SO_4 is both oxidized and reduced [46]. However, this is only a hypothesis right now, and there is no specific research that has been done on disproportionation of silver sulphate. Further investigation is needed to test this hypothesis.

Reason to the stopping of silver growth

With reference to Chapter 4, silver growth stopped at around 432 °C in all reflections. Phase transition of silver sulphate is suspected to cause the stop of silver growth, as the stopping temperature (432 °C) is very close to the phase transition temperature (427 °C).

To test the hypothesis, the silver sulphate powder have to be heated up from 380 °C to 530 °C and then cool down back to 380 °C. Then, it is needed to check if silver crystallites will grow again at temperature lower than the phase transition temperature of silver sulphate. If the silver crystallites grow again, then very likely the phase transition of sulphate silver is prohibiting the growth of metallic silver.

TEM can also be used for doing further investigation in the system, because TEM can be used to look at the local structure of the system, and might be able to find evidence to the site saturation of silver sulphate matrix during the silver growth.

Appendix A

Diffraction angles of silver

Table [A.1](#) and table [A.2](#) were calculated by Excel function, Data Table.

Table A.1: Diffraction angles of silver estimated by linear regression

Temperature, °C	Reflections, 2θ (degree)				
	111	200	220	311	222
380	16.784	19.404	27.576	32.457	33.942
382	16.783	19.403	27.575	32.455	33.941
384	16.783	19.402	27.573	32.454	33.939
386	16.782	19.401	27.572	32.452	33.938
388	16.781	19.400	27.571	32.451	33.936
390	16.780	19.400	27.570	32.449	33.935
392	16.780	19.399	27.568	32.448	33.933
394	16.779	19.398	27.567	32.446	33.931
396	16.778	19.397	27.566	32.445	33.930
398	16.777	19.396	27.564	32.443	33.928
400	16.777	19.395	27.563	32.442	33.927
402	16.776	19.394	27.562	32.440	33.925
404	16.775	19.393	27.561	32.439	33.924
406	16.774	19.393	27.559	32.437	33.922
408	16.773	19.392	27.558	32.436	33.921
410	16.773	19.391	27.557	32.434	33.919
412	16.772	19.390	27.556	32.433	33.917
414	16.771	19.389	27.554	32.431	33.916
416	16.770	19.388	27.553	32.430	33.914
418	16.770	19.387	27.552	32.428	33.913
420	16.769	19.386	27.551	32.427	33.911
422	16.768	19.386	27.549	32.425	33.910
424	16.767	19.385	27.548	32.424	33.908
426	16.767	19.384	27.547	32.422	33.906
428	16.766	19.383	27.546	32.421	33.905
430	16.765	19.382	27.544	32.419	33.903
432	16.764	19.381	27.543	32.418	33.902
434	16.764	19.380	27.542	32.416	33.900
436	16.763	19.379	27.541	32.415	33.899
438	16.762	19.379	27.539	32.413	33.897
440	16.761	19.378	27.538	32.412	33.895
442	16.761	19.377	27.537	32.410	33.894
444	16.760	19.376	27.535	32.409	33.892
446	16.759	19.375	27.534	32.407	33.891
448	16.758	19.374	27.533	32.406	33.889
450	16.758	19.373	27.532	32.404	33.888
452	16.757	19.372	27.530	32.403	33.886
454	16.756	19.372	27.529	32.401	33.884
456	16.755	19.371	27.528	32.400	33.883
458	16.755	19.370	27.527	32.398	33.881

Temperature, °C	Reflections, 2θ (degree)				
	111	200	220	311	222
460	16.754	19.369	27.525	32.397	33.880
462	16.753	19.368	27.524	32.395	33.878
464	16.752	19.367	27.523	32.394	33.877
466	16.752	19.366	27.522	32.392	33.875
468	16.751	19.365	27.520	32.391	33.874
470	16.750	19.364	27.519	32.389	33.872
472	16.749	19.364	27.518	32.388	33.870
474	16.749	19.363	27.517	32.386	33.869
476	16.748	19.362	27.515	32.385	33.867
478	16.747	19.361	27.514	32.383	33.866
480	16.746	19.360	27.513	32.382	33.864
482	16.745	19.359	27.512	32.380	33.863
484	16.745	19.358	27.510	32.379	33.861
486	16.744	19.357	27.509	32.377	33.859
488	16.743	19.357	27.508	32.376	33.858
490	16.742	19.356	27.507	32.374	33.856
492	16.742	19.355	27.505	32.373	33.855
494	16.741	19.354	27.504	32.371	33.853
496	16.740	19.353	27.503	32.370	33.852
498	16.739	19.352	27.502	32.368	33.850
500	16.739	19.351	27.500	32.367	33.849
502	16.738	19.350	27.499	32.365	33.847
504	16.737	19.350	27.498	32.364	33.845
506	16.736	19.349	27.497	32.362	33.844
508	16.736	19.348	27.495	32.361	33.842
510	16.735	19.347	27.494	32.360	33.841
512	16.734	19.346	27.493	32.358	33.839
514	16.733	19.345	27.491	32.357	33.838
516	16.733	19.344	27.490	32.355	33.836
518	16.732	19.343	27.489	32.354	33.835
520	16.731	19.343	27.488	32.352	33.833
522	16.730	19.342	27.486	32.351	33.831
524	16.730	19.341	27.485	32.349	33.830
526	16.729	19.340	27.484	32.348	33.828
528	16.728	19.339	27.483	32.346	33.827
530	16.727	19.338	27.481	32.345	33.825
532	16.727	19.337	27.480	32.343	33.824
534	16.726	19.337	27.479	32.342	33.822
536	16.725	19.336	27.478	32.340	33.820
538	16.724	19.335	27.476	32.339	33.819
540	16.724	19.334	27.475	32.337	33.817

Table A.2: Diffraction angles of silver estimated by exponential regression

Temperature, °C	Reflections, 2θ (degree)				
	111	200	220	311	222
380	16.784	19.404	27.576	32.457	33.943
382	16.784	19.404	27.575	32.456	33.942
384	16.783	19.403	27.574	32.454	33.940
386	16.782	19.402	27.573	32.453	33.939
388	16.781	19.401	27.571	32.451	33.937
390	16.781	19.400	27.570	32.450	33.935
392	16.780	19.399	27.569	32.448	33.934
394	16.779	19.398	27.568	32.447	33.932
396	16.778	19.397	27.566	32.445	33.931
398	16.778	19.397	27.565	32.444	33.929
400	16.777	19.396	27.564	32.442	33.928
402	16.776	19.395	27.563	32.441	33.926
404	16.775	19.394	27.561	32.439	33.924
406	16.775	19.393	27.560	32.438	33.923
408	16.774	19.392	27.559	32.436	33.921
410	16.773	19.391	27.558	32.435	33.920
412	16.772	19.390	27.556	32.433	33.918
414	16.772	19.389	27.555	32.432	33.917
416	16.771	19.389	27.554	32.430	33.915
418	16.770	19.388	27.552	32.429	33.913
420	16.769	19.387	27.551	32.427	33.912
422	16.769	19.386	27.550	32.426	33.910
424	16.768	19.385	27.549	32.424	33.909
426	16.767	19.384	27.547	32.423	33.907
428	16.766	19.383	27.546	32.421	33.906
430	16.766	19.382	27.545	32.420	33.904
432	16.765	19.382	27.544	32.418	33.903
434	16.764	19.381	27.542	32.417	33.901
436	16.763	19.380	27.541	32.415	33.899
438	16.763	19.379	27.540	32.414	33.898
440	16.762	19.378	27.539	32.412	33.896
442	16.761	19.377	27.537	32.411	33.895
444	16.760	19.376	27.536	32.409	33.893
446	16.759	19.375	27.535	32.408	33.892
448	16.759	19.375	27.534	32.406	33.890
450	16.758	19.374	27.532	32.405	33.888
452	16.757	19.373	27.531	32.404	33.887
454	16.756	19.372	27.530	32.402	33.885
456	16.756	19.371	27.529	32.401	33.884
458	16.755	19.370	27.527	32.399	33.882

Temperature, °C	Reflections, 2θ (degree)				
	111	200	220	311	222
460	16.754	19.369	27.526	32.398	33.881
462	16.753	19.368	27.525	32.396	33.879
464	16.753	19.368	27.524	32.395	33.877
466	16.752	19.367	27.522	32.393	33.876
468	16.751	19.366	27.521	32.392	33.874
470	16.750	19.365	27.520	32.390	33.873
472	16.750	19.364	27.519	32.389	33.871
474	16.749	19.363	27.517	32.387	33.870
476	16.748	19.362	27.516	32.386	33.868
478	16.747	19.361	27.515	32.384	33.867
480	16.747	19.361	27.513	32.383	33.865
482	16.746	19.360	27.512	32.381	33.863
484	16.745	19.359	27.511	32.380	33.862
486	16.744	19.358	27.510	32.378	33.860
488	16.744	19.357	27.508	32.377	33.859
490	16.743	19.356	27.507	32.375	33.857
492	16.742	19.355	27.506	32.374	33.856
494	16.741	19.354	27.505	32.372	33.854
496	16.741	19.354	27.503	32.371	33.852
498	16.740	19.353	27.502	32.369	33.851
500	16.739	19.352	27.501	32.368	33.849
502	16.738	19.351	27.500	32.366	33.848
504	16.738	19.350	27.498	32.365	33.846
506	16.737	19.349	27.497	32.363	33.845
508	16.736	19.348	27.496	32.362	33.843
510	16.735	19.347	27.495	32.360	33.842
512	16.735	19.347	27.493	32.359	33.840
514	16.734	19.346	27.492	32.357	33.838
516	16.733	19.345	27.491	32.356	33.837
518	16.732	19.344	27.490	32.354	33.835
520	16.732	19.343	27.488	32.353	33.834
522	16.731	19.342	27.487	32.351	33.832
524	16.730	19.341	27.486	32.350	33.831
526	16.729	19.340	27.485	32.348	33.829
528	16.729	19.340	27.483	32.347	33.827
530	16.728	19.339	27.482	32.345	33.826
532	16.727	19.338	27.481	32.344	33.824
534	16.726	19.337	27.480	32.342	33.823
536	16.725	19.336	27.478	32.341	33.821
538	16.725	19.335	27.477	32.339	33.820
540	16.724	19.334	27.476	32.338	33.818

Appendix B

Scaling factors of exponential decay of synchrotron beam

Table B.1 was calculated by Equation 3.6 with half life equals to 10 hours and the elapsed time before the first recorded data equals to 1500 s and time interval between data sets equals to 60 s.

Table B.1: Scaling factor K for the samples at different elapsed time

Data set	Elapsed time, s	Scaling factor K	Data set	Elapsed time, s	Scaling factor K
1	1500	1.0425	16	2400	1.0689
2	1560	1.0443	17	2460	1.0707
3	1620	1.0460	18	2520	1.0725
4	1680	1.0478	19	2580	1.0743
5	1740	1.0495	20	2640	1.0761
6	1800	1.0513	21	2700	1.0779
7	1860	1.0530	22	2760	1.0797
8	1920	1.0548	23	2820	1.0815
9	1980	1.0565	24	2880	1.0833
10	2040	1.0583	25	2940	1.0851
11	2100	1.0601	26	3000	1.0869
12	2160	1.0618	27	3060	1.0887
13	2220	1.0636	28	3120	1.0905
14	2280	1.0654	29	3180	1.0924
15	2340	1.0672	30	3240	1.0942

Data set	Elapsed time, s	Scaling factor K	Data set	Elapsed time, s	Scaling factor K
31	3300	1.0960	65	5340	1.1599
32	3360	1.0978	66	5400	1.1618
33	3420	1.0997	67	5460	1.1638
34	3480	1.1015	68	5520	1.1657
35	3540	1.1033	69	5580	1.1677
36	3600	1.1052	70	5640	1.1696
37	3660	1.1070	71	5700	1.1716
38	3720	1.1089	72	5760	1.1735
39	3780	1.1107	73	5820	1.1755
40	3840	1.1126	74	5880	1.1774
41	3900	1.1144	75	5940	1.1794
42	3960	1.1163	76	6000	1.1814
43	4020	1.1181	77	6060	1.1833
44	4080	1.1200	78	6120	1.1853
45	4140	1.1219	79	6180	1.1873
46	4200	1.1237	80	6240	1.1893
47	4260	1.1256	81	6300	1.1912
48	4320	1.1275	82	6360	1.1932
49	4380	1.1294	83	6420	1.1952
50	4440	1.1313	84	6480	1.1972
51	4500	1.1331	85	6540	1.1992
52	4560	1.1350	86	6600	1.2012
53	4620	1.1369	87	6660	1.2032
54	4680	1.1388	88	6720	1.2052
55	4740	1.1407	89	6780	1.2072
56	4800	1.1426	90	6840	1.2092
57	4860	1.1445	91	6900	1.2113
58	4920	1.1464	92	6960	1.2133
59	4980	1.1484	93	7020	1.2153
60	5040	1.1503	94	7080	1.2173
61	5100	1.1522	95	7140	1.2194
62	5160	1.1541	96	7200	1.2214
63	5220	1.1560	97	7260	1.2234
64	5280	1.1580	98	7320	1.2255

Appendix C

Maximum instrumental broadening due to energy dispersion

Appendix D

Mathematica Code

Listing D.1: Import data set

```
1 ClearAll["Global'*"]
2 testlist =sample=re111=re200=re220=re311=re222=re111IntenVsTemp=re200IntenVsTemp=
   re220IntenVsTemp=re311IntenVsTemp=re222IntenVsTemp=Table[1,{i,3}];
3
4 (* testlist [[1]] to testlist [[3]] represent sample 1, sample 2 and sample 3;
5 teslist [[AlI ]][[1]] to [[83]] and then to [[98]] respresent temperature from 380\{Degree}C to 540\{
   Degree}C and then back to 510\{Degree}C;
6 for each teslist , it contains three values: 1. 2\{Theta} in degrees 2. recorded diffracted intensity (
   arbitrary units) 3. ucertainty of the intensity measurement *)
7 testlist [[1]]=Table[Import["C:\\Users\\roy\\Desktop\\thesis\\Ag_2SO_4_powder\\ramp_1\\dat\\
   Agramp1s"<>ToString[i]<>".dat","Data"],{i,98}];
8 testlist [[2]]=Table[Import["C:\\Users\\roy\\Desktop\\thesis\\Ag_2SO_4_powder\\ramp_2\\dat\\
   Agramp2s"<>ToString[i]<>".dat","Data"],{i,98}];
9 testlist [[3]]=Table[Import["C:\\Users\\roy\\Desktop\\thesis\\Ag_2SO_4_powder\\ramp_3\\dat\\
   Agramp3s"<>ToString[i]<>".dat","Data"],{i,98}];
10
11 (*Scaling of the synchrotron beams because of the reduction in intensity of synchrotron beams along time
   *)
12 scaling =Flatten[Import["C:\\Users\\roy\\Desktop\\thesis\\scaling factor result .xlsx "]];
13
14 (*Extract the values of the recorded diffracted intensity ( arbitrary units) and the corresponding
   diffraction angle (2\{Theta})*)
```



```

15 Do[sample[[n]]=Table[Thread[{testlist [[n]][[i]][[All,1]], testlist [[n]][[i]][[All,2]]* scaling [[i]]}, {i
    ,98}],{n,3}];
16
17 (*Data list of peak intensity and the corresponding diffraction angle (2\Theta) for 5 lowest
    reflection of silver of the three different samples*)
18 Do[re111[[n]]=Table[Flatten[MaximalBy[Select[sample[[n]][[i]],(16.65<#[[1]]<16.95)&],Last]],{i,98}],{n
    ,3}];
19 Do[re200[[n]]=Table[Flatten[MaximalBy[Select[sample[[n]][[i]],(19.25<#[[1]]<19.55)&],Last]],{i,98}],{n
    ,3}];
20 Do[re220[[n]]=Table[Flatten[MaximalBy[Select[sample[[n]][[i]],(27.35<#[[1]]<27.75)&],Last]],{i,98}],{n
    ,3}];
21 Do[re311[[n]]=Table[Flatten[MaximalBy[Select[sample[[n]][[i]],(32.25<#[[1]]<32.65)&],Last]],{i,98}],{n
    ,3}];
22 Do[re222[[n]]=Table[Flatten[MaximalBy[Select[sample[[n]][[i]],(33.75<#[[1]]<34.05)&],Last]],{i,98}],{n
    ,3}];
23
24 (* fix side peak*)
25 re220 [[2,1;;15]]= Table[Flatten[MaximalBy[Select[sample [[2]][[i]],(27.55<#[[1]]<27.75)&],Last]],{i,15}];
26
27 (*Data list of the temperature*)
28 Temp=Flatten[Import["C:\\Users\\roy\\Desktop\\thesis\\temp.xlsx"]];
29
30 (*Data list of time in minutes*)
31 time=Flatten[Import["C:\\Users\\roy\\Desktop\\thesis\\timeintervaloframpminutes.xlsx"]];
32
33 (* Reflections intensity vs Temperature*)
34 Do[re111IntenVsTemp[[n]]=Thread[{Temp,re111[[n]][[All,2]]}],{n,3}];
35 Do[re200IntenVsTemp[[n]]=Thread[{Temp,re200[[n]][[All,2]]}],{n,3}];
36 Do[re220IntenVsTemp[[n]]=Thread[{Temp,re220[[n]][[All,2]]}],{n,3}];
37 Do[re311IntenVsTemp[[n]]=Thread[{Temp,re311[[n]][[All,2]]}],{n,3}];
38 Do[re222IntenVsTemp[[n]]=Thread[{Temp,re222[[n]][[All,2]]}],{n,3}];

```

Listing D.2: Chapter 2

```

1 (*Example of diffractograms of sample2 at 380\DegreeC*)
2 ListPlot[{sample [[2,1]]}, PlotRange->All,Joined->True,AxesLabel->{"2\Theta(degree)","Intensity (
    arbitrary units)"},ImageSize->500,AspectRatio->0.5]

```

Listing D.3: Chapter 3

```

1  (*Plot: Subscript[Ag, 2]Subscript[SO, 4] peak nearby silver 220 reflection peak*)
2  ListPlot[sample[[2,1;;4]], PlotRange->{{27.35,27.75},{20,80}},Joined->True,Mesh->All,ImageSize
   ->500,PlotMarkers->Automatic,PlotLegends->{"380\ [Degree]C", "382\ [Degree]C", "384\ [Degree]C", "
   386\ [Degree]C"},PlotLegends->{"380\ [Degree]C", "382\ [Degree]C", "384\ [Degree]C", "386\ [Degree]C"},
   AxesLabel->{"2\ [Theta](degree)", "Intensity (arbitrary units)"}, Epilog->{Text["Subscript[Ag, 2]
   Subscript[SO, 4] peak", Scaled[ {.52, .94} ]], Text["Silver peak", Scaled[ {.72, .81} ]]}]
3
4  (*Plot: To show the influence without proper scaling of the silver 111 reflection intensity *)
5  sample2withoutScaling=Table[Thread[{{testlist[[2]][[i]][[All,1]], testlist[[2]][[i]][[All,2]]},{i,98}}];
6  re111withoutScaling=Table[Flatten[MaximalBy[Select[sample2withoutScaling[[i]],(16.65<#[[1]]<16.95)&],
   Last]],{i,98}];
7  re111withoutScalingIntenVsTemp=Thread[{Temp,re111withoutScaling[[All,2]]];ListPlot[{
   re111withoutScalingIntenVsTemp,re111IntenVsTemp[[2]]},PlotRange->All,Mesh->All,PlotMarkers->{
   Automatic,7},Joined->True,AxesLabel->{"Temperature(\ [Degree]C)", "Intensity (arbitrary units)"},
   PlotLegends->{"Sample2 without scaling", "Sample2 with scaling"},ImageSize->500]
8  ListPlot[{re111withoutScalingIntenVsTemp,re111IntenVsTemp[[2]]},PlotRange->{{420,540},{500,700}},
   Joined->True,Mesh->All,PlotMarkers->{Automatic,7},AxesLabel->{"Temperature(\ [Degree]C)", "
   Intensity (arbitrary units)"},PlotLegends->{"Sample2 without scaling", "Sample2 with scaling"},
   ImageSize->500]
9
10 (*Plot: : Intensity of silver 111 reflection of the 3 different samples along with temperature*)
11 ListPlot[re111IntenVsTemp,PlotRange->All,Joined->True,Mesh->All,PlotMarkers->{Automatic,7},
   AxesLabel->{"Temperature(\ [Degree]C)", "Intensity (arbitrary units)"},PlotLegends->{"Sample1", "
   Sample2", "Sample3"},ImageSize->500]
12
13 (*Plot: Diffractogram to examining the presence of silver in the samples at temperature530\ [PlusMinus]
   Cin 111 reflection *)
14 ListPlot[sample[[All,83]], PlotRange->{{16.60,16.85},{0,700}},Joined->True,Mesh->All,PlotMarkers->
   Automatic,AxesLabel->{"2\ [Theta](degree)", "Intensity (arbitrary units)"},PlotLegends->{"Sample1", "
   Sample2", "Sample3"},ImageSize->500,PlotMarkers->Automatic]

```

Listing D.4: Chapter 4

```

1  (*Showing the diffraction peak broadening by crystallites size *)
2  Plot[Sin[500x]^2/Sin[x]^2,{x,0,3 Pi/2},Ticks->{{0,Pi/2,Pi,3 Pi/2},Automatic},PlotRange->All,
   PlotLegends->"N = 500"]

```

```

3 Plot[ Sin[5x]^2/Sin[x]^2,{x,0,3 Pi/2}, Ticks->{{0,Pi/2,Pi,3 Pi/2},Automatic},PlotRange->All,
  PlotLegends->"N = 5"]
4
5 (*Size estimation by FWHM*)
6 data1=Table[Select[sample [[2]][[ i ]],(16.6<#[[1]]<16.85)&],{i ,98}];
7 For[i=1,i<99,i++,data1[[i]]=Thread[{data1[[i ]][ All ,1], data1 [[i ]][ All ,2]}-Mean[data1[[i
  ]][[1;;3,2]]]];
8 nlm1=Table[1,{i,98}];
9 nlm1=Table[NonlinearModelFit[data1[[i ]], A * Exp[(-1)*(1/2) *(x-[Mu])^2*(1/[Sigma])^2],{{[Sigma
  ],0.05},{[Mu],16.75},{A,600}},x],{i,98}];
10 FWHM1=Table[nlm1[[i]]["ParameterTableEntries"][[1,1]]*2*Sqrt[2*Log[2]],{i ,98}];
11
12 data2=Table[Select[sample [[2]][[ i ]],(19.25<#[[1]]<19.55)&],{i ,98}];
13 For[i=1,i<99,i++,data2[[i]]=Thread[{data2[[i ]][ All ,1], data2 [[i ]][ All ,2]}-Mean[data2[[i
  ]][[-3;;2]]]];
14 nlm2=Table[1,{i,98}];
15 nlm2=Table[NonlinearModelFit[data2[[i ]], A * Exp[(-1)*(1/2) *(x-[Mu])^2*(1/[Sigma])^2],{{[Sigma
  ],0.05},{[Mu],19.4},{A,600}},x],{i,98}];
16 FWHM2=Table[nlm2[[i]]["ParameterTableEntries"][[1,1]]*2*Sqrt[2*Log[2]],{i ,98}];
17
18 data3=Table[{1,1},{i,98}];
19 data3 [[1;;11]]= Table[Select[sample [[2]][[ i ]],(27.56<#[[1]]<27.75)&],{i ,1,11}]; data3 [[12;;22]]= Table[
  Select[sample [[2]][[ i ]],(27.55<#[[1]]<27.75)&],{i ,12,22}]; data3 [[23;;30]]= Table[Select[sample [[2]][[
  i ]],(27.54<#[[1]]<27.75)&],{i ,23,30}]; data3 [[31;;98]]= Table[Select[sample [[2]][[ i
  ]],(27.35<#[[1]]<27.75)&],{i ,31,98}];
20 For[i=1,i<99,i++,data3[[i]]=Thread[{data3[[i ]][ All ,1], data3 [[i ]][ All ,2]}-Mean[data3[[i
  ]][[-3;;2]]]];
21 nlm3=Table[1,{i,98}];
22 nlm3 [[1;;11]]= Table[NonlinearModelFit[data3 [[i ]], A * Exp[(-1)*(1/2) *(x-[Mu])^2*(1/[Sigma])^2],{{[
  Sigma],0.05},{[Mu],27.55},{A,200}},x],{i,1,11}]; nlm3 [[11;;22]]= Table[NonlinearModelFit[data3 [[i ]], A *
  Exp[(-1)*(1/2) *(x-[Mu])^2*(1/[Sigma])^2],{{[Sigma],0.05},{[Mu],27.55},{A,200}},x],{i,11,22}];
  nlm3 [[23;;30]]= Table[NonlinearModelFit[data3 [[i ]], A * Exp[(-1)*(1/2) *(x-[Mu])^2*(1/[Sigma])
  ^2],{{[Sigma],0.05},{[Mu],27.55},{A,200}},x],{i,23,30}]; nlm3 [[31;;98]]= Table[NonlinearModelFit[data3
  [[i ]], A * Exp[(-1)*(1/2) *(x-[Mu])^2*(1/[Sigma])^2],{{[Sigma],0.05},{[Mu],27.55},{A,200}},x],{i
  ,31,98}];
23 FWHM3=Table[nlm3[[i]]["ParameterTableEntries"][[1,1]]*2*Sqrt[2*Log[2]],{i ,98}];

```

```

24
25 data4=Table[Select[sample [[2]][[ i ]],(32.25<#[[1]]<32.65)&],{i ,98}];
26 For[i=1,i<99,i++,data4[[i]]=Thread[{data4[[i ]][[ All ,1]], data4 [[ i ]][[ All ,2]]-Mean[data4[[i
    ]][[-3;:,2]]]}];
27 nlm4=Table[1,{i,98}];
28 nlm4=Table[NonlinearModelFit[data4[[i ]], A * Exp[(-1)*(1/2) *(x-[Mu])^2*(1/[Sigma])^2],{{[Sigma
    ],0.05},{[Mu],32.4},{A,200}},x],{i,98}];
29 FWHM4=Table[nlm4[[i]]["ParameterTableEntries"][[1,1]]*2*Sqrt[2*Log[2]],{i ,98}];
30
31 data5=Table[Select[sample [[2]][[ i ]],(33.75<#[[1]]<34.15)&],{i ,98}];
32 For[i=1,i<99,i++,data5[[i]]=Thread[{data5[[i ]][[ All ,1]], data5 [[ i ]][[ All ,2]]-Mean[data5[[i
    ]][[-3;:,2]]]}];
33 nlm5=Table[1,{i,98}];
34 nlm5=Table[NonlinearModelFit[data5[[i ]], A * Exp[(-1)*(1/2) *(x-[Mu])^2*(1/[Sigma])^2],{{[Sigma
    ],0.05},{[Mu],33.95},{A,12}},x],{i,98}];
35 FWHM5=Table[nlm5[[i]]["ParameterTableEntries"][[1,1]]*2*Sqrt[2*Log[2]],{i ,98}];
36
37 (*y-axis: thickness*)
38 thickness1=(0.8551*(0.6941/10^10))/((FWHM1*Pi/180)*Cos[re111[[2,All,1]]/2Degree]);
39 thickness2=(0.8859*(0.6941/10^10))/((FWHM2*Pi/180)*Cos[re200[[2,All,1]]/2Degree]);
40 thickness3=(0.8340*(0.6941/10^10))/((FWHM3*Pi/180)*Cos[re220[[2,All,1]]/2Degree]);
41 thickness4=(0.9082*(0.6941/10^10))/((FWHM4*Pi/180)*Cos[re311[[2,All,1]]/2Degree]);
42 thickness5=(0.8551*(0.6941/10^10))/((FWHM5*Pi/180)*Cos[re222[[2,All,1]]/2Degree]);
43
44 (*thickness vs temperature, assuming cubic crystallite and SC with Langfor's table*)
45 thickness1VsTemp=Thread[{Temp,thickness1}];
46 thickness2VsTemp=Thread[{Temp,thickness2}];
47 thickness3VsTemp=Thread[{Temp,thickness3}];
48 thickness4VsTemp=Thread[{Temp,thickness4}];
49 thickness5VsTemp=Thread[{Temp,thickness5}];
50
51 (*thickness vs time, assuming cubic crystallite and SC with Langfor's table*)
52 thickness1VsTime=Thread[{time,thickness1*10^9}];
53 thickness2VsTime=Thread[{time,thickness2*10^9}];
54 thickness3VsTime=Thread[{time,thickness3*10^9}];
55 thickness4VsTime=Thread[{time,thickness4*10^9}];

```

```

56 thickness5VsTime=Thread[[{time,thickness5*10^9}];
57
58 (*thickness vs time, assuming spherical crystallite and SC 0.94 *)
59 thickness1CS=(0.94*(0.6941/10^10))/((FWHM1*Pi/180)*Cos[re111[[2,All,1]]/2Degree]);
60 thickness2CS=(0.94*(0.6941/10^10))/((FWHM2*Pi/180)*Cos[re200[[2,All,1]]/2Degree]);
61 thickness3CS=(0.94*(0.6941/10^10))/((FWHM3*Pi/180)*Cos[re220[[2,All,1]]/2Degree]);
62 thickness4CS=(0.94*(0.6941/10^10))/((FWHM4*Pi/180)*Cos[re311[[2,All,1]]/2Degree]);
63 thickness5CS=(0.94*(0.6941/10^10))/((FWHM5*Pi/180)*Cos[re222[[2,All,1]]/2Degree]);
64
65 thickness1CSVsTime=Thread[[{time,thickness1CS*10^9}];
66 thickness2CSVsTime=Thread[[{time,thickness2CS*10^9}];
67 thickness3CSVsTime=Thread[[{time,thickness3CS*10^9}];
68 thickness4CSVsTime=Thread[[{time,thickness4CS*10^9}];
69 thickness5CSVsTime=Thread[[{time,thickness5CS*10^9}];
70
71 (*To show the Gaussian fitting , e.g. 200 reflection at 398\ [Degree]C*)
72 ListPlot [data2 [[10]], PlotStyle->Red,PlotRange->All,AxesLabel->{"2\[Theta](degree)","Intensity (
    arbitrary units)"},ImageSize->500]
73 Show[ListPlot[Thread[[{data2[[10]][[All ,1]], data2 [[10]][[ All ,2]]-Mean[data2 [[10]][[1;;3,2]]}], PlotStyle
    ->Red,PlotRange->All,ImageSize->500,AxesLabel->{"2\[Theta](degree)","Intensity (arbitrary units
    )"}],Plot[Nlm2[[10]][x],{x,19.25,19.55},PlotRange->All,ImageSize->500,AxesLabel->{"2\[Theta](
    degree)","Intensity (arbitrary units)"}]]
74
75 (*Show cancelling of background intensity *)
76 databg2=Table[Select[sample [[2]][[i]],(19.25<#[[1]]<19.55)&,{i ,98}];
77 For[i=1,i<99,i++,databg2[[i]]=Thread[[{databg2[[i]][[ All ,1]], databg2[[i ]][[ All ,2]]]];
78 nImbg2=Table[1,{i,98}];
79 nImbg2=Table[NonlinearModelFit[databg2[[i]],A * Exp[(-1)*(1/2) *(x-[Mu])^2*(1/[Sigma])^2],{{\ [Sigma
    ],0.05},{\ [Mu],19.4},{A,600}},x],{i,98}];
80 ListPlot [{data2 [[10]], databg2 [[10]]}, PlotRange->All,AxesLabel->{"2\[Theta](degree)","Intensity (
    arbitrary units)"},ImageSize->500,PlotRange->{x,16.7,17.95},PlotLegends->{"With background
    intensity","Without background intensity"}]Show[ListPlot[Thread[[{data2[[10]][[All,1]],data2[[10]][[All
    ,2]]-Mean[data2 [[10]][[1;;3,2]]}], PlotStyle->Red,PlotRange->All,ImageSize->500,AxesLabel->{"
    2\[Theta](degree)","Intensity (arbitrary units)"},Plot[Nlm2[[10]][x],{x,19.25,19.55},PlotRange->All,
    Filling->Bottom,ImageSize->500,AxesLabel->{"2\[Theta](degree)","Intensity (arbitrary units)"}]]

```

```

82 (*Plot: FWHM vs time, by FWHM method*)ListPlot[{FWHM1,FWHM2,FWHM3,FWHM4,FWHM5},
      PlotRange->All,Joined->True,AxesLabel->{"Time (minutes)","FWHM (degree)"},PlotLegends->{"
      111","200","220","311","222"},Mesh->All,PlotMarkers->{Automatic,7},ImageSize->500]
83
84 (*Plot: thickness vs temperature, by FWHM method*)
85 ListPlot[{thickness1VsTemp},PlotRange->All,Joined->True,Mesh->All,PlotMarkers->{Automatic,7},
      AxesLabel->{"Temperature(\[Degree]C)","Thickness(m)"},ImageSize->500]
86 ListPlot[{thickness2VsTemp},PlotRange->All,Joined->True,Mesh->All,PlotMarkers->{Automatic,7},
      AxesLabel->{"Temperature(\[Degree]C)","Thickness(m)"},ImageSize->500]
87 ListPlot[{thickness3VsTemp},PlotRange->All,Joined->True,Mesh->All,PlotMarkers->{Automatic,7},
      AxesLabel->{"Temperature(\[Degree]C)","Thickness(m)"},ImageSize->500]
88 ListPlot[{thickness4VsTemp},PlotRange->All,Joined->True,Mesh->All,PlotMarkers->{Automatic,7},
      AxesLabel->{"Temperature(\[Degree]C)","Thickness(m)"},ImageSize->500]
89 ListPlot[{thickness5VsTemp},PlotRange->All,Joined->True,Mesh->All,PlotMarkers->{Automatic,7},
      AxesLabel->{"Temperature(\[Degree]C)","Thickness(m)"},ImageSize->500]
90
91 (*Plot: thickness vs time, by FWHM method*)
92 ListPlot[{thickness1VsTime},PlotRange->All,Joined->True,Mesh->All,PlotMarkers->{Automatic,7},
      AxesLabel->{"Time (minutes)","Thickness (nm)"},ImageSize->500]
93 ListPlot[{thickness2VsTime},PlotRange->All,Joined->True,Mesh->All,PlotMarkers->{Automatic,7},
      AxesLabel->{"Time (minutes)","Thickness (nm)"},ImageSize->500]
94 ListPlot[{thickness3VsTime},PlotRange->All,Joined->True,Mesh->All,PlotMarkers->{Automatic,7},
      AxesLabel->{"Time (minutes)","Thickness (nm)"},ImageSize->500]
95 ListPlot[{thickness4VsTime},PlotRange->All,Joined->True,Mesh->All,PlotMarkers->{Automatic,7},
      AxesLabel->{"Time (minutes)","Thickness (nm)"},ImageSize->500]
96 ListPlot[{thickness5VsTime},PlotRange->All,Joined->True,Mesh->All,PlotMarkers->{Automatic,7},
      AxesLabel->{"Time (minutes)","Thickness (nm)"},ImageSize->500]
97
98 (*Plot: comparing with using constant Scherrer constant 0.94 *)
99 ListPlot[{thickness1VsTime,thickness1CSVsTime},PlotRange->All,Joined->True,AxesLabel->{"Time (
      minutes)","Thickness (nm)"},PlotLegends->{"Cubic crystallite","Spherical crystallite"},Mesh->All,
      PlotMarkers->{Automatic,7},ImageSize->500]
100 ListPlot[{thickness2VsTime,thickness2CSVsTime},PlotRange->All,Joined->True,AxesLabel->{"Time (
      minutes)","Thickness (nm)"},PlotLegends->{"Cubic crystallite","Spherical crystallite"},Mesh->All,
      PlotMarkers->{Automatic,7},ImageSize->500]
101 ListPlot[{thickness3VsTime,thickness3CSVsTime},PlotRange->All,Joined->True,AxesLabel->{"Time (

```

```

minutes)", "Thickness (nm)"}}, PlotLegends -> {"Cubic crystallite", "Spherical crystallite"}, Mesh -> All,
PlotMarkers -> {Automatic, 7}, ImageSize -> 500
102 ListPlot[{thickness4VsTime, thickness4CSVsTime}, PlotRange -> All, Joined -> True, AxesLabel -> {"Time (
minutes)", "Thickness (nm)"}}, PlotLegends -> {"Cubic crystallite", "Spherical crystallite"}, Mesh -> All,
PlotMarkers -> {Automatic, 7}, ImageSize -> 500
103 ListPlot[{thickness5VsTime, thickness5CSVsTime}, PlotRange -> All, Joined -> True, AxesLabel -> {"Time (
minutes)", "Thickness (nm)"}}, PlotLegends -> {"Cubic crystallite", "Spherical crystallite"}, Mesh -> All,
PlotMarkers -> {Automatic, 7}, ImageSize -> 500
104
105 (*Size estimation by IntegralBreadth method*)
106 IntegralBreadth1 = Table[1, {i, 98}];
107 IntegralBreadth1 = Table[Integrate[nlm1[[i]][x], {x, 16.65, 16.95}]/nlm1[[i]]["ParameterTableEntries"
]][[3, 1]], {i, 98}];
108 IntegralBreadth2 = Table[1, {i, 98}];
109 IntegralBreadth2 = Table[Integrate[nlm2[[i]][x], {x, 19.25, 19.55}]/nlm2[[i]]["ParameterTableEntries"
]][[3, 1]], {i, 98}];
110 IntegralBreadth3 = Table[1, {i, 98}];
111 IntegralBreadth3 = Table[Integrate[nlm3[[i]][x], {x, 27.35, 27.75}]/nlm3[[i]]["ParameterTableEntries"
]][[3, 1]], {i, 98}];
112 IntegralBreadth4 = Table[1, {i, 98}];
113 IntegralBreadth4 = Table[Integrate[nlm4[[i]][x], {x, 32.25, 32.65}]/nlm4[[i]]["ParameterTableEntries"
]][[3, 1]], {i, 98}];
114 IntegralBreadth5 = Table[1, {i, 98}];
115 IntegralBreadth5 = Table[Integrate[nlm5[[i]][x], {x, 33.75, 34.05}]/nlm5[[i]]["ParameterTableEntries"
]][[3, 1]], {i, 98}];
116
117 (*Find thickness*)
118 thicknessIB1 = (1.1547*(0.6941/10^10))/((IntegralBreadth1*Pi/180)*Cos[re111[[2, All, 1]]/2Degree]);
119 thicknessIB2 = (1.0*(0.6941/10^10))/((IntegralBreadth2*Pi/180)*Cos[re200[[2, All, 1]]/2Degree]);
120 thicknessIB3 = (1.0607*(0.6941/10^10))/((IntegralBreadth3*Pi/180)*Cos[re220[[2, All, 1]]/2Degree]);
121 thicknessIB4 = (1.1359*(0.6941/10^10))/((IntegralBreadth4*Pi/180)*Cos[re311[[2, All, 1]]/2Degree]);
122 thicknessIB5 = (1.1547*(0.6941/10^10))/((IntegralBreadth5*Pi/180)*Cos[re222[[2, All, 1]]/2Degree]);
123
124 thicknessIB1VsTime = Thread[{time, thicknessIB1*10^9}];
125 thicknessIB2VsTime = Thread[{time, thicknessIB2*10^9}];
126 thicknessIB3VsTime = Thread[{time, thicknessIB3*10^9}];

```

```

127 thicknessB4VsTime=Thread[{time,thicknessB4*10^9}];
128 thicknessB5VsTime=Thread[{time,thicknessB5*10^9}];
129
130 (*Plot: thickness vs temperature, by integral breadth method*)
131 ListPlot[{IntegralBreadth1, IntegralBreadth2, IntegralBreadth3, IntegralBreadth4, IntegralBreadth5},
PlotRange->All,Joined->True,AxesLabel->{"Time (minutes)", "IntegralBreadth (degree)"},
PlotLegends->{"111", "200", "220", "311", "222"},Mesh->All,PlotMarkers->{Automatic,7},ImageSize
->500]
132
133 (*Plot: thickness vs time, by integral breadth method*)
134 ListPlot[thicknessB1VsTime,PlotRange->All,Joined->True,AxesLabel->{"Time (minutes)", "Thickness (
nm)"},Mesh->All,PlotMarkers->{Automatic,7},ImageSize->500]
135 ListPlot[thicknessB2VsTime,PlotRange->All,Joined->True,AxesLabel->{"Time (minutes)", "Thickness (
nm)"},Mesh->All,PlotMarkers->{Automatic,7},ImageSize->500]
136 ListPlot[thicknessB3VsTime,PlotRange->All,Joined->True,AxesLabel->{"Time (minutes)", "Thickness (
nm)"},Mesh->All,PlotMarkers->{Automatic,7},ImageSize->500]
137 ListPlot[thicknessB4VsTime,PlotRange->All,Joined->True,AxesLabel->{"Time (minutes)", "Thickness (
nm)"},Mesh->All,PlotMarkers->{Automatic,7},ImageSize->500]
138 ListPlot[thicknessB5VsTime,PlotRange->All,Joined->True,AxesLabel->{"Time (minutes)", "Thickness (
nm)"},Mesh->All,PlotMarkers->{Automatic,7},ImageSize->500]
139
140 (*Plot: comparing size estimated by FWHM and IntegralBreadth method*)
141 ListPlot[{thickness1VsTime,thicknessB1VsTime},PlotRange->All,Joined->True,AxesLabel->{"Time (
minutes)", "Thickness (nm)"},PlotLegends->Placed[{"FWHM", "Integral breadth"},{0.85,0.2}],Mesh->
All,PlotMarkers->{Automatic,7},ImageSize->500]
142 ListPlot[{thickness2VsTime,thicknessB2VsTime},PlotRange->All,Joined->True,AxesLabel->{"Time (
minutes)", "Thickness (nm)"},PlotLegends->Placed[{"FWHM", "Integral breadth"},{0.85,0.2}],Mesh->
All,PlotMarkers->{Automatic,7},ImageSize->500]
143 ListPlot[{thickness3VsTime,thicknessB3VsTime},PlotRange->All,Joined->True,AxesLabel->{"Time (
minutes)", "Thickness (nm)"},PlotLegends->Placed[{"FWHM", "Integral breadth"},{0.85,0.2}],Mesh->
All,PlotMarkers->{Automatic,7},ImageSize->500]
144 ListPlot[{thickness4VsTime,thicknessB4VsTime},PlotRange->All,Joined->True,AxesLabel->{"Time (
minutes)", "Thickness (nm)"},PlotLegends->Placed[{"FWHM", "Integral breadth"},{0.85,0.2}],Mesh->
All,PlotMarkers->{Automatic,7},ImageSize->500]
145 ListPlot[{thickness5VsTime,thicknessB5VsTime},PlotRange->All,Joined->True,AxesLabel->{"Time (
minutes)", "Thickness (nm)"},PlotLegends->Placed[{"FWHM", "Integral breadth"},{0.85,0.2}],Mesh->

```



```

All,PlotMarkers->{Automatic,7},ImageSize->500]
146
147 (*{Comparing the estimated size growth rate of silver by FWHM and integral breadth method by shifting up
    the plot of size estimated by integral breadth method*})
148 thickness1fVsTime=Thread[{time,thickness1B1*10^9}];
149 thickness1B2fVsTime=Thread[{time,thickness1B2*10^9}];
150 thickness1B3fVsTime=Thread[{time,thickness1B3*10^9}];
151 thickness1B4fVsTime=Thread[{time,thickness1B4*10^9}];
152 thickness1B5fVsTime=Thread[{time,thickness1B5*10^9}];thickness1fVsTime=Thread[{time,thickness1*10^9+
    Mean[thickness1B1*10^9-thickness1*10^9]}}];
153 thickness2fVsTime=Thread[{time,thickness2*10^9+Mean[thickness1B2*10^9-thickness2*10^9]}}];
154 thickness3fVsTime=Thread[{time,thickness3*10^9+Mean[thickness1B3*10^9-thickness3*10^9]}}];
155 thickness4fVsTime=Thread[{time,thickness4*10^9+Mean[thickness1B4*10^9-thickness4*10^9]}}];
156 thickness5fVsTime=Thread[{time,thickness5*10^9+Mean[thickness1B5*10^9-thickness5*10^9]}}];ListPlot[{
    thickness1fVsTime,thickness1B1VsTime},PlotRange->All,Joined->True,AxesLabel->{"Time (minutes)"
    ,"Thickness (nm)"},PlotLegends->Placed[{"FWHM","Integral breadth"},{0.85,0.35}],Mesh->All,
    PlotMarkers->{Automatic,7},ImageSize->500]
157 ListPlot[{thickness2fVsTime,thickness1B2VsTime},PlotRange->All,Joined->True,AxesLabel->{"Time (
    minutes)" ,"Thickness (nm)"},PlotLegends->Placed[{"FWHM","Integral breadth"},{0.85,0.35}],Mesh->
All,PlotMarkers->{Automatic,7},ImageSize->500]
158 ListPlot[{thickness3fVsTime,thickness1B3VsTime},PlotRange->All,Joined->True,AxesLabel->{"Time (
    minutes)" ,"Thickness (nm)"},PlotLegends->Placed[{"FWHM","Integral breadth"},{0.85,0.35}],Mesh->
All,PlotMarkers->{Automatic,7},ImageSize->500]
159 ListPlot[{thickness4fVsTime,thickness1B4VsTime},PlotRange->All,Joined->True,AxesLabel->{"Time (
    minutes)" ,"Thickness (nm)"},PlotLegends->Placed[{"FWHM","Integral breadth"},{0.85,0.35}],Mesh->
All,PlotMarkers->{Automatic,7},ImageSize->500]
160 ListPlot[{thickness5fVsTime,thickness1B5VsTime},PlotRange->All,Joined->True,AxesLabel->{"Time (
    minutes)" ,"Thickness (nm)"},PlotLegends->Placed[{"FWHM","Integral breadth"},{0.85,0.35}],Mesh->
All,PlotMarkers->{Automatic,7},ImageSize->500]
161
162 (*Size estimation error of FWHM and IntegralBreadth*)
163 nlm1bands95[x_]=Table[1,{i,98}];
164 nlm1bands95[x_]=Table[nlm1[[i]]["MeanPredictionBands",ConfidenceLevel->.95],{i,98}];
165 nlm2bands95[x_]=Table[1,{i,98}];
166 nlm2bands95[x_]=Table[nlm2[[i]]["MeanPredictionBands",ConfidenceLevel->.95],{i,98}];
167 nlm3bands95[x_]=Table[1,{i,98}];

```

```

168 nlm3bands95[x_]=Table[nlm3[[i]]["MeanPredictionBands",ConfidenceLevel->.95],{i,98}];
169 nlm4bands95[x_]=Table[1,{i,98}];
170 nlm4bands95[x_]=Table[nlm4[[i]]["MeanPredictionBands",ConfidenceLevel->.95],{i,98}];
171 nlm5bands95[x_]=Table[1,{i,98}];
172 nlm5bands95[x_]=Table[nlm5[[i]]["MeanPredictionBands",ConfidenceLevel->.95],{i,98}];
    IntergralBreadth1delta=Table[1,{i,98}];
173 IntergralBreadth1delta=Table[(Abs[Integrate[nlm1bands95[x][[i,1]],{x,16.65,16.95}]/nlm1[[i]]["
    ParameterConfidenceIntervals",ConfidenceLevel->.95][[3,2]]-IntergralBreadth1[[i]]+Abs[Integrate[
    nlm1bands95[x][[i,2]],{x,16.65,16.95}]/nlm1[[i]]["ParameterConfidenceIntervals",ConfidenceLevel
    ->.95][[3,1]]-IntergralBreadth1[[i]])]/2,{i,98}];
174 IntergralBreadth2delta=Table[1,{i,98}];
175 IntergralBreadth2delta=Table[(Abs[Integrate[nlm2bands95[x][[i,1]],{x,19.25,19.55}]/nlm2[[i]]["
    ParameterConfidenceIntervals",ConfidenceLevel->.95][[3,2]]-IntergralBreadth2[[i]]+Abs[Integrate[
    nlm2bands95[x][[i,2]],{x,19.25,19.55}]/nlm2[[i]]["ParameterConfidenceIntervals",ConfidenceLevel
    ->.95][[3,1]]-IntergralBreadth2[[i]])]/2,{i,98}];
176 IntergralBreadth3delta=Table[1,{i,98}];
177 IntergralBreadth3delta=Table[(Abs[Integrate[nlm3bands95[x][[i,1]],{x,27.35,27.75}]/nlm3[[i]]["
    ParameterConfidenceIntervals",ConfidenceLevel->.95][[3,2]]-IntergralBreadth3[[i]]+Abs[Integrate[
    nlm3bands95[x][[i,2]],{x,27.35,27.75}]/nlm3[[i]]["ParameterConfidenceIntervals",ConfidenceLevel
    ->.95][[3,1]]-IntergralBreadth3[[i]])]/2,{i,98}];
178 IntergralBreadth4delta=Table[1,{i,98}];
179 IntergralBreadth4delta=Table[(Abs[Integrate[nlm4bands95[x][[i,1]],{x,32.25,32.65}]/nlm4[[i]]["
    ParameterConfidenceIntervals",ConfidenceLevel->.95][[3,2]]-IntergralBreadth4[[i]]+Abs[Integrate[
    nlm4bands95[x][[i,2]],{x,32.25,32.65}]/nlm4[[i]]["ParameterConfidenceIntervals",ConfidenceLevel
    ->.95][[3,1]]-IntergralBreadth4[[i]])]/2,{i,98}];
180 IntergralBreadth5delta=Table[1,{i,98}];
181 IntergralBreadth5delta=Table[(Abs[Integrate[nlm5bands95[x][[i,1]],{x,33.75,34.05}]/nlm5[[i]]["
    ParameterConfidenceIntervals",ConfidenceLevel->.95][[3,2]]-IntergralBreadth5[[i]]+Abs[Integrate[
    nlm5bands95[x][[i,2]],{x,33.75,34.05}]/nlm5[[i]]["ParameterConfidenceIntervals",ConfidenceLevel
    ->.95][[3,1]]-IntergralBreadth5[[i]])]/2,{i,98}];FWHM1delta=Table[1,{i,98}];
182 FWHM2delta=Table[1,{i,98}];
183 FWHM3delta=Table[1,{i,98}];
184 FWHM4delta=Table[1,{i,98}];
185 FWHM5delta=Table[1,{i,98}];
186 FWHM1delta=Table[(Abs[nlm1[[i]]["ParameterConfidenceIntervals",ConfidenceLevel->.95][[1,1]]*2*Sqrt[2*
    Log[2]]-FWHM1[[i]]+Abs[nlm1[[i]]["ParameterConfidenceIntervals",ConfidenceLevel->.95][[1,2]]*2*Sqrt

```

```

[2*Log[2]]-FWHM1[[i]])/2,{i,98}];
187 FWHM2delta= Table[(Abs[nlm2[[i]]["ParameterConfidenceIntervals",ConfidenceLevel->.95][[1,1]]*2*Sqrt[2*
Log[2]]-FWHM2[[i]]+Abs[nlm2[[i]]["ParameterConfidenceIntervals",ConfidenceLevel->.95][[1,2]]*2*Sqrt
[2*Log[2]]-FWHM2[[i]])]/2,{i,98}];
188 FWHM3delta= Table[(Abs[nlm3[[i]]["ParameterConfidenceIntervals",ConfidenceLevel->.95][[1,1]]*2*Sqrt[2*
Log[2]]-FWHM3[[i]]+Abs[nlm3[[i]]["ParameterConfidenceIntervals",ConfidenceLevel->.95][[1,2]]*2*Sqrt
[2*Log[2]]-FWHM3[[i]])]/2,{i,98}];
189 FWHM4delta= Table[(Abs[nlm4[[i]]["ParameterConfidenceIntervals",ConfidenceLevel->.95][[1,1]]*2*Sqrt[2*
Log[2]]-FWHM4[[i]]+Abs[nlm4[[i]]["ParameterConfidenceIntervals",ConfidenceLevel->.95][[1,2]]*2*Sqrt
[2*Log[2]]-FWHM4[[i]])]/2,{i,98}];
190 FWHM5delta= Table[(Abs[nlm5[[i]]["ParameterConfidenceIntervals",ConfidenceLevel->.95][[1,1]]*2*Sqrt[2*
Log[2]]-FWHM5[[i]]+Abs[nlm5[[i]]["ParameterConfidenceIntervals",ConfidenceLevel->.95][[1,2]]*2*Sqrt
[2*Log[2]]-FWHM5[[i]])]/2,{i,98}];

191
192 (*Delta D_hkl of FWHM*)
193 deltathicknessFWHM1= Sqrt [
194 ( ((0.6941/10^10)*0.0849) / ( (FWHM1*Pi/180)* ((Cos[re111[[2,All,1]]/2Degree])) ) )^2+
195 ( ((0.8551) *(0.0000000000000006941)) / ( (FWHM1*Pi/180)*(Cos[re111[[2,All,1]]/2Degree]) ) )^2+
196 ( ( (0.8551) *(0.6941/10^10) * (FWHM1delta*Pi/180) ) / ( (FWHM1*Pi/180)^2 * (Cos[re111[[2,All,1]]/2
Degree)))^2 +
197 ( ( (0.8551) *(0.6941/10^10) * (Sin[re111 [[2, All ,1]]/2 Degree] )*(0.034842237140) ) / ( (FWHM1*Pi/180)*
(Cos[re111[[2,All,1]]/2Degree]^2))^2 ];
198 deltathicknessFWHM2= Sqrt [
199 ( ((0.6941/10^10)*0.2069) / ( (FWHM2*Pi/180)* ((Cos[re200[[2,All,1]]/2Degree])) ) )^2+
200 ( ((0.8551) *(0.0000000000000006941)) / ( (FWHM2*Pi/180)*(Cos[re200[[2,All,1]]/2Degree]) ) )^2+
201 ( ( (0.8551) *(0.6941/10^10) * (FWHM2delta*Pi/180) ) / ( (FWHM2*Pi/180)^2 * (Cos[re200[[2,All,1]]/2
Degree)))^2 +
202 ( ( (0.8551) *(0.6941/10^10) * (Sin[re200 [[2, All ,1]]/2 Degree] )*(0.034842237140) ) / ( (FWHM2*Pi/180)*
(Cos[re200[[2,All,1]]/2Degree]^2))^2 ];
203 deltathicknessFWHM3= Sqrt [
204 ( ((0.6941/10^10)*0.2138) / ( (FWHM3*Pi/180)* ((Cos[re220[[2,All,1]]/2Degree])) ) )^2+
205 ( ((0.8551) *(0.0000000000000006941)) / ( (FWHM3*Pi/180)*(Cos[re220[[2,All,1]]/2Degree]) ) )^2+
206 ( ( (0.8551) *(0.6941/10^10) * (FWHM3delta*Pi/180) ) / ( (FWHM3*Pi/180)^2 * (Cos[re220[[2,All,1]]/2
Degree)))^2 +
207 ( ( (0.8551) *(0.6941/10^10) * (Sin[re220 [[2, All ,1]]/2 Degree] )*(0.034842237140) ) / ( (FWHM3*Pi/180)*
(Cos[re220[[2,All,1]]/2Degree]^2))^2 ];deltathicknessFWHM4= Sqrt [

```

```

208 ( ((0.6941/10^10)*0.0426 ) / ( (FWHM4*Pi/180)* ((Cos[re311[[2,All,1]]/2Degree])) ) )^2+
209 ( ((0.8551) *(0.000000000000006941)) / ( (FWHM4*Pi/180)*(Cos[re311[[2,All,1]]/2Degree]) ) )^2+
210 ( ( (0.8551) *(0.6941/10^10) * (FWHM4delta*Pi/180) ) / ( (FWHM4*Pi/180)^2 * (Cos[re311[[2,All,1]]/2
Degree])) )^2 +
211 ( ( (0.8551) *(0.6941/10^10) * (Sin[re311 [[2, All ,1]]/2 Degree])*(0.034842237140) ) / ( (FWHM4*Pi/180)*
(Cos[re311[[2,All,1]]/2Degree]^2) )^2 ];deltathicknessFWHM5= Sqrt [
212 ( ((0.6941/10^10)*0.0849 ) / ( (FWHM5*Pi/180)* ((Cos[re222[[2,All,1]]/2Degree])) ) )^2+
213 ( ((0.8551) *(0.000000000000006941)) / ( (FWHM5*Pi/180)*(Cos[re222[[2,All,1]]/2Degree]) ) )^2+
214 ( ( (0.8551) *(0.6941/10^10) * (FWHM5delta*Pi/180) ) / ( (FWHM5*Pi/180)^2 * (Cos[re222[[2,All,1]]/2
Degree])) )^2 +
215 ( ( (0.8551) *(0.6941/10^10) * (Sin[re222 [[2, All ,1]]/2 Degree])*(0.034842237140) ) / ( (FWHM5*Pi/180)*
(Cos[re222[[2,All,1]]/2Degree]^2) )^2 ];
216
217 (*Delta D_hkl of Integral Breadth*)
218 deltathicknessIntegralBreadth1 = Sqrt [
219 ( ((0.6941/10^10)*0.2544 ) / ( (IntegralBreadth1*Pi/180)* ((Cos[re111 [[2, All ,1]]/2 Degree])) ) )^2+
220 ( ((0.8551) *(0.000000000000006941)) / ( (IntegralBreadth1*Pi/180)*(Cos[re111[[2,All,1]]/2 Degree]
) )^2+
221 ( ( (0.8551) *(0.6941/10^10) * (IntegralBreadth1delta *Pi/180) ) / ( (IntegralBreadth1*Pi/180)^2 * (
Cos[re111 [[2, All ,1]]/2 Degree])) )^2 +
222 ( ( (0.8551) *(0.6941/10^10) * (Sin[re111 [[2, All ,1]]/2 Degree])*(0.034842237140) ) / ( (IntegralBreadth1 *
Pi/180)* (Cos[re111 [[2, All ,1]]/2 Degree]^2) )^2 ];
223 deltathicknessIntegralBreadth2 = Sqrt [
224 ( ((0.6941/10^10)*0.3120) / ( (IntegralBreadth2*Pi/180)* ((Cos[re200 [[2, All ,1]]/2 Degree])) ) )^2+
225 ( ((0.8551) *(0.000000000000006941)) / ( (IntegralBreadth2*Pi/180)*(Cos[re200[[2,All,1]]/2 Degree]
) )^2+
226 ( ( (0.8551) *(0.6941/10^10) * (IntegralBreadth2delta *Pi/180) ) / ( (IntegralBreadth2*Pi/180)^2 * (
Cos[re200 [[2, All ,1]]/2 Degree])) )^2 +
227 ( ( (0.8551) *(0.6941/10^10) * (Sin[re200 [[2, All ,1]]/2 Degree])*(0.034842237140) ) / ( (IntegralBreadth2 *
Pi/180)* (Cos[re200 [[2, All ,1]]/2 Degree]^2) )^2 ];
228 deltathicknessIntegralBreadth3 = Sqrt [
229 ( ((0.6941/10^10)*0.0941) / ( (IntegralBreadth3*Pi/180)* ((Cos[re220 [[2, All ,1]]/2 Degree])) ) )^2+
230 ( ((0.8551) *(0.000000000000006941)) / ( (IntegralBreadth3*Pi/180)*(Cos[re220[[2,All,1]]/2 Degree]
) )^2+
231 ( ( (0.8551) *(0.6941/10^10) * (IntegralBreadth3delta *Pi/180) ) / ( (IntegralBreadth3*Pi/180)^2 * (
Cos[re220 [[2, All ,1]]/2 Degree])) )^2 +

```

```

232 ( ( (0.8551) *(0.6941/10^10) * (Sin[re220 [[2, All ,1]]/2 Degree])* (0.034842237140) ) / ( (IntegralBreadth3 *
    Pi/180)* (Cos[re220 [[2, All ,1]]/2 Degree]^2))^2 ]; deltathicknessIntegralBreadth4 = Sqrt [
233 ( ((0.6941/10^10)*0.2409) / ( (IntegralBreadth4*Pi/180)* ((Cos[re311 [[2, All ,1]]/2 Degree])) ) )^2+
234 ( ((0.8551) *(0.0000000000000006941)) / ( (IntegralBreadth4*Pi/180)*(Cos[re311 [[2, All ,1]]/2 Degree]
    ) ) )^2+
235 ( ( (0.8551) *(0.6941/10^10) * (IntegralBreadth4delta *Pi/180) ) / ( (IntegralBreadth4*Pi/180)^2 * (
    Cos[re311 [[2, All ,1]]/2 Degree])) )^2 +
236 ( ( (0.8551) *(0.6941/10^10) * (Sin[re311 [[2, All ,1]]/2 Degree])* (0.034842237140) ) / ( (IntegralBreadth4 *
    Pi/180)* (Cos[re311 [[2, All ,1]]/2 Degree]^2))^2 ]; deltathicknessIntegralBreadth5 = Sqrt [
237 ( ((0.6941/10^10)*0.1262) / ( (IntegralBreadth5*Pi/180)* ((Cos[re222 [[2, All ,1]]/2 Degree])) ) )^2+
238 ( ((0.8551) *(0.0000000000000006941)) / ( (IntegralBreadth5delta *Pi/180)*(Cos[re222 [[2, All ,1]]/2
    Degree]) ) )^2+
239 ( ( (0.8551) *(0.6941/10^10) * (IntegralBreadth5delta *Pi/180) ) / ( (IntegralBreadth5*Pi/180)^2 * (
    Cos[re222 [[2, All ,1]]/2 Degree])) )^2 +
240 ( ( (0.8551) *(0.6941/10^10) * (Sin[re222 [[2, All ,1]]/2 Degree])* (0.034842237140) ) / ( (IntegralBreadth5 *
    Pi/180)* (Cos[re222 [[2, All ,1]]/2 Degree]^2))^2 ];
241
242 (* Plot: Uncertainty in Gaussianfitting *) Show[ListPlot[Thread[{data2[[10]][[All ,1]], data2 [[10]][[ All
    ,2]]-Mean[data2 [[10]][[1;;3,2]]]}, PlotStyle->Red,PlotRange->All,ImageSize->500,AxesLabel
    ->{"2\Theta(degree)","Intensity (arbitrary units)"},Plot[{nlm2[[10]][x],nlm2bands95[x][[10]],{x
    ,19.25,19.55}],PlotLegends->{"Gaussian fitting model","95\% confidence interval"}]]
243
244 (*Plot: uncertainty in sizeestiimation *)
245 ListPlot[{thickness1*10^9,thickness1*10^9+deltathicknessFWHM1*10^9,thickness1*10^9-
    deltathicknessFWHM1*10^9},Joined->True,PlotRange->All,PlotLegends->Placed[{"size estiamtion",
    "upper limit of size estimation","lower limit of size estimation",{0.7,0.2}],AxesLabel->{"Time (minutes)
    ","Thickness (nm)"},ImageSize->500]
246 ListPlot[{thickness2*10^9,thickness2*10^9+deltathicknessFWHM2*10^9,thickness2*10^9-
    deltathicknessFWHM2*10^9},Joined->True,PlotRange->All,PlotLegends->Placed[{"size estiamtion",
    "upper limit of size estimation","lower limit of size estimation",{0.7,0.2}],AxesLabel->{"Time (minutes)
    ","Thickness (nm)"},ImageSize->500]
247 ListPlot[{thickness3*10^9,thickness3*10^9+deltathicknessFWHM3*10^9,thickness3*10^9-
    deltathicknessFWHM3*10^9},Joined->True,PlotRange->All,PlotLegends->Placed[{"size estiamtion",
    "upper limit of size estimation","lower limit of size estimation",{0.7,0.2}],AxesLabel->{"Time (minutes)
    ","Thickness (nm)"},ImageSize->500]
248 ListPlot[{thickness4*10^9,thickness4*10^9+deltathicknessFWHM4*10^9,thickness4*10^9-

```

```

deltathicknessFWHM4*10^9},Joined->True,PlotRange->All,PlotLegends->Placed[{"size estiamtion",
upper limit of size estimation","lower limit of size estimation"},{0.7,0.2}],AxesLabel->{"Time (minutes)
","Thickness (nm)"},ImageSize->500]
249 ListPlot[{thickness5*10^9,thickness5*10^9+deltathicknessFWHM5*10^9,thickness5*10^9-
deltathicknessFWHM5*10^9},Joined->True,PlotRange->All,PlotLegends->Placed[{"size estiamtion",
upper limit of size estimation","lower limit of size estimation"},{0.7,0.2}],AxesLabel->{"Time (minutes)
","Thickness (nm)"},ImageSize->500]
250
251 ListPlot[{thicknessB1*10^9,thicknessB1*10^9+deltathicknessIntegralBreadth1*10^9,thicknessB1*10^9-
deltathicknessIntegralBreadth1*10^9},Joined->True,PlotRange->All,PlotLegends->Placed[{"size
estiamtion","upper limit of size estimation","lower limit of size estimation "},{0.7,0.2}], AxesLabel->{
"Time (minutes)","thicknessB (nm)"},ImageSize->500]
252 ListPlot[{thicknessB2*10^9,thicknessB2*10^9+deltathicknessIntegralBreadth2*10^9,thicknessB2*10^9-
deltathicknessIntegralBreadth2*10^9},Joined->True,PlotRange->All,PlotLegends->Placed[{"size
estiamtion","upper limit of size estimation","lower limit of size estimation "},{0.7,0.2}], AxesLabel->{
"Time (minutes)","thicknessB (nm)"},ImageSize->500]
253 ListPlot[{thicknessB3*10^9,thicknessB3*10^9+deltathicknessIntegralBreadth3*10^9,thicknessB3*10^9-
deltathicknessIntegralBreadth3*10^9},Joined->True,PlotRange->All,PlotLegends->Placed[{"size
estiamtion","upper limit of size estimation","lower limit of size estimation "},{0.7,0.2}], AxesLabel->{
"Time (minutes)","thicknessB (nm)"},ImageSize->500]
254 ListPlot[{thicknessB4*10^9,thicknessB4*10^9+deltathicknessIntegralBreadth4*10^9,thicknessB4*10^9-
deltathicknessIntegralBreadth4*10^9},Joined->True,PlotRange->All,PlotLegends->Placed[{"size
estiamtion","upper limit of size estimation","lower limit of size estimation "},{0.7,0.2}], AxesLabel->{
"Time (minutes)","thicknessB (nm)"},ImageSize->500]
255 ListPlot[{thicknessB5*10^9,thicknessB5*10^9+deltathicknessIntegralBreadth5*10^9,thicknessB5*10^9-
deltathicknessIntegralBreadth5*10^9},Joined->True,PlotRange->All,PlotLegends->Placed[{"size
estiamtion","upper limit of size estimation","lower limit of size estimation "},{0.7,0.2}], AxesLabel->{
"Time (minutes)","thicknessB (nm)"},ImageSize->500]

```

Listing D.5: Chapter 5

```

1 (*to show the jumping of diffraction angle due to insufficient diffraction angle resolution *)
2 ListPlot[sample [[2,5;;8]], PlotRange->{{19.25,19.55},{20,120}},Joined->True,Mesh->All,ImageSize
->500,PlotMarkers->Automatic,PlotLegends->{"388\[Degree]C","390\[Degree]C","392\[Degree]C",
394\[Degree]C"},AxesLabel->{"2\[Theta](degree)","Intensity (arbitrary units)"}]
3
4 (*Comparing theoretical and experiment values of diffraction angle of reflection 200*)

```

```

5 theoreticalExpo2=Flatten[Import["C:\\Users\\roy\\Desktop\\thesis\\theoretical diffraction angle - 200
   expo.xlsx" ]];
6 theoreticalExpoc2=Flatten[Import["C:\\Users\\roy\\Desktop\\thesis\\theoretical diffraction angle - 200
   expoc.xlsx" ]];
7 ListPlot [{ Thread [{Temp,theoreticalExpoc2}], Thread [{Temp,re200[[2,All,1]]}], PlotLegends -> {"Theoretical",
   "Experimental"}, AxesLabel -> {"Temperature([Degree]C)", "2\\[Theta](degree)"}, Joined -> True,
   ImageSize -> 500, PlotMarkers -> {"", {\\[FilledSmallCircle], 10}}]
8
9 (*Comparing thickness with and without energy dispersion broadening for reflection 111*)
10 FWHMEnergyDispersion=Flatten[Import["C:\\Users\\roy\\Desktop\\thesis\\broadening due to energy
   dispersion result(111).xlsx" ]];
11 FWHMWithoutEnergyDispersion=Sqrt[FWHM12-FWHMEnergyDispersion2];
12 thicknessWithoutEnergyDispersion=(0.8551*(0.6941/1010))/((FWHMWithoutEnergyDispersion*Pi/180)*Cos[
   re111[[2,All,1]]/2Degree]);
13 thicknessWithoutEnergyDispersionVsTime=Thread [{time,thicknessWithoutEnergyDispersion*109};
14
15 ListPlot [{thickness1VsTime,thicknessWithoutEnergyDispersionVsTime}, PlotRange -> All, Joined -> True,
   Mesh -> All, ImageSize -> 500, PlotMarkers -> {Automatic, 7}, AxesLabel -> {"Time (minutes)", "
   Thickness (nm)"}, PlotLegends -> Placed [{"thickness(with energy dispersion broadening)", "thickness(
   without energy dispersion broadening)"}, {0.66, 0.3}]

```

Listing D.6: Chapter 6

```

1 (*Isothermal kinetics*)
2 yfwhm01=Table[1,{i,25}];
3 yfwhm01=Table[thickness1[[i]]3/thickness1 [[27]]3,{ i ,2,26}];
4 yfwhm1=Log[-Log[1-yfwhm01]];
5 xfwhm1=Log[time[[2;;26]]*60];
6 yvsxfwhm1=Thread [{xfwhm1,yfwhm1}];
7
8 yfwhm02=Table[1,{i,25}];
9 yfwhm02=Table[thickness2[[i]]3/thickness2 [[27]]3,{ i ,2,26}];
10 yfwhm2=Log[-Log[1-yfwhm02]];
11 xfwhm2=Log[time[[2;;26]]*60];
12 yvsxfwhm2=Thread [{xfwhm2,yfwhm2}];
13
14 yfwhm03=Table[1,{i,25}];

```

```

15 yfwhm03=Table[thickness3[[i]]^3/thickness3 [[27]]^3,{ i ,2,26}];
16 yfwhm3=Log[-Log[1-yfwhm03]];
17 xfwhm3=Log[time[[2;;26]]*60];
18 yvsxfwhm3=Thread[{xfwhm3,yfwhm3}];
19
20 yfwhm04=Table[1,{i,25}];
21 yfwhm04=Table[thickness1[[i]]^3/thickness1 [[27]]^3,{ i ,2,26}];
22 yfwhm4=Log[-Log[1-yfwhm01]];
23 xfwhm4=Log[time[[2;;26]]*60];
24 yvsxfwhm4=Thread[{xfwhm1,yfwhm1}];
25
26 yfwhm05=Table[1,{i,25}];
27 yfwhm05=Table[thickness5[[i]]^3/thickness5 [[27]]^3,{ i ,2,26}];
28 yfwhm5=Log[-Log[1-yfwhm05]];
29 xfwhm5=Log[time[[2;;26]]*60];
30 yvsxfwhm5=Thread[{xfwhm5,yfwhm5}];
31
32 yIB01=Table[1,{i,25}];
33 yIB01=Table[thicknessIB1[[i]]^3/ thicknessIB1 [[27]]^3,{ i ,2,26}];
34 yIB1=Log[-Log[1-yIB01]];
35 xIB1=Log[time [[2;;26]]*60];
36 yvsxIB1=Thread[{xIB1,yIB1}];
37
38 yIB02=Table[1,{i,25}];
39 yIB02=Table[thicknessIB2[[i]]^3/ thicknessIB2 [[27]]^3,{ i ,2,26}];
40 yIB2=Log[-Log[1-yIB02]];
41 xIB2=Log[time [[2;;26]]*60];
42 yvsxIB2=Thread[{xIB2,yIB2}];
43
44 yIB03=Table[1,{i,25}];
45 yIB03=Table[thicknessIB3[[i]]^3/ thicknessIB3 [[27]]^3,{ i ,2,26}];
46 yIB3=Log[-Log[1-yIB03]];
47 xIB3=Log[time [[2;;26]]*60];
48 yvsxIB3=Thread[{xIB3,yIB3}];
49
50 yIB04=Table[1,{i,25}];

```



```

51 yIB04=Table[thicknessIB1[[i]]^3/thicknessIB1 [[27]]^3,{ i ,2,26}];
52 yIB4=Log[-Log[1-yIB01]];
53 xIB4=Log[time [[2;;26]]*60];
54 yvsxIB4=Thread[{xIB1,yIB1}];
55
56 yIB05=Table[1,{i,25}];
57 yIB05=Table[thicknessIB5[[i]]^3/thicknessIB5 [[27]]^3,{ i ,2,26}];
58 yIB5=Log[-Log[1-yIB05]];
59 xIB5=Log[time [[2;;26]]*60];
60 yvsxIB5=Thread[{xIB5,yIB5}];
61
62 ListPlot [yvsxfwhm1,PlotRange->All,AxesLabel->{"ln(t)", "ln[-ln(1-x(t))]"},ImageSize->500]
63 ListPlot [yvsxfwhm2,PlotRange->All,AxesLabel->{"ln(t)", "ln[-ln(1-x(t))]"},ImageSize->500]
64 ListPlot [yvsxfwhm3,PlotRange->All,AxesLabel->{"ln(t)", "ln[-ln(1-x(t))]"},ImageSize->500]
65 ListPlot [yvsxfwhm4,PlotRange->All,AxesLabel->{"ln(t)", "ln[-ln(1-x(t))]"},ImageSize->500]
66 ListPlot [yvsxfwhm5,PlotRange->All,AxesLabel->{"ln(t)", "ln[-ln(1-x(t))]"},ImageSize->500]
67
68 ListPlot [yvsxIB1, PlotRange->All,AxesLabel->{"ln(t)", "ln[-ln(1-x(t))]"},ImageSize->500]
69 ListPlot [yvsxIB2, PlotRange->All,AxesLabel->{"ln(t)", "ln[-ln(1-x(t))]"},ImageSize->500]
70 ListPlot [yvsxIB3, PlotRange->All,AxesLabel->{"ln(t)", "ln[-ln(1-x(t))]"},ImageSize->500]
71 ListPlot [yvsxIB4, PlotRange->All,AxesLabel->{"ln(t)", "ln[-ln(1-x(t))]"},ImageSize->500]
72 ListPlot [yvsxIB5, PlotRange->All,AxesLabel->{"ln(t)", "ln[-ln(1-x(t))]"},ImageSize->500]
73 Show[Graphics3D[Ellipsoid [{0,0,0},{92.37',76.71',86.57'}]], ViewPoint->{1.3',-2.4',2.'}]
74 Show[Graphics3D[Ellipsoid [{0,0,0},{72.82',72.34',72.45'}],{ ViewPoint->{1.3',-2.4',2.'}],ViewPoint
->{1.3',-2.4',2.'}]

```

Bibliography

- [1] Nanoparticle (2016). In Encyclopaedia Britannica. Retrieved from <http://academic.eb.com/EBchecked/topic/1109065/nanoparticle>.
- [2] Welles, A. E. (2010). *Silver nanoparticles: properties, characterization and applications*. Nova Science Publishers.
- [3] Ameen, K. B., Rajasekar, K. and Rajasekharan, T. (2007). Silver nanoparticles in mesoporous aerogel exhibiting selective catalytic oxidation of benzene in CO₂ free air. *Catalysis Letters*, 119(3-4), 289–295.
- [4] Jiang, Z.-J., Liu, C.-Y. and Sun, L.-W. (2005). Catalytic properties of silver nanoparticles supported on silica spheres. *The Journal of Physical Chemistry B*, 109(5), 1730–1735.
- [5] Larsen, H. B., Thorkildsen, G., Nicholson, D. G. and Pattison, P. (2016). Thermal induced structural properties of silver(I) sulphate (Ag₂SO₄). *Submitted for publication to Physical Review B*.
- [6] Dorofeev, G., Streletskii, A., Povstugar, I., Protasov, A. and Elsukov, E. (2012). Determination of nanoparticle sizes by X-ray diffraction. *Colloid Journal*, 74(6), 675–685.
- [7] Merkus, H. G. (2009). *Particle size measurements: fundamentals, practice, quality*, volume 17. Springer Science & Business Media.
- [8] Sette, F. (2016). Station Bending Magnet 1A. Retrieved from <http://www.esrf.eu/UsersAndScience/Experiments/CRG/BM01/bm01-a>.
- [9] Masciocchi, N. and Parrish, W. (1990). New Crystal Data for High Temperature Hexagonal Silver Sulfate. *Powder Diffraction*, 5(01), 50–52.

- [10] Bragg, W. H. and Bragg, W. L. (1913). The reflection of X-rays by crystals. *Proceedings of the Royal Society of London Series A, Containing Papers of a Mathematical and Physical Character*, 88(605), 428–438.
- [11] Kittel, C. (2005). *Introduction to solid state physics*. Wiley.
- [12] Prince, E., Wilson, A. J. C., Hahn, T. and Shmueli, U. (1999). *International tables for crystallography*. International Union of Crystallography.
- [13] Moruzzi, V. L., Janak, J. F. and Schwarz, K. (1988). Calculated thermal properties of metals. *Physical Review B*, 37(2), 790.
- [14] Sands, D. E. (2012). *Introduction to crystallography*. Courier Corporation.
- [15] Spreadborough, J. and Christian, J. W. (1959). High-temperature X-ray diffractometer. *Journal of Scientific Instruments*, 36(3), 116.
- [16] Draper, N. R., Smith, H. and Pownell, E. (1966). *Applied regression analysis*, volume 3. Wiley New York.
- [17] Hyndman, R. J. and Koehler, A. B. (2006). Another look at measures of forecast accuracy. *International journal of forecasting*, 22(4), 679–688.
- [18] Patel, S. B. (1991). *Nuclear physics: an introduction*. New Age International.
- [19] Warren, B. E. (1969). *X-ray diffraction*. Courier Corporation.
- [20] Stribeck, N. (2007). *X-ray scattering of soft matter*. Springer Science & Business Media.
- [21] Klug, H. P., Alexander, L. E. et al. (1954). *X-ray diffraction procedures*, volume 2. Wiley New York.
- [22] Langford, J. I. and Wilson, A. (1978). Scherrer after sixty years: a survey and some new results in the determination of crystallite size. *Journal of Applied Crystallography*, 11(2), 102–113.
- [23] Scherrer, P. (1918). Zsigmondy's Kolloidchemie. *Nachrichten der Göttinger Gesellschaft*, 98, 394.

- [24] Wilson, A. (1968). On variance as a measure of line broadening in diffractometry: effect of a distribution of sizes on the apparent crystallite size. *Journal of Applied Crystallography*, 1(3), 194–196.
- [25] Wilson, A. (1971). Some further considerations in particle-size broadening. *Journal of Applied Crystallography*, 4(6), 440–443.
- [26] Hammond, C. (2009). *The basics of crystallography and diffraction*. Oxford University Press Oxford.
- [27] Leineweber, A. and Mittemeijer, E. J. (2006). Anisotropic microstrain broadening due to compositional inhomogeneities and its parametrisation. *Zeitschrift für Kristallographie Suppl*, 23, 117–122.
- [28] Snyder, R. L., Fiala, J. and Bunge, H. J. (1999). *Defect and microstructure analysis by diffraction*, volume 10. Courier Corporation.
- [29] York, B. R. (1997). New X-ray diffraction line profile function based on crystallite size and strain distributions determined from mean field theory and statistical mechanics. *Advances in X-ray Analysis*, 41, 544–554.
- [30] Patterson, A. (1939). The diffraction of X-rays by small crystalline particles. *Physical Review*, 56(10), 972–978.
- [31] Patterson, A. (1939). The Scherrer formula for X-ray particle size determination. *Physical review*, 56(10), 978–982.
- [32] Guo, H. (2011). A simple algorithm for fitting a Gaussian function. *IEEE Signal Processing Magazine*, 28(9), 134–137.
- [33] Ekström, P. (1996). *Statistics and the treatment of experimental data*. Lunds Universitet.
- [34] Laue, M. (1936). Die äussere Form der Kristalle in ihrem Einfluss auf die Interferenzerscheinungen an Raumgittern. *Annalen der Physik*, 418, 55–68.

- [35] Stokes, A. and Wilson, A. (1942). A method of calculating the integral breadths of Debye-Scherrer lines. *Mathematical Proceedings of the Cambridge Philosophical Society*, 38, 313–322.
- [36] Jones, F. W. (1938). The measurement of particle size by the X-ray method. *Proceedings of the Royal Society of London A: Mathematical, Physical and Engineering Sciences*, 166, 16–43.
- [37] Holzwarth, U. and Gibson, N. (2011). The Scherrer equation versus the 'Debye-Scherrer equation'. *Nature Nanotechnology*, 6(9), 534–534.
- [38] Klimovich, P. V., Shirts, M. R. and Mobley, D. L. (2015). Guidelines for the analysis of free energy calculations. *Journal of computer-aided molecular design*, 29(5), 397–411.
- [39] Taylor, J. R. and Cohen, E. (1998). An introduction to error analysis: the study of uncertainties in physical measurements. *Measurement Science and Technology*, 9(6), 1015.
- [40] Balzar, D., Audebrand, N., Daymond, M., Fitch, A., Hewat, A., Langford, J. I., Le Bail, A., Louër, D., Masson, O., McCowan, C. N. et al. (2004). Size-strain line-broadening analysis of the ceria round-robin sample. *Journal of Applied Crystallography*, 37(6), 911–924.
- [41] Cullity, B. D. and Weymouth, J. W. (1957). Elements of X-ray Diffraction. *American Journal of Physics*, 25(6), 394–395.
- [42] Guinier, A. (1994). *X-ray diffraction in crystals, imperfect crystals, and amorphous bodies*. Courier Corporation.
- [43] Als-Nielsen, J. and McMorrow, D. (2011). *Elements of modern X-ray physics*. John Wiley & Sons.
- [44] Vazquez, J., Lopez, A. P. L., Villares, P. and Jimenez, G. R. (2000). Generalization of the Avrami equation for the analysis of non-isothermal transformation kinetics. Application to the crystallization of the Cu 0.20 As 0.30 Se 0.50 alloy. *Journal of Physics and Chemistry of Solids*, 61(4), 493–500.
- [45] Smith, A., Datta, S. P., Smith, G. H., Campbell, P. N., Bentley, R., McKenzie, H. et al. (2000). *Oxford dictionary of biochemistry and molecular biology*. Oxford University Press.

- [46] Chen, Q. A., Wang, D. S., Zhou, Y. G., Duan, Y., Fan, H. J., Yang, Y. and Zhang, Z. (2011). Convergent asymmetric disproportionation reactions: metal/Brønsted acid relay catalysis for enantioselective reduction of quinoxalines. *Journal of the American Chemical Society*, 133(16), 6126–6129.